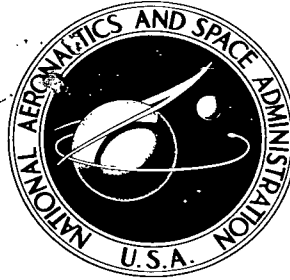


NASA TECHNICAL NOTE



NASA TN D-3478

NASA TN D-3478

cl

LOCAL COPY REF
RISAL TAVEL
RINDA 10 PER.

0130399



STUDY OF SURFACE PITOTS FOR MEASURING TURBULENT SKIN FRICTION AT SUPERSONIC MACH NUMBERS - ADIABATIC WALL

by Edward J. Hopkins and Earl R. Keener

Ames Research Center

Moffett Field, Calif.





STUDY OF SURFACE PITOTS FOR MEASURING TURBULENT
SKIN FRICTION AT SUPERSONIC MACH NUMBERS -
ADIABATIC WALL

By Edward J. Hopkins and Earl R. Keener

Ames Research Center
Moffett Field, Calif.

NATIONAL AERONAUTICS AND SPACE ADMINISTRATION

For sale by the Clearinghouse for Federal Scientific and Technical Information
Springfield, Virginia 22151 - Price \$4.00

TABLE OF CONTENTS

	<u>Page</u>
SUMMARY	1
INTRODUCTION	1
NOTATION	4
FACILITY	9
TEST CONDITIONS	9
INSTRUMENTATION	9
General Arrangement	9
Skin-Friction Balance	10
Stanton Tube	10
Preston Tubes	10
Traversing Impact-Pressure Probe	10
Boundary-Layer Rake	11
Pressure Sensors	11
Temperature Sensors	11
DATA REDUCTION AND ACCURACY	11
Boundary-Layer-Edge Conditions	11
Momentum Thickness	12
Skin Friction	12
Pressures	13
Geometric Measurements	13
DEVELOPMENT OF NEW CALIBRATION FACTORS	13
Equivalent Incompressible Pressure Coefficient, C_p	13
Reference Temperature Conditions	14
COMPRESSIBILITY AND HEAT-TRANSFER EFFECTS ON THE PRESTON TUBE	
CALIBRATIONS	15
Sharp Leading Edge	15
Blunt Leading Edge	16
RESULTS AND DISCUSSION	17
Preston Tube Calibrations	17
Subsonic $R_d^2 C_p$ vs. $R_d^2 C_f$	17
Supersonic $f_2(T_w) R_d^2 C_p$ vs. $f_2(T_w) R_d^2 C_f$	18
Supersonic $f_2(T_w) R_d^2 (M_s/M_\infty)^2$ vs. $f_2(T_w) R_d^2 C_f$	18
Supersonic $f_2(T') R_d^2 (M_s/M_\infty)^2$ vs. $f_2(T') R_d^2 C_f$	18
Supersonic $[f_1(T_w) (R_d/\sqrt{\sigma_\infty}) \sin^{-1}(\sqrt{\sigma_\infty} V_s/V_\infty)]^2$ vs. $f_2(T_w) R_d^2 C_f$	18
Detailed analysis of the linear part of the Preston tube calibration	19

TABLE OF CONTENTS - Concluded

	<u>Page</u>
Selection of Critical Preston Tube Diameters	19
Maximum tube diameter	19
Minimum critical size	20
Estimated Effects of Mach Number and Heat Transfer on the Preston	
Tube Calibration	20
Sharp leading edge	20
Blunt leading edge	21
Stanton Tube Calibrations	21
$f_2(T_w)R_d^2 C_p$ vs. $f_2(T_w)R_d^2 C_f$	21
$f_2(T_w)R_d^2 (M_S/M_\infty)^2$ vs. $f_2(T_w)R_d^2 C_f$	22
$f_2(T')R_d^2 (M_S/M_\infty)^2$ vs. $f_2(T')R_d^2 C_f$	22
$[f_1(T_w)(R_d/\sqrt{\sigma_\infty})\sin^{-1}(\sqrt{\sigma_\infty} V_S/V_\infty)]^2$ vs. $f_2(T_w)R_d^2 C_f$	22
Local Skin Friction	22
Data From Present Investigation	23
Data From Past Investigations	23
CONCLUSIONS	24
APPENDIX A - SKIN-FRICTION EQUATIONS	26
APPENDIX B - SURFACE PITOT-TUBE CALIBRATION FACTORS USED IN THE PAST	29
APPENDIX C - CRITICAL PRESTON TUBE DIAMETERS	32
APPENDIX D - C_f DERIVED FROM $d\theta/dx$	35
REFERENCES	36
TABLES	40
FIGURES	45

STUDY OF SURFACE PITOTS FOR MEASURING TURBULENT
SKIN FRICTION AT SUPERSONIC MACH NUMBERS -
ADIABATIC WALL

By Edward J. Hopkins and Earl R. Keener

Ames Research Center

SUMMARY

Two types of surface pitot tubes were investigated for measuring local turbulent skin friction at supersonic speeds. These tubes consisted of a circular tube, called a Preston tube, and a two-dimensional blade over a static orifice, hereinafter called a Stanton tube. They were calibrated in air against the measured skin friction throughout a Mach number range from 2.4 to 3.4 and a Reynolds number range from about 16 to 100 million. The boundary layer in which the surface tubes were mounted varied in thickness from about 5 to 7 inches, and the wall temperature was close to adiabatic. The surface pitot data are presented on the basis of several calibration factors that have been used in the past and on the basis of a newly developed calibration factor.

The new calibration factor collapsed the supersonic Preston tube results onto a single calibration curve, which is invariant with changes in Reynolds number, Mach number, or tube size within wide limits. This curve is the same as Preston's incompressible curve.

It was found that the calibration curve for the Stanton tube was affected by the streamwise position of the tube leading edge relative to the static orifice over which it was mounted.

In addition to the surface tube calibrations, some existing local skin-friction results, measured for turbulent boundary layers on adiabatic flat plates, are compared with theoretical values on the basis of equal momentum thickness Reynolds numbers throughout a Mach number range from 0.06 to 6.7. In general, the theory of Wilson and the T' method of Sommer and Short bracketed all the experimental skin-friction data of both past and present investigations.

INTRODUCTION

Skin-friction drag is a significant part of the total drag for a typical supersonic transport flying near maximum lift-to-drag ratio (about 35 percent of the total drag at a Mach number of 3.0); therefore, accurate knowledge of this drag component is important for this type airplane. One simple way to measure the local skin friction on airplanes at high Reynolds numbers is with

calibrated surface pitot tubes. Obviously, the use of surface pitot tubes for obtaining accurate values of skin friction in flight has a considerable advantage over the use of skin-friction balances, which would be more difficult to install and would need to be insensitive to temperature, vibration, and acceleration.

An accurate calibration of a surface pitot tube depends upon how accurately the local skin friction can be measured. In recent years, several direct measuring skin-friction balances have been perfected for use at both subsonic and supersonic speeds. Schultz-Grunow made some of the earliest successful direct measurements with a skin-friction balance at subsonic speeds (ref. 1). More recently, direct measurements of the skin friction were made at low speeds by Liepmann and Dhawan, by Dhawan, and by Smith and Walker (refs. 2 through 4). At supersonic speeds, skin-friction balances have been used in numerous investigations reported in references 5 through 11. In general, skin-friction balances have been used successfully in wind tunnels in which the floating surface element can be relatively large to give large values of the local shearing stress; therefore, an accurate calibration of a surface pitot against readings from these skin-friction balances can be obtained in a wind tunnel.

The use of a surface impact tube was first reported by Stanton, Marshall, and Bryant in 1920 (ref. 12). In their investigation, the surface pitot consisted of a two-dimensional tube with an adjustable upper wall for changing the tube height. This type of surface pitot has become commonly known as a Stanton tube. They used such a tube to deduce the existence of the laminar sublayer of a turbulent boundary layer in incompressible flow. As reported in 1930, Fage and Falkner (ref. 13) used the Stanton tube to measure the turbulent skin friction, but assumed that the velocity profiles very close to the surface were the same for the turbulent and laminar boundary layers; therefore, it was assumed that the Stanton tube calibration obtained in a laminar boundary layer was applicable to the turbulent boundary layer. In 1938, Taylor (ref. 14) studied the effect of Stanton tube height on the "effective distance" from the surface at which the dynamic pressure in incompressible flow is equal to the difference between the Stanton tube and static pressures. Fage and Sargent in 1947 (ref. 15) calibrated a Stanton tube in a turbulent boundary layer up to a Mach number of 0.855. In 1952, Cope (ref. 16) used a Stanton tube to make the first supersonic measurements at a Mach number of 2.5 and concluded that this device is reliable for making skin-friction measurements. Hakkinen found in 1954 (ref. 17) that the subsonic calibration he obtained for a Stanton tube agreed reasonably well with other subsonic calibrations, but that the supersonic calibration had an apparent Mach number effect when based on the usual calibration factors. In the light of Hakkinen's results, the Stanton tube was critically examined further by Trilling and Hakkinen (ref. 18) as a skin-friction measuring device. Their analysis showed that the skin friction indicated by a Stanton tube is a function of the Stanton tube pressure to some power, depending on the flow conditions and the tube height relative to the boundary-layer thickness. A genuine Mach number effect on the Stanton tube calibration was also indicated. Further theoretical work was done by Gadd in 1958 on the Stanton tube (ref. 19) in which the calibration curve was predicted at high Reynolds numbers. In 1959, Bradshaw and Gregory (ref. 20) showed that the Stanton tube calibration made in a laminar boundary

layer at subsonic speeds is not the same as that for a turbulent boundary layer. The first reliable calibration of the Stanton tube at supersonic speeds was made by Abarbanel, Hakkinen, and Trilling in 1959 (ref. 21). They found that, with the usual calibration factors based on the wall temperature, the Stanton tube calibration for a laminar boundary layer was not affected by Mach number, but that the calibration for a turbulent boundary layer was affected by Mach number. In 1962, Smith, Gaudet, and Winter (ref. 22) calibrated a Stanton tube consisting of a razor blade cemented over a static orifice at Mach numbers of 1.8 and 2.7. In reference 22 they stated that the supersonic calibration was sensibly independent of Mach number but later stated that different calibration curves were obtained for subsonic and supersonic Mach numbers with a transitional region for Mach numbers between 0.8 and 1.5 (ref. 23, footnote on p. 11). They based their calibration factors on wall temperature. In 1963, Edwards (ref. 24) used the calibration curve presented in reference 23 to measure the skin friction in free flight between Mach numbers of 1.2 and 2.2.

In 1953, Preston (ref. 25) developed calibration factors for circular surface pitot tubes (Preston tubes), based on the universality of the law of the wall for turbulent boundary layers, and showed that these factors collapsed the incompressible Preston tube data into a single curve for a large range of tube diameters. Preston showed that it is not necessary to limit the tube size to the laminar sublayer to obtain a single calibration curve, because of the large extent of the boundary layer over which the law of the wall is applicable. In a more recent investigation in 1955 (ref. 26), Hsu demonstrated that Preston tubes can be used for measuring skin friction accurately in the presence of adverse pressure gradients and thereby showed the applicability of the method to nonisobaric surfaces. Hsu also showed a theoretical relationship between the shearing stress and the Preston tube pressure and the minor importance of having a particular ratio of inside-to-outside tube diameter on the Preston tube calibration. In 1957, Fenter and Stalmach (ref. 27) developed calibration factors based on the Von Kármán mixing-length theory, following the compressible skin-friction theory of Wilson (ref. 28), which collapsed their supersonic Preston tube data into a single curve between Mach numbers of 1.7 and 3.7. A brief summary of the Fenter and Stalmach development is presented in reference 29. This curve corresponded very closely to the incompressible generalized law of the wall functions of Coles, which are listed in table I of reference 30; therefore, no displacement effect due to the presence of the tubes was indicated, a result which was somewhat contrary to that given by Preston for incompressible flow. In 1958 Naleid (ref. 7) showed that Preston tubes are reliable instruments for measuring skin friction in the presence of an adverse pressure gradient with zero heat transfer. Smith and Walker showed in 1959 (ref. 4) that the form of the Preston calibration factors is correct for low subsonic speeds, but that the constants used to define the calibration curve were slightly different from Preston's. In 1961 the staff of NPL (ref. 31) showed that the form of the incompressible calibration curve for flat plates is similar to that obtained in pipe flow, but that for a given Preston tube reading the local skin friction is about 11 percent higher on the flat plate than in a circular pipe with a fully developed turbulent boundary layer as used by Preston in his original calibration (ref. 25). This result was in contradiction to Hsu's result in 1955 (ref. 26) which appeared to confirm Preston's calibration curve. In 1962, Head and Rechenberg (ref. 32) showed

that for a given Preston tube reading the skin friction was the same for both the boundary layer and fully developed pipe flow, thus vindicating Preston's pipe-flow calibration and confirming the existence of a universal region of flow similarity near the wall. In 1963, Rechenberg (ref. 33) further demonstrated the existence of a universal Preston tube calibration in incompressible flow for either the fully developed turbulent boundary layer in pipe flow or turbulent boundary-layer flow. He also confirmed in reference 33 that the Preston tube method is valid for nonisobaric flow conditions. In reference 34, Rechenberg showed that because of the universal nature of the boundary layer adjacent to the wall the effect of Mach number on the Preston tube calibration is predictable.

The present experimental investigation was undertaken to calibrate surface pitot tubes at high Reynolds numbers near a Mach number of 3 in a thick boundary layer similar to that expected for large supersonic airplanes. Two types of surface pitots, the Preston tube and the Stanton tube, were calibrated on the side wall of the Ames 8- by 7-foot supersonic wind tunnel where the boundary layer in air is 5 to 7 inches thick. This investigation covered a Mach number range from 2.4 to 3.4 and a Reynolds number range from about 16 to 100 million. The surface-pitot data are reduced both on the basis of calibration factors which have been developed in the past and on the basis of a newly developed calibration factor. The adequacy of the calibration factors in reducing the results to a single calibration curve which would be insensitive to Mach number and Reynolds number effects is examined.

Recently, at a Mach number of 2.8 and a Reynolds number up to about one billion, Moore and Harkness (ref. 8) measured the local skin friction on the floor of a wind-tunnel supersonic diffuser. They showed that the theory of either Wilson or Van Driest II gives excellent agreement with experiment but that the reference enthalpy theory of Schultz-Grunow underpredicts the measured values by 10 to 15 percent. There is some indication in the Moore-Harkness report that the Wilson theory tends to overpredict the measured skin friction previously obtained at the lower Reynolds numbers. Because of this anomaly in agreement between theory and experiment, depending on the Reynolds number and, possibly the Mach number, the skin friction measured in the present investigation and the majority of existing experimental skin-friction results obtained throughout a Mach number range from 0.06 to 6.7 for turbulent flow on adiabatic flat plates are compared herein with predicted results from the theory of Wilson (ref. 35) and the method of Sommer and Short (ref. 36).

NOTATION

- C_F average skin-friction coefficient, $\frac{2\theta}{x}$
- C_f local skin-friction coefficient, $\frac{\tau}{q_\infty}$
- C_{f_i} local skin-friction coefficient for incompressible flow

- C_p measured pressure coefficient, $\frac{p_s - p_\infty}{q_\infty}$
- C_{pi} equivalent incompressible pressure coefficient, $\left(\frac{M_s}{M_\infty}\right)^2$
- d diameter of the Preston tubes or the height of the Stanton tubes
- d_i inside diameter
- d_o outside diameter
- $(d_{cr})_{max}$ maximum critical diameter of Preston tube for which the Preston tube calibration is expected to be valid (defined by eq. (C1))
- $(d_{cr})_{min}$ minimum critical diameter of Preston tube allowable to remain within the linear portion of the calibration curve (defined by eq. (C9))
- F_w factor for determining the effects of Mach number and heat transfer on the Preston tube calibration when the flow properties are based on wall temperature, $\left(\frac{T'}{T_w}\right)^{2.536}$, (see eqs. (10) and (11))
- $f, f_p, F_p, f_k, f_h, F_h, f_f, F_f$ } functions relating certain factors appearing in the equation-development sections of this report
- $f_1(T_w)$ factor for converting Reynolds number based on free-stream static temperature to Reynolds number based on wall temperature, $\frac{\mu_\infty \rho_w}{\mu_w \rho_\infty}$
- $f_2(T_w)$ factor for converting Reynolds number squared divided by density, based on free-stream static temperature, to that based on wall temperature, $\left(\frac{\mu_\infty}{\mu_w}\right)^2 \frac{\rho_w}{\rho_\infty}$
- $f_2(T')$ factor for converting Reynolds number squared divided by density, based on free-stream static temperature, to that based on the reference temperature (T') of Sommer and Short, $\left(\frac{\mu_\infty}{\mu'}\right)^2 \frac{\rho'}{\rho_\infty}$
- K constant used in equation (C5), $\frac{1 + 0.2M_\infty^2}{0.2M_\infty^2}$ or $\frac{1}{\sigma}$
- M_z local Mach number defined by equation (14) when leading-edge bluntness is considered

- M_S Mach number indicated by the ratio of the wall static pressure to the pressure of the Preston or Stanton tubes. (When this pressure ratio indicates supersonic flow ahead of the tubes, then the normal shock relationships are used to obtain the Mach number, M_S , ahead of the shock.)
- M_∞ free-stream Mach number indicated by the ratio of surface static pressure to the total pressure from a total pressure tube located just outside the boundary layer, assuming normal shock relationships (see footnote 1)
- $p_{i,\infty}$ free-stream impact pressure (pitot pressure)
- p_S pressure indicated by the Preston or Stanton tubes
- p_∞ static pressure on the side wall of the wind tunnel in the vicinity of the Preston and Stanton tubes
- q_S dynamic pressure indicated by the Preston or Stanton tubes,

$$\frac{\gamma}{2} p_\infty M_S^2$$
- q_∞ free-stream dynamic pressure, $\frac{\gamma}{2} p_\infty M_\infty^2$
- R gas constant for air when treated as a perfect gas
- R_d Reynolds number based on the free-stream flow conditions and the outside diameter of the Preston tube or the height of the Stanton tube,

$$\frac{\rho_\infty V_\infty d}{\mu_\infty}$$
- R_x Reynolds number based on free-stream flow conditions and distance x from the leading edge,

$$\frac{\rho_\infty V_\infty x}{\mu_\infty}$$
- $R_{x,v}$ Reynolds number based on free-stream conditions and distance x_v from the virtual origin,

$$\frac{\rho_\infty V_\infty x_v}{\mu_\infty}$$
- R_θ Reynolds number based on free-stream flow conditions and the momentum thickness,

$$\frac{\rho_\infty V_\infty \theta}{\mu_\infty}$$
- T_S static temperature indicated by the surface pitot tubes, assuming isoenergetic flow conditions,

$$\frac{T_t}{1 + 0.2M_S^2}$$

- T_t total temperature measured in the settling chamber
- T_w wall temperature
- $(T_w)_{ad}$ adiabatic wall temperature for an assumed temperature recovery factor of 0.88, $T_\infty(1 + 0.176M_\infty^2)$
- $(T_w)_{meas}$ measured wall temperature
- T' reference temperature used by Sommer and Short,

$$T_\infty \left[1 + 0.035M_\infty^2 + 0.45 \left(\frac{T_w}{T_\infty} - 1 \right) \right]$$
- T_∞ free-stream static temperature, $\frac{T_t}{1 + 0.2M_\infty^2}$
- t ratio of inside-to-outside diameter of Preston tube
- u local velocity within the boundary layer
- u_τ friction velocity based on the wall temperature, $\sqrt{\frac{\tau}{\rho_w}}$
- u_τ' friction velocity based on the Sommer and Short T' temperature,

$$\sqrt{\frac{\tau}{\rho'}}$$
- V_S velocity indicated by the ratio of the Preston or Stanton tube pressure to the wall static pressure, assuming isoenergetic flow conditions and a normal shock relationship, $(49\sqrt{T_S})M_S$
- V_∞ free-stream velocity, $(49\sqrt{T_\infty})M_\infty$
- X_H function used in the generalization of Wilson's theory,

$$\frac{(T_w/T_\infty)C_f}{[(\sin^{-1}\sqrt{\sigma_\infty})/\sqrt{\sigma_\infty}]^2}$$
- X_S function used in the generalization of Sommer and Short's method,

$$\left(\frac{T'}{T_\infty} \right) C_f$$
- x length from the leading edge or characteristic length used in forming Reynolds number
- x_V distance from the virtual origin of the turbulent boundary layer to the point at which θ is measured

$(Y_\theta)_H$	function used in the generalization of Wilson's theory, $\frac{\mu_\infty}{\mu_w} R_\theta$
$(Y_\theta)_S$	function used in the generalization of Sommer and Short's method, $\frac{\mu_\infty}{\mu'} R_\theta$
y	distance from surface
γ	ratio of specific heats (assumed herein to be 1.4 for air)
Δp	difference between the surface pitot pressure and the static pressure, $p_s - p_\infty$
δ_c	boundary-layer thickness for compressible flow, $\frac{C_F x}{2(\theta/\delta)_c}$
$\left(\frac{\delta^*}{\delta}\right)_i$	ratio of displacement thickness to boundary-layer thickness for an incompressible boundary layer (see eq. (C6))
θ	boundary-layer momentum thickness, $\frac{C_F x}{2}$
θ_c	momentum thickness for a compressible boundary layer
μ_w	viscosity from Sutherland's formula in which the wall temperature is used
μ'	viscosity from Sutherland's formula in which the T' temperature from Sommer and Short is used
μ_∞	viscosity from Sutherland's formula in which the free-stream static temperature is used
ν_w	kinematic viscosity based on wall temperature
ν'	kinematic viscosity based on Sommer and Short's reference temperature, T'
ν_∞	kinematic viscosity based on free-stream static temperature
ρ_w	mass density based on the wall temperature
ρ'	mass density based on the reference temperature (T') of Sommer and Short
ρ_∞	mass density based on the free-stream static temperature
σ_∞	factor used in the Wilson theory, $1 - \frac{T_\infty}{T_t}$ or $\frac{0.2M_\infty^2}{1 + 0.2M_\infty^2}$
τ	surface shear stress
ω	exponent (0.768) for the approximate viscosity formula

FACILITY

The experiment was conducted in air in the Ames 8- by 7-foot supersonic wind tunnel. This facility is a closed-circuit, continuous flow wind tunnel capable of producing a relatively constant Mach number ranging from 2.4 to 3.4 in the test section which is 16 feet long. The Mach number is varied by changing the wind-tunnel nozzle contour by moving the flexible vertical side walls. Reynolds number is varied by changing the stagnation pressure over a range of about 2 atmospheres.

TEST CONDITIONS

To provide changes in Reynolds number, the wind-tunnel total pressure was varied after the Mach number had been set at one of the following nominal Mach numbers: 2.4, 2.9, or 3.4. Unit Reynolds numbers covered in the investigation ranged from nominal values of 0.5 to 3.2 million per foot, inclusive. Four Preston tubes of different diameters and a Stanton tube were tested simultaneously for a given flow condition. For part of the investigation, two of the Preston tube diameters and the Stanton tube height were changed. Two different Stanton tube geometries were also tested by changing the position of the blade relative to the orifice over which the blade was mounted as shown in figure 1. Measured values of Mach number, Reynolds number, tube height, and streamwise Stanton tube positions are given in table I.

Flow conditions correspond to that for a turbulent boundary layer acting on a flat surface with nearly zero pressure gradient and nearly adiabatic wall conditions (no heat transfer). Table I gives the measured wall temperatures and the estimated adiabatic wall temperatures. The boundary layer was from 5 to 7 inches thick, depending on the flow conditions. Location of the origin of the turbulent boundary layer was unknown; however, the nozzle throat of the wind tunnel was about 32 feet upstream of the measuring station. Impact-probe traverses were made only at unit Reynolds numbers of 1.0, 2.5, and 3.2 million per foot to reduce the running time of the wind tunnel.

INSTRUMENTATION

General Arrangement

Figure 2 shows the relative locations of the boundary-layer instrumentation used in the experiment: the skin-friction balance, the Preston tubes, a Stanton tube, the traversing probe, and the 5-inch boundary-layer rake. The probes and balance were mounted on the wind-tunnel side wall. In addition to the reference orifice shown in figure 2, three static-pressure orifices were located 6 inches ahead of the reference orifice, the Stanton tube, and the rake.

Skin-Friction Balance

The skin-friction balance was designed mechanically and electrically by the Ames Instrumentation Division. A complete description of the balance is given in reference 4. The balance had a floating element 2 inches in diameter attached to flexure pivots. An electrical nulling circuit centered the floating element in the hole for each measurement. A special low-friction pulley was used to calibrate the balance in the operating position. Before and after the test, several calibrations were made at 40°, 70°, and 100° Fahrenheit. During the test the approximate temperature of the balance was indicated by a thermocouple inserted in the cavity of the balance.

The floating-element disk had an edge tapered to 0.025 inch to minimize the possible buoyancy effect from the gap pressures. A buoyancy force correction was obtained by integrating the measured pressures in the gap at six stations spaced equally around the disk as shown in reference 4.

Stanton Tube

Geometric details of the Stanton tube are shown in figure 1. The Stanton tube used in the present experiment consisted of a sharp blade mounted over a static-pressure orifice. The blade was tested in two different streamwise positions as well as at two different vertical heights in each position, since Dr. K. G. Winter had suggested in a private communication that streamwise position might affect the calibration.

Preston Tubes

The Preston tubes consisted of circular impact-pressure tubes similar to those suggested and used by Preston (ref. 25) as indirect sensors of skin friction. These tubes were mounted as shown in figure 1 so that the tube leading edge rested firmly on the surface of the tunnel wall. The ratio of inside-to-outside diameters was held to 0.60 as in Preston's experiment. Tube diameters of 0.061, 0.090, 0.126, and 0.188 inch were tested first, followed by tube diameters of 0.031, 0.090, 0.126, and 0.250 inch in the locations shown in figure 2.

Traversing Impact-Pressure Probe

A traversing impact-pressure probe was used in this investigation to define in detail the boundary-layer profile at selected Reynolds numbers for the purpose of obtaining the momentum thickness. Figure 3 shows the geometry of the traversing probe, which was designed to minimize the flow disturbance from the tip and the deflection under load. The tip was carefully constructed to be free of burrs and imperfections. The probe was moved perpendicular to the wall by means of a screw device to which a height gage with a vernier was attached for measuring the probe height accurately.

Boundary-Layer Rake

A boundary-layer rake was used in place of the traversing probe to obtain the momentum thickness at some Reynolds numbers, to reduce the running time necessary for a survey with the traversing probe. The geometry of the rake is shown in figure 4.

Pressure Sensors

Precision mercury manometers were used to measure reference pressure, calibration pressure, and impact pressure outside of the boundary layer ($p_{i,\infty}$). The manometers were mounted in temperature controlled cabinets.

The test pressures were measured by Ames designed precision electrical strain-gage type transducers, referred to as slack-diaphragm pressure cells, mounted in a temperature controlled cabinet. The cells were used to measure the differential between the test pressure and a reference pressure. The reference pressure was set so that the lowest range cells available of ± 4 psid could be utilized. Each cell was individually check-calibrated over its range in the laboratory and selected to meet the tolerances described in the section, Data Reduction and Accuracy. The length of the tubes was minimized to eliminate pressure lag. Sufficient time was allowed for the pressures to stabilize before each data point was taken.

Temperature Sensors

Total temperature probes were located in the low-speed leg of the wind tunnel upstream of the throat section. The thermocouple probes were connected to a hot-box junction of the data recording system, and were calibrated with a laboratory reference thermocouple in crushed ice. The approximate static wall temperature was monitored by a thermocouple inserted into a hole in the wall drilled to within 1/4 inch of the inside surface, and connected to a hot-box junction.

DATA REDUCTION AND ACCURACY

Boundary-Layer-Edge Conditions

Mach number,¹ Reynolds number, total pressure, dynamic pressure, and static temperature at the boundary-layer edge were calculated from the measured impact pressure outside the boundary layer, the wall static pressure, and the tunnel total temperature. The compressible-flow relations in

¹The following approximation to the Rayleigh pitot equation (derived by N. K. Delany of Ames Research Center) was used to compute the Mach number, M_∞ . The expression gives Mach number to within 0.0005 for $1.08 < M_\infty < 4.11$.

$$M_\infty = \{0.88185 - 0.2147(p_\infty/p_{i,\infty}) - 0.2478[(p_\infty/p_{i,\infty}) + 0.06]^{3.44}\} (p_\infty/p_{i,\infty})^{-1/2}$$

reference 37 were used in the calculations. The edge, or free-stream impact, pressure was measured at a height of 8.50 inches by an impact probe on a boundary-layer rake. This pressure was taken to be the edge impact pressure for all of the measurements in the experiment because previous tunnel surveys showed that nearly uniform flow existed across the test area. In addition, this impact pressure was compared to that of the traversing probe at the same height and found to agree generally within 0.5 percent. The wall static pressure measured at the location shown in figure 2 was assumed to be constant through the boundary layer. The static pressures at the three other orifice locations mentioned in the discussion of Instrumentation agreed to within 0.5 psf of the reference wall static pressure.

Momentum Thickness

The momentum thickness, θ , of the boundary layer was obtained from the velocity profile determined with the traversing impact probe for unit Reynolds numbers of 1.0, 2.5, and 3.2 million per foot. Boundary-layer rake profiles were used to determine θ at the other Reynolds numbers. In the calculation of the local velocity ratio, the flow was assumed to be isoenergetic (constant total temperature) and the static pressure to be constant through the boundary layer; reference 38 shows that these assumptions result in negligible errors in momentum thickness for adiabatic flow at supersonic speeds. An interference effect from the traversing probe, negligible except near the wall, should not affect θ noticeably. A comparison of the momentum thickness obtained from the rake with that obtained from the traversing probe showed that the difference in momentum thickness was in fact negligible.

Skin Friction

The estimated probable error of the floating-element skin-friction balance is a function of Mach and Reynolds number and is listed in the following table for the nominal test conditions. Total errors were estimated to be the root-sum-square (RSS) of four individual estimated errors - the RSS having been used as representative of a combination of individual random errors. Calibration error was estimated to be ± 2 percent from several repeated calibrations, before and after the test, in the laboratory with the balance in the same position as mounted in the tunnel side wall. The balance temperature error was estimated to be less than ± 1 percent. The estimated probable error was ± 0.7 psf for the gap differential pressures used in the buoyancy correction, and the probable error in fairing the pressure distribution in the gap could be as high as 100 percent for the six orifices or about ± 2 percent. Resulting RSS values and also the apparent error in the data, as indicated by the scatter in repeated points, are as follows:

Estimated and Apparent Error of Skin-Friction Balance, Percent

$(V_\infty/v_\infty)10^{-6}$ per ft	M = 2.4		M = 2.9		M = 3.4	
	RSS	Data	RSS	Data	RSS	Data
3.2	±3.1	---	±3.2	---	---	---
3.0	---	---	3.2	---	---	---
2.5	3.2	±2.0	3.3	±2.2	±3.6	±1.2 ^a
2.0	3.3	2.6	3.5	4.9	4.0	---
1.5	3.5	3.4	3.9	6.1	4.6	---
1.0	4.1	---	4.8	6.3	6.2	6.1 ^a
0.5	---	---	---	---	12	---

^aLimited data.

Note that the data scatter from the test was approximately of the same magnitude as the estimated probable error. In general, the effect of the wall temperature not being exactly adiabatic was estimated to change the skin friction less than 1 percent and therefore was ignored. Values of both the estimated adiabatic and measured wall temperatures are listed in table I.

Pressures

Estimated probable errors of the pressures were determined to be the RSS of the following individual errors: reference pressure from precision manometer, ±0.28 psf; differential pressure from slack-diaphragm transducers, ±0.05 percent of 4 psi, or ±0.29 psf; zero shift of transducers during test, ±0.3 psf. The RSS value for these errors is ±0.5 psf.

Geometric Measurements

The traversing-impact probe error in height was a total of about 0.003 inch; the maximum play in the mechanism was about ±0.002 inch at the probe tip; and the reading error from the height gage with vernier was ±0.001 inch. The diameter of the Preston tubes and the height of the Stanton tubes were measured to within ±0.0005 inch. The height of boundary-layer rakes was measured to within ±0.005 inch.

DEVELOPMENT OF NEW CALIBRATION FACTORS

Equivalent Incompressible Pressure Coefficient, C_p

Appendix B gives a functional equation similar to that used by Smith, Gaudet and Winter (ref. 23) for calibrating surface pitot tubes. Results from the present investigation and reference 23 indicated that equation (B6) still contains a compressibility effect since this equation did not collapse the calibration curves obtained at supersonic Mach numbers onto the calibration

curves obtained at low subsonic Mach numbers. The development of equation (B6) for compressible boundary layers indicates that the pressure coefficient (C_p) was left in its compressible form. The equivalent incompressible C_p is obtained by replacing the measured pressure rise for the surface tube with an incompressible pressure rise which is indicated by the dynamic pressure of the tube ($(\gamma/2)\rho_\infty M_S^2$). The equivalent incompressible pressure coefficient, therefore, becomes

$$C_{pi} = \frac{q_s}{q_\infty} = \frac{(\gamma/2)\rho_\infty M_S^2}{(\gamma/2)\rho_\infty M_\infty^2} \quad \text{or} \quad C_{pi} = \left(\frac{M_S}{M_\infty}\right)^2 \quad (1)$$

since the static pressure is assumed to be constant through the boundary layer. By substituting the incompressible form of C_p given by equation (1) in equation (B6) for C_p , we obtain another functional equation

$$f_2(T_w)R_d^2(M_S/M_\infty)^2 = f_k[f_2(T_w)R_d^2C_f] \quad (2)$$

Reference Temperature Conditions

Although several investigators have shown that the compressible law of the wall equation, in which the fluid properties are based on wall temperature in general, collapses boundary-layer profiles onto a single curve, Coles in reference 30 shows that if the fluid properties are based on a reference temperature, then even better collapsibility is obtained for turbulent boundary-layer profiles for Mach numbers of 2.6 through 4.5. Following the work of Coles a more generalized law of the wall may be written as

$$\frac{u}{u_\tau'} = f_h \left(\frac{yu_\tau'}{v'} \right) \quad (3)$$

where the primed quantities are based on a reference temperature which is a function of Mach number; for example, $u_\tau' = \sqrt{\tau/\rho'}$. It follows that for calibrating surface tubes a functional equation similar to equation (2) can be written if the wall temperature is replaced by a reference temperature² as

$$f_2(T')R_d^2(M_S/M_\infty)^2 = F_h[f_2(T')R_d^2C_f] \quad (4)$$

where for the Sommer and Short reference temperature method and by Sutherland's formula for viscosity following the definition of $f_2(\)$ in the notation

$$f_2(T') = \left(\frac{\mu_\infty}{\mu'}\right)^2 \frac{\rho'}{\rho_\infty} \quad (5a)$$

When specialized for adiabatic wall conditions in air in which $T' = T_\infty(1 + 0.1142M_\infty^2)$, equation (5a) becomes

²During the final preparation of this report, Sigalla (ref. 39) presented a reference temperature equation similar to equation (4) for calibrating surface pitots, except he replaced Δp in C_p with $(1/2)\rho'V_S^2$ instead of $(1/2)\rho_S V_S^2$ or $\Delta p = (\gamma/2)\rho_\infty M_S^2$ as the author's did herein.

$$f_2(T') = \left(\frac{T' + 198.6}{T_\infty + 198.6} \right)^2 \left(\frac{1}{1 + 0.1142M_\infty^2} \right)^4 \quad (5b)$$

COMPRESSIBILITY AND HEAT-TRANSFER EFFECTS
ON THE PRESTON TUBE CALIBRATIONS

Although it will be shown that the calibration factors based on the reference temperature (T') given by Sommer and Short (eq. (4)) completely collapse the supersonic Preston tube data onto the Preston incompressible curve, in some cases it may be desirable to base the calibration factors on wall conditions that can be easily measured.³ In the development that follows, the estimated effects of compressibility and heat transfer on the calibration curve thus based will be indicated.

Sharp Leading Edge

If equation (4) is rewritten in its expanded form containing the equivalent equation for Mach number squared,

$$\left(\frac{M_S}{M_\infty} \right)^2 = \frac{(\gamma/2)(\rho'RT')M_S^2}{(1/2)\rho_\infty V_\infty^2} \quad (6)$$

then, assuming $\gamma = 1.4$ for air, we obtain

$$\left(\frac{\rho'V_\infty d}{\mu'} \right)^2 \frac{M_S^2(1.4RT')}{V_\infty^2} = F_h \left[\left(\frac{\rho'V_\infty d}{\mu'} \right)^2 \frac{\tau}{(1/2)\rho'V_\infty^2} \right] \quad (7)$$

Equation (7) can be simplified to

$$1.4RM_S^2 \left[\left(\frac{1}{\nu'} \right)^2 T' \right] d^2 = F_h \left\{ (2\tau d^2) \left[\frac{1}{\rho'(\nu')^2} \right] \right\} \quad (8)$$

If the flow properties are assumed to be based on wall temperature, then equation (8) can be written as

$$1.4RM_S^2 \left[\left(\frac{1}{\nu_w} \right)^2 T_w \right] d^2 \frac{1}{F_w} = F_h \left\{ (2\tau d^2) \left[\frac{1}{\rho_w(\nu_w)^2} \right] \frac{1}{F_w} \right\} \quad (9)$$

³For example, the boundary-layer-edge conditions may be unobtainable as is the case at hypersonic Mach numbers where the boundary-layer edge may be obscured by the thick entropy layer induced by leading-edge bluntness.

where if the equation of state is used

$$F_W = \left(\frac{\nu'}{\nu_W}\right)^2 \frac{T_W}{T'} = \left(\frac{\nu'}{\nu_W}\right)^2 \frac{\rho'}{\rho_W} = \left(\frac{\mu'}{\mu_W}\right)^2 \frac{T'}{T_W} \quad (10)$$

If the approximate viscosity equation (B12) is used with T_∞ replaced by T' , equation (10) becomes

$$F_W = \left(\frac{T'}{T_W}\right)^{1.536} \times \frac{T'}{T_W} = \left(\frac{T'}{T_W}\right)^{2.536} \quad (11)$$

It should be emphasized that the factor F_W can be calculated only if the local Mach number at the boundary-layer edge is known. In the discussion to be presented hereinafter the effect on the calibration of assuming that this Mach number is unknown and that the flow quantities are based on a known T_W (or $F_W = 1.0$ in eq. (9)) will be shown. The F_W factor in equation (9) can be considered dependent on Mach number and/or heat transfer through the following equation from reference 36 for the reference temperature ratio

$$\frac{T'}{T_W} = \frac{1 + 0.035M_\infty^2 + 0.45[(T_W/T_\infty) - 1]}{T_W/T_\infty} \quad (12)$$

in which T_W/T_∞ is defined for a turbulent boundary layer by the adiabatic recovery temperature equation (using a temperature recovery factor of 0.88)

$$\frac{T_W}{T_\infty} = \frac{T_W}{(T_W)_{ad}} (1 + 0.176M_\infty^2) \quad (13)$$

It follows that the effects of Mach number and heat-transfer variations on the Preston calibration curve when flow properties are based on wall conditions can be evaluated by multiplying the F_W factor for a particular flow condition times the calibration factors given by equation (4).

Blunt Leading Edge

Provided the leading edge is sufficiently blunt that the full bluntness effect is realized (see refs. 40 and 41), then the reduced local Mach number instead of the free-stream Mach number should be substituted in equations (12) and (13). This reduced Mach number can be computed by the following equation which is given in reference 41 (eq. (A7)):

$$M_l = \left[(6M_\infty^2) \left(\frac{6}{7M_\infty^2 - 1} \right)^{5/7} - 5 \right]^{1/2} \quad (14)$$

Again, the effects of bluntness, Mach number, and heat-transfer variations on the Preston tube calibration, when the flow properties are based on wall conditions, can be evaluated from the effects of these properties on the F_w factor (eq. (11)).

RESULTS AND DISCUSSION

Skin-friction equations for the theory of Wilson and of Sommer and Short, which will be used throughout this report, are presented in appendix A. Some of the surface tube calibration factors which were used in the past are presented in appendix B. Equations for obtaining the maximum and minimum critical Preston tube diameters are given in appendix C. Equations used for deriving C_f from measured values of θ as a function of longitudinal distance, when skin friction in other investigations was not measured directly, are given in appendix D.

Preston Tube Calibrations

Calibration curves for Preston tubes obtained at subsonic speeds in other investigations are presented⁴ in figure 5. Complete calibration curves are presented in figures 6, 7, 8, and 9 on the basis of the functions contained in each of the four calibration functional equations (eqs. (B6), (2), (4), and (B11)), respectively. The linear portions of the present data (approximately $f_2(\pi')R_d^2C_f \geq 10^4$) are replotted with the Mach number and unit Reynolds number identified in figures 10 and 11 for two of the calibration factors. The solid line on figures 10 and 11 represents a least-squares fit of all the present data for a particular calibration factor within the linear portion of the calibration curve. The least-squares-fit equations for the linear part of all the calibration curves are given, respectively, on each figure. All data presented in figures 5 through 11 are also listed in tables I and II.

Subsonic $R_d^2C_p$ vs. $R_d^2C_f$.-- In figure 5(a) the incompressible Preston tube curve of Preston or Hsu is compared with the Coles' functional data curve. The latter curve represents an average of several experimental data curves obtained from boundary-layer surveys and includes no displacement effect due to tube size. The difference in these two curves can be considered, therefore, as being produced by the displacement effect of the Preston tube. Both of these curves given in figure 5(a) will be presented on each Preston tube calibration curve to help evaluate the various calibration factors. Smith and Walker's Preston tube curve (fig. 5(b)) lies below Coles' functional curve, thereby showing an opposite displacement effect from that of Preston. Head and Rechenberg's calibration curve (fig. 5(c)) agrees with Preston's curve at

⁴Calibration results presented herein are plotted on log-log paper for reasons set forth by Preston (ref. 25). Preston found that it was indecisive whether a "log" law or a "power" law best represented the law of the wall equation from which his calibration factors were developed. For circular pitots he favored the "power" law.

$R_d^2 C_p \cong 10^6$ and with Smith and Walker's curve at $R_d^2 C_p \cong 10^8$ and shows a slightly different slope from all the other calibration curves.

Supersonic $f_2(T_w)R_d^2 C_p$ vs. $f_2(T_w)R_d^2 C_f$.- In figure 6, it can be seen that the experimental results are considerably above the Preston curve; therefore, basing the flow properties on wall temperature alone is insufficient to collapse the experimental data onto the Preston incompressible curve. The Coles' curve is shown for reference purposes only, representing the incompressible case for zero displacement effect.

Supersonic $f_2(T_w)R_d^2 (M_s/M_\infty)^2$ vs. $f_2(T_w)R_d^2 C_f$.- If for a compressible fluid, the measured pressure coefficient C_p contained in the calibration factor used in figure 6 is replaced by the equivalent incompressible form $C_{p_i} = (M_s/M_\infty)^2$, then the experimental data obtained at supersonic Mach numbers move considerably closer to but still slightly above the Preston incompressible curve as shown in figure 7.

Supersonic $f_2(T')R_d^2 (M_s/M_\infty)^2$ vs. $f_2(T')R_d^2 C_f$.- If the flow properties are based on the reference temperature (T') given by Sommer and Short (ref. 36), the function $f_2(T_w)$ becomes $f_2(T')$ and the experimental results based on this new function are very close to the Preston incompressible curve as shown in figure 8(a). It can also be observed in figure 8(a) that even in the nonlinear portion of the curve this new function seems to collapse the data, although fewer points were measured over this nonlinear range. Above a value of $[f_2(T')R_d^2]C_f$ of about 10^4 the experimental points fall nearly on a straight line, the same result as for the incompressible Preston calibration. Since the supersonic data are so close to the Preston incompressible curve, it can be reasoned that the displacement effects from the Preston tubes are almost the same at subsonic and supersonic Mach numbers when the data are based on the new calibration factors. This displacement effect can be thought of as accounting for the difference between the Coles' functional values (ref. 30) and the incompressible experimental curve of Preston (ref. 25).

The supersonic Preston tube data of Stalmach (ref. 6) have been recomputed on the basis of the new T' calibration factor given above with the viscosity computed by the Sutherland formula (see eqs. (B13) and (B14)) and are presented in figure 8(b). It can be seen that these data also fall near the linear part of the Preston incompressible curve and therefore agree with the present results for this part of the curve. Compare figures 8(a) and 8(b). Within the nonlinear part of the calibration curves, the Stalmach data fall below the Preston curve and near the Coles' functional curve, thereby indicating zero displacement effect. Until the nonlinear part of the curve is substantiated by other experiments, it is suggested that Preston tube diameters be chosen so that only the linear part of the calibration curve is used.

Supersonic $[f_1(T_w)(R_d/\sqrt{\sigma_\infty})\sin^{-1}(\sqrt{\sigma_\infty} V_s/V_\infty)]^2$ vs. $f_2(T_w)R_d^2 C_f$.- If the present experimental data are based on the Fenter-Stalmach calibration factors, then the points fall somewhat above the nonlinear part of the Preston curve then cross somewhat below the linear part of the Preston curve as shown

in figure 9(a). The slope of the linear part of the supersonic curve is slightly less than either of the incompressible curves in figure 9(a).

In figure 9(b), Stalmach's Preston tube data, corrected for viscosity being based on the Sutherland formula, fall nearly on the Coles' functional curve at values of $f_2(T_w)R_d^2C_f$ greater than about 10^4 , thereby indicating zero displacement effect. At the smaller values of this function the Stalmach data fall between the Preston and the Coles' functional curves.

Detailed analysis of the linear part of the Preston tube calibration.- In figures 6 through 9 no attempt was made to identify each data point for a specific Mach number or unit Reynolds number, since only a general evaluation of the four different calibration factors was made. A further analysis was made, therefore, within the linear portions of two of the calibration curves for the new calibration factors based on reference temperature and the Fenter-Stalmach calibration factors by identifying the Mach number and unit Reynolds numbers, the results being presented in figures 10 and 11, respectively. The solid curves represent a least-squares fit of all the experimental data within the linear range for a given calibration factor. It can be seen in figures 10 and 11 that variation in neither Mach number nor Reynolds number had any consistent effect on the calibration curves and that any small displacement of the data from this least-squares curve was within the experimental accuracy.

The present data presented on the basis of the new calibration factors based on reference temperature fall very close to the Preston incompressible curve but the same data presented on the basis of the Fenter-Stalmach calibration factor fall on a curve with a somewhat lesser slope than the Preston incompressible curve. Compare figures 10 and 11.

Selection of Critical Preston Tube Diameters

Maximum tube diameter.- In reference 6 an equation is given for computing the maximum diameter of Preston tubes for which a single calibration curve would be expected to be valid. A modified version of the equation is given herein as equation (C7). This equation is represented in figure 12 from which it is possible to select the maximum tube diameter for a given Reynolds number and Mach number. An example for using figure 12 is given below.

Assumed flow conditions:

1. $M_\infty = 3.0$
2. $V_\infty/\nu_\infty = 10^5/\text{in.}$
3. $x = 10^3$ in. (Therefore, $R_x = 10^8$.)
4. $T_t = 560^\circ$ R and adiabatic wall

For the above flow conditions $(d_{cr}/x)_{max} = 3.9 \times 10^{-3}$ from figure 12. Therefore, the maximum critical diameter becomes

$$(d_{cr})_{max} = (d_{cr}/x)_{max}(x) = (3.9 \times 10^{-3})(10^3) = 3.9 \text{ in.}$$

Minimum critical size.— The curves for selecting the minimum critical Preston tube diameter, presented in figure 13, are based on the findings herein that the calibration is linear above a value of $f_2(T')R_d^2C_f = 10^4$ and that the data within the linear part of the calibration generally agreed with previous experimental results (ref. 6). See equation (C9).

An example for using figure 13 is given below.

Assumed flow conditions:

1. $M_\infty = 3.0$
2. $V_\infty/v_\infty = 10^5/\text{in.}$
3. $x = 10^3 \text{ in.}$ (Therefore, $R_x = 10^8$.)
4. $T_t = 560^\circ \text{ R}$ and adiabatic wall

For the above flow conditions, $(d_{cr}/x)_{min} = 7.5 \times 10^{-5}$ from figure 13. Therefore, the minimum critical diameter becomes

$$(d_{cr})_{min} = (7.5 \times 10^{-5})(10^3) = 0.075 \text{ in.}$$

It can be seen, then, that any Preston tube between 0.075 and 3.9 inches for the above assumed flow conditions would be a valid tube size for remaining within a single linear calibration curve.

Estimated Effects of Mach Number and Heat Transfer on the Preston Tube Calibration

Sharp leading edge.— It was shown in the equation development section that if the flow properties in the calibration factors are based on wall conditions instead of the reference temperature conditions⁵ of Sommer and Short, the effect of Mach number and heat transfer is given by F_W (eq. (11)). This effect has been calculated for a sharp-edged flat plate at Mach numbers of 3, 5, and 7 for several heat-transfer rates and is shown in figure 14.

It can be seen in figure 14 that for the adiabatic wall case ($T_w/(T_w)_{ad} = 1.0$) with the flow conditions based on wall temperature, that the skin friction given by the Preston curve would differ less than 10 percent from the true value. With heat transfer and the temperature ratio ($T_w/(T_w)_{ad}$)

⁵Provided the flow conditions at the edge of the boundary layer can be defined, then it is assumed that a calibration based on $f_2(T')R_d^2(M_S/M_\infty)^2 = F_h[f_2(T')R_d^2C_f]$ will not be affected by changes in either Mach number or heat transfer.

of 0.6, the Preston curve for Mach numbers from 3 through 7 would give the skin friction to within about 5 percent of the true value. For very low values of $T_w/(T_w)_{ad}$ (e.g., 0.2 as shown), larger errors in skin friction would be incurred if the Preston incompressible curve were used, particularly at the lower Mach numbers.

Blunt leading edge.- When leading-edge bluntness is incorporated in the design of a hypersonic vehicle, an inviscid entropy layer is formed having a vertical gradient of reduced Mach number near the leading edge which persists on the surface in the streamwise direction until the boundary layer becomes thick enough to envelop the entropy layer. If this entropy gradient is comingled with a vertical gradient of static pressure emanating from a curved surface, it becomes virtually impossible to define even by measurement the flow conditions at the boundary-layer edge. For this reason, the effects of Mach number and heat transfer on the Preston tube calibration curve (based on measurable wall conditions and the Preston tube Mach number) were estimated for a surface having full leading-edge bluntness effects.⁶

For the adiabatic wall case, it can be seen by comparing figures 14 and 15 that accounting for full leading-edge bluntness slightly reduced the error in predicting the skin friction from the Preston curve for Mach numbers from 3 through 7. For the intermediate value of heat transfer represented by $T_w/(T_w)_{ad} = 0.6$, the Preston curve happens to give the correct values of skin friction when bluntness is included as shown in figure 15. If heat transfer is large (e.g., $T_w/(T_w)_{ad} = 0.2$), then the error involved by using wall conditions was predicted to be even greater for the blunt edge than for the sharp edge, but for either case the error was, in general, so large as to be nonacceptable.

Stanton Tube Calibrations

It should be mentioned again that the Stanton tube in the present investigation was calibrated in two different streamwise positions relative to the static orifice over which it was mounted as shown in figure 1. The position called the rearward position with the leading edge of the blade coincident with the leading edge of the orifice corresponds closest to the configurations investigated by Bradshaw and Gregory and by Winter.

$f_2(T_w)R_d^2 C_p$ vs. $f_2(T_w)R_d^2 C_f$.- It can be seen in figure 16 that the position of the blade relative to the orifice had a large effect on the calibration curve and that basing the calibration factors on wall conditions and the Stanton tube pressure coefficient did not collapse the data onto either of the experimental incompressible curves. The supersonic curve of Winter falls closest to the data from the present investigation with the blade in the rearward position as would be expected from geometrical considerations.

⁶Full leading-edge bluntness effect on Mach number was computed by equation (14) following the bluntness theory set forth in reference 40.

$f_2(T_W)R_d^2(M_S/M_\infty)^2$ vs. $f_2(T_W)R_d^2C_f$.-- In figure 17, the Stanton tube data are presented with the pressure coefficient replaced by its equivalent incompressible form, $C_{p_i} = (M_S/M_\infty)^2$ (see eq. (2)). By comparing figure 17 with figure 16, we can see that this calibration factor, containing $(M_S/M_\infty)^2$, shifts the measured supersonic data closer to the incompressible curves at the low values of $f_2(T_W)R_d^2C_f$ but somewhat below Bradshaw and Gregory's curve at the high values of this calibration factor. Again, the comparison with the incompressible curves should be only for the present data with the blade in the rearward position.

$f_2(T')R_d^2(M_S/M_\infty)^2$ vs. $f_2(T')R_d^2C_f$.-- When, in addition to replacing C_p with its equivalent incompressible form $C_{p_i} = (M_S/M_\infty)^2$, the flow properties are based on the Sommer and Short reference temperature (T'), the data in figure 18 for the blade in the rearward position fall, in general, between the two incompressible curves at low values of $f_2(T')R_d^2C_f$. At high values of this calibration factor, the use of T' in place of T_W tended to rotate the curves slightly so that slopes of the present data curves agree more closely with the incompressible curve of Bradshaw and Gregory. Compare figure 18 with figure 17.

$[f_1(T_W)(R_d/\sqrt{\sigma_\infty})\sin^{-1}(\sqrt{\sigma_\infty} V_S/V_\infty)]^2$ vs. $f_2(T_W)R_d^2C_f$.-- With the data presented on the basis of the Fenter-Stalmach calibration factors (ref. 27), it can be seen in figure 19 that the data fall closer to the Bradshaw and Gregory incompressible curve but have somewhat less slope than this curve.

The present Stanton tube data, based on any of the four calibration factors (figs. 16 through 19), indicate that the blade position relative to the orifice, over which it is mounted, has a large effect on the calibration curves. Also, all of the calibration curves are nonlinear, even at the higher coordinates where the Preston tubes had linear curves. For these reasons, especially since it may be difficult to match exactly the geometry of a given Stanton tube, Preston tubes appear to be superior devices for making skin-friction measurements.

Local Skin Friction

The present experimental results obtained by direct measurement of skin friction are presented in figure 20. Local skin-friction data obtained in other investigations are presented in figure 21. In both figures, the data are presented on the basis of C_f vs. R_θ . The use of R_θ avoids having to establish the virtual origin of the turbulent boundary layer for each investigation. The majority of the skin-friction data presented in figure 21 were obtained by direct measurement of the skin friction; however, in a few cases it was necessary to derive the local skin friction from a differentiation of the momentum thickness with respect to streamwise distance (x). For the latter cases, the equations and differentiation performed are presented in appendix D. For each experimental case, theoretical curves are presented for the theories of Wilson (eq. (A1)) and Sommer and Short (eq. (A4)). All the skin friction results presented in figures 20 and 21 are also presented on a

generalized basis of the Sommer and Short theory (eq. (A5)) in figure 22 and of the Wilson theory (eq. (A2)) in figure 23. The relationship between R_θ and R_x as given by the Sommer and Short method for several different Mach numbers is given in figure 24. In figure 25, the variation in both the average skin-friction coefficient and the local skin-friction coefficient with Reynolds number is given for several different Mach numbers. Figures 24 and 25, which are based on the Sommer and Short method, can be used to convert the data presented in figures 20 and 21 to equivalent values of R_x and C_F .

Data From Present Investigation

The directly measured skin-friction data from the present investigation fall, in general, between the two theoretical curves at Mach numbers of 2.46 and 2.96 as shown in figure 20. At a Mach number of 3.45, the data fall closer to the Sommer and Short curve; however, the difference between the two theories at any of these Mach numbers is only about 10 percent.

Data From Past Investigations

It can be seen in figure 21(a) that the two theories give essentially the same curves at $M_\infty = 0.06$ (the incompressible case), and both curves agree well with the experimental results. In figure 21(n), at the highest Mach number investigated ($M_\infty = 6.7$ (ref. 9)), the Sommer and Short theoretical curve agrees well with the measured C_F and the Wilson curve is considerably above the measured C_F . At a slightly lower Mach number ($M_\infty = 5.8$), the data from Korkegi (ref. 11) lie on the Wilson theoretical curve and do not agree with the curve estimated by the Sommer and Short method. In general, at supersonic Mach numbers of 4.2 and less, and $R_\theta \cong 10^4$, the theory of Sommer and Short gave results which agreed somewhat better with the experimental results than did the values from the theory of Wilson (e.g., figs. 21(b) to 21(l)), but at the higher values of $R_\theta \geq 5 \times 10^4$ the reverse was true. (See the Moore-Harkness data in fig. 21(i).) At the higher Mach numbers ($M_\infty \geq 5.8$), where the results from the two theories differ the most, data are insufficient at all values of R_θ to draw definite conclusions regarding the adequacy of these theories.⁷

With the skin-friction data presented on a generalized basis (X_S vs. $(Y_\theta)_S$) from the Sommer and Short theory (eq. (A5)), it can again be seen in figure 22 that at values of $(Y_\theta)_S$ slightly less than 10^4 and Mach numbers ≤ 4.2 , this theory in general collapses the data onto the incompressible curve. At values of $(Y_\theta)_S \cong 3 \times 10^4$ and at Mach numbers close to 3.0 both the present results and the Moore-Harkness results are slightly above the theoretical curve (fig. 22(b)). As shown in figure 23(b), with the skin-friction data presented

⁷In a report by Peterson (ref. 50) in which the experimental skin friction is compared with values from seven different theories on the basis of equivalent length Reynolds numbers ($R_{x,v}$), it is concluded the Sommer and Short T' method provides the most accurate estimate of the available compressible turbulent skin friction, but that further verification is required at the higher Mach numbers (above $M = 6$) where data are scarce and the theories show their greatest differences.

on a generalized basis (X_H vs. $(Y_\theta)_H$) from the Wilson theory (eq. (A2)), at values of $(Y_\theta)_H > 2.4 \times 10^4$, the Moore-Harkness data fall onto the theoretical curve and the present data are slightly below this curve. At intermediate values of $(Y_\theta)_H \cong 5 \times 10^3$, the experimental values of X_H lie, in general, below the theoretical curve at supersonic Mach numbers of 4.2 and less as shown in figures 23. At the higher Mach numbers shown in figure 23(c) ($M \geq 5.8$) insufficient data are available to assess the two theories.

CONCLUSIONS

From an experimental investigation of surface pitot tubes for measuring local skin friction and from an analysis of existing local skin-friction data for turbulent boundary layers on adiabatic flat plates the following conclusions can be drawn.

1. It was shown that a Preston tube can be used for measuring local skin friction accurately, provided the new compressible calibration factors presented herein are employed and the tube size is selected so that only the linear part of the calibration curve is used. The present calibration curve agreed closely with that of StaImach only within the linear part of the calibration curve.
2. With the Preston tube data reduced on the basis of the new calibration factors which include an equivalent incompressible pressure coefficient and the flow properties based on the Sommer and Short reference temperature, the supersonic data obtained from Mach numbers 2.4 through 3.4 fall on the Preston incompressible calibration curve, even duplicating the nonlinear part of the curve.
3. It was estimated that if a moderate amount of heat transfer is encountered (wall temperature about 60 percent of the adiabatic wall temperature) and full leading-edge bluntness effects are realized, then the Preston tube calibration based on wall temperature and the Mach number indicated by the Preston tube would be almost identical with the Preston incompressible calibration. Knowledge of this result may be useful if the boundary-layer-edge conditions are not measurable. For much larger amounts of heat transfer, the estimates indicate that a calibration curve based on wall conditions does not fall close to the Preston incompressible curve.
4. The Stanton tube calibration was nonlinear and was greatly affected by the streamwise location of the tube leading edge relative to the static orifice over which it was mounted. For these reasons it is believed that a Preston tube, which is geometrically easier to duplicate than a Stanton tube, is a superior device for measuring local skin friction.
5. Experimental skin-friction data from the present investigation fell generally between the values predicted from the theory of Sommer and Short and that of Wilson at Mach numbers of 2.46 and 2.96 but tended to favor the predicted values from Sommer and Short at a Mach number of 3.45; however, values from these theories differ by only about 10 percent at these Mach numbers.

6. Turbulent skin-friction theories of Wilson and of Sommer and Short, in general, bracketed all the skin-friction data measured in past investigations. Insufficient skin-friction data were available at the higher Mach numbers where these theories differed by as much as 25 percent to assess the adequacy of the theories. At $R_\theta \cong 10^4$ the theory of Sommer and Short gave skin-friction values which agreed better with the experimental values than did the values from the theory of Wilson; however, at $R_\theta \geq 5 \times 10^4$, the opposite occurred.

Ames Research Center
National Aeronautics and Space Administration
Moffett Field, Calif., Dec. 21, 1965

APPENDIX A

SKIN-FRICTION EQUATIONS

In this report only two theories were chosen for analyzing the skin-friction data: the theory of Wilson (ref. 35) and the reference temperature method of Sommer and Short (ref. 36). Both the local and the average skin-friction coefficients will be given in terms of the Reynolds number based on the momentum thickness for each of these theories. Only the skin friction on a flat plate with a turbulent boundary layer, zero pressure gradient, and adiabatic wall conditions will be considered.

LOCAL SKIN FRICTION

Wilson's Theory

This theory is based on the assumption that Von Kármán's differential equation for the velocity distribution in the incompressible boundary layer applies for compressible flow when the variation in density through the boundary layer is taken into account (see ref. 35). In reference 8, Moore and Harkness give the skin-friction equation for this theory as

$$\left(\frac{\sin^{-1}\sqrt{\sigma_\infty}}{\sqrt{\sigma_\infty}}\right)^{-2} \left(\frac{T_w}{T_\infty}\right) C_f = \frac{1}{\left[4.15 \log_{10}\left(R_\theta \frac{\mu_\infty}{\mu_w}\right) + 2.78\right]^2} \quad (A1)$$

or on a generalized basis as

$$X_H = \frac{1}{\left[4.15 \log_{10}(Y_\theta)_H + 2.78\right]^2} \quad (A2)$$

in which the constant term 2.78 was evaluated from available incompressible experimental data by Moore and Harkness in a manner consistent with the rest of Wilson's analysis. For incompressible flow, equation (A1) can be simplified to

$$C_f = \frac{1}{\left[4.15 \log_{10} R_\theta + 2.78\right]^2} \quad (A3)$$

Sommer and Short's Reference Temperature Method

In this method the fluid properties such as density and viscosity are assumed to be based on a reference temperature (T'), the equation for which was empirically derived in reference 36. Because of the good agreement between the experimental and the Von Kármán-Schoenherr theoretical values of average skin friction for incompressible flow over a wide range of Reynolds numbers (from about 5×10^5 to 5×10^8) shown in references 4 and 51, this incompressible theory was chosen for applying the Sommer and Short reference enthalpy properties for compressible flow. The complete compressible equation for local skin friction in terms of Reynolds number based on momentum thickness and the Von Kármán-Schoenherr incompressible equation can be derived from equations (10) and (11) of reference 52 as

$$\left(\frac{T'}{T_\infty}\right) C_f = \frac{1}{17.076 \left[\log_{10} \left(R_\theta \frac{\mu_\infty}{\mu'} \right) \right]^2 + 25.112 \log_{10} \left(R_\theta \frac{\mu_\infty}{\mu'} \right) + 6.012} \quad (A4)$$

or on a generalized basis as

$$X_s = \frac{1}{17.076 [\log_{10}(Y_\theta)_s]^2 + 25.112 \log_{10}(Y_\theta)_s + 6.012} \quad (A5)$$

For incompressible flow, equation (A4) can be simplified to

$$C_f = \frac{1}{17.076 (\log_{10} R_\theta)^2 + 25.112 \log_{10} R_\theta + 6.012} \quad (A6)$$

AVERAGE SKIN FRICTION

Wilson's Theory

From equations (58) and (60) of reference 28, and since

$$R_X C_F = 2R_\theta \quad (A7)$$

Wilson's equation for average skin friction can be written as

$$C_F = \left[\frac{0.242 \sin^{-1} \sqrt{\sigma_\infty}}{\sqrt{\sigma_\infty} \log_{10} \left(2R_\theta \frac{\mu_\infty}{\mu_w} \right)} \right]^2 \left(\frac{T_\infty}{T_w} \right) \quad (A8)$$

Sommer and Short's Reference Temperature Method

An equation, similar in form to equation (A8), can be written for the Sommer and Short theory from the Von Kármán-Schoenherr incompressible equation (eq. (10) of ref. 52) as

$$C_F = \left[\frac{0.242}{\log_{10} \left(2R_\theta \frac{\mu_\infty}{\mu'} \right)} \right]^2 \left(\frac{T_\infty}{T'} \right) \quad (A9)$$

APPENDIX B

SURFACE PITOT-TUBE CALIBRATION FACTORS USED IN THE PAST

$$\underline{f_2(T_w)R_d^2 C_p \text{ vs. } f_2(T_w)R_d^2 C_f}$$

Correlation factors which relate wall shear stress to the surface pitot-tube pressure have been developed in the past from the "law of the wall." For incompressible flow, it was shown in reference 53 that a universal relationship exists for the part of the velocity profile near the wall (commonly known as the law of the wall) that can be expressed as a function of wall shear stress by

$$\frac{u}{u_\tau} = f\left(\frac{u_\tau y}{\nu_\infty}\right) \quad (B1)$$

In reference 25, Preston shows that the calibration factor from a dynamical similarity analysis for surface pitots when assuming the universality of the law of the wall (e.g., eq. (B1)) is

$$\frac{\Delta p d^2}{4\rho_\infty \nu_\infty^2} = f_p \left(\frac{\tau d^2}{4\rho_\infty \nu_\infty^2} \right) \quad (B2)$$

In the development of equation (B2) it is assumed that Δp (the difference between the pitot pressure and the static pressure) acts at $y = d/2$; therefore, no displacement effects due to the tube are assumed. For compressible flow, several authors have used a compressible form of equation (B2) in which the fluid properties (ρ_∞ and ν_∞) are based on wall temperature in place of free-stream temperature. Following the development of equation (B2) from (B1), a similar equation can be written for compressible flow

$$\frac{\Delta p d^2}{4\rho_w \nu_w^2} = F_p \left(\frac{\tau d^2}{4\rho_w \nu_w^2} \right) \quad (B3)$$

where u_τ in equation (B1) is now defined by $\tau = \rho_w u_\tau^2$. Equation (B3) without the factor 4 has been used by several investigators as the functional equation for calibrating surface pitots at supersonic Mach numbers (e.g., see refs. 21 and 22). Another useful form of equation (B3), particularly for wind-tunnel tests, is obtained when this equation is written in terms of pressure coefficients, Reynolds number, and skin-friction coefficient

$$\frac{\Delta p d^2}{4\rho_w \nu_w^2} = \frac{1}{8} \left(\frac{\nu_\infty}{\nu_w} \right)^2 \left(\frac{\rho_\infty}{\rho_w} \right) \left(\frac{V_\infty d}{\nu_\infty} \right)^2 \left(\frac{\Delta p}{\frac{1}{2} \rho_\infty V_\infty^2} \right) = \frac{1}{8} f_2(T_w) R_d^2 C_p \quad (B4)$$

and in a similar manner

$$\frac{\tau d^2}{4\rho_w v_w^2} = \frac{1}{8} f_2(T_w) R_d^2 C_f \quad (B5)$$

where $f_2(T_w)$ is as defined in the notation. Then, if equations (B4) and (B5) are substituted in equation (B3)

$$\frac{1}{8} f_2(T_w) R_d^2 C_p = F_p \left[\frac{1}{8} f_2(T_w) R_d^2 C_f \right] \quad (B6)$$

The constant $1/8$ was not used in plotting the data herein, so to relate the calibration factors to the original Preston factors, the following relationship is applicable

$$8 \left(\frac{\Delta p d^2}{4\rho_w v_w^2} \right) = f_2(T_w) R_d^2 C_p \quad (B7)$$

Using the Sutherland equation for low temperatures ($T_\infty < 300^\circ \text{R}$) as given in reference 37 and the equation of state in which the pressure is assumed constant through the boundary layer, the viscosity-density factor in equation (B4) can be written as

$$\left(\frac{\mu_\infty}{\mu_w} \right)^2 \left(\frac{\rho_w}{\rho_\infty} \right) = \left(\frac{T_w + 198.6}{T_\infty + 198.6} \right)^2 \left(\frac{T_\infty}{T_w} \right)^4 \quad (B8)$$

For adiabatic wall conditions, if a temperature recovery factor of 0.88 is assumed, equation (B8) becomes

$$\left(\frac{\mu_\infty}{\mu_w} \right)^2 \left(\frac{\rho_w}{\rho_\infty} \right) = \left(\frac{T_w + 198.6}{T_\infty + 198.6} \right)^2 \left(\frac{1}{1 + 0.176 M_\infty^2} \right)^4 \quad (B9)$$

All data presented herein are based on the viscosity-density factor given by equation (B9).

$$\left[f_1(T_w) \frac{R_d}{\sqrt{\sigma_\infty}} \sin^{-1} \left(\sqrt{\sigma_\infty} \frac{V_s}{V_\infty} \right) \right]^2 \text{ vs. } f_2(T_w) R_d^2 C_f$$

Fenter and Stalmach in reference 27 developed a functional equation for use in calibrating surface pitot tubes at supersonic speeds by following Wilson's theoretical approach for skin friction (ref. 35 and eq. (A1) herein). A form of the resulting equation is given below.

$$\frac{f_1(T_w) R_d}{\sqrt{\sigma_\infty}} \sin^{-1} \left(\sqrt{\sigma_\infty} \frac{V_s}{V_\infty} \right) = f_f \left[\sqrt{f_2(T_w) R_d^2 C_f} \right] \quad (B10)$$

Note that the right-hand side of equation (B10) is the same as the right-hand side of equation (B6) except for the radical. If both sides of equation (B10)

are squared, then this equation will become another functional equation that reduces in form to Preston's original equation for incompressible flow (see p. 7 of ref. 23). The squared form of equation (B10) was used for the data presented here in order to be consistent with Preston's original work. In this form equation (B10) becomes

$$\left[\frac{f_1(T_w) R_d}{\sqrt{\sigma_\infty}} \sin^{-1} \left(\sqrt{\sigma_\infty} \frac{V_S}{V_\infty} \right) \right]^2 = F_f \left[f_2(T_w) R_d^2 C_f \right] \quad (B11)$$

wherein $f_1(T_w)$ and $f_2(T_w)$ are as defined in the notation. In reference 6, the approximate viscosity formula

$$\frac{\mu_\infty}{\mu_w} = \left(\frac{T_\infty}{T_w} \right)^{0.768} \quad (B12)$$

was used to compute the functions $f_1(T_w)$ and $f_2(T_w)$, although the free-stream static temperatures would be below the acceptable minimum temperature (300° R) for this formula. For this reason and to be consistent with the presentation of the present results which were reduced on the basis of the more exact Sutherland formula, the data from reference 6 presented herein were corrected by multiplying the calibration functions $f_1(T_w)$ and $f_2(T_w)$ by the following ratios:

$$\frac{[f_1(T_w)]_{\text{Sutherland}}}{[f_1(T_w)]_{\text{Approx. viscosity formula}}} = \left(\frac{T_w + 198.6}{T_\infty + 198.6} \right) \left(\frac{1}{1 + 0.176 M_\infty^2} \right)^{0.732} \quad (B13)$$

$$\frac{[f_2(T_w)]_{\text{Sutherland}}}{[f_2(T_w)]_{\text{Approx. viscosity formula}}} = [\text{eq. (B13)}]^2 \quad (B14)$$

APPENDIX C

CRITICAL PRESTON TUBE DIAMETERS

MAXIMUM

In reference 27 an equation is given for calculating the maximum Preston tube diameter for which a single calibration curve would be expected to be applicable. This equation, which is based on the maximum distance from the surface for which the law of the wall was found experimentally to be applicable, is given below

$$(d_{cr})_{\max} = (0.1061) \left(\frac{2}{t+1} \right) \left(\frac{\delta_c}{\sqrt{C_{f_i}}} \right) \left(\frac{\delta^*}{\delta} \right)_i \quad (C1)$$

For the present investigation t (the ratio of inside-to-outside tube diameter) is 0.6 and the incompressible local skin-friction coefficient was computed by Sivells and Payne's approximate formula (ref. 54) which is shown in reference 52 to give accurately the Kármán-Schoenherr skin-friction values in the range $10^5 < R_x < 10^9$. This formula is:

$$C_{f_i} = \frac{0.088(\log_{10} R_x - 2.3686)}{(\log_{10} R_x - 1.5)^3} \quad (C2)$$

The boundary-layer thickness for compressible flow was computed as

$$\delta_c = \frac{\theta_c}{(\theta/\delta)_c} = \frac{x C_F}{2(\theta/\delta)_c} \quad (C3)$$

in which C_F was defined by the Sivells-Payne approximate formula for average skin friction (ref. 54) as

$$C_F = \left(\frac{T_\infty}{T^*} \right) \frac{0.088}{\left[\log_{10} \left(R_x \frac{\mu_\infty T_\infty}{\mu^* T^*} \right) - 1.5 \right]^2} \quad (C4)$$

and $(\theta/\delta)_c$ was computed from reference 55 (eq. (24)) in which a 1/7-power velocity profile was assumed. For the computations herein, 50 terms were summed, so that

$$\left(\frac{\theta}{\delta} \right)_c = \frac{7}{1 + 0.2M_\infty^2} \sum_{i=0}^{i=50} \frac{1}{(8+2i)(9+2i)K^i} \quad (C5)$$

where

where

$$K = \frac{1 + 0.2M_\infty^2}{0.2M_\infty^2}$$

and as

$$M_\infty \rightarrow 0, \quad \frac{\theta}{\delta} \rightarrow \frac{7}{12}$$

Also, for this boundary layer

$$\left(\frac{\delta^*}{\delta}\right)_i = \frac{1}{8} \quad (C6)$$

therefore, by substituting equations (C3) and (C6) in equation (C1), we obtain

$$\frac{(d_{cr})_{max}}{x} = \frac{0.00829C_F}{\sqrt{C_{f_i}}(\theta/\delta)_c} \quad (C7)$$

MINIMUM

In the present investigation it was found that the Preston tube calibration was linear on a log-log plot above a value of $f_2(T')R_d^2C_f \approx 10^4$. For this reason and because only the present data within the linear part of the calibration curve agreed with values measured in reference 6, it was considered prudent to limit the Preston tube minimum size for a given application to $f_2(T')R_d^2C_f = 10^4$. From this assumption, the Reynolds number based on the minimum tube diameter becomes

$$\frac{\rho_\infty V_\infty (d_{cr})_{min}}{\mu_\infty} = \sqrt{\frac{10^4}{f_2(T')C_f}} \quad (C8)$$

By employing the approximate viscosity relationship (eq. (B12)) and the reference temperature of Sommer and Short for the adiabatic wall case [$T' = T_\infty(1 + 0.1142M_\infty^2)$] in equation (C8), we can obtain the following equation

$$\left(\frac{d_{cr}}{x}\right)_{min} = \frac{10^2(1 + 0.1142M_\infty^2)^{1.268}}{R_x \sqrt{C_f}} \quad (C9)$$

For the figures presented herein, the local skin-friction coefficient (C_f) in equation (C9) was computed by the compressible Sivells and Payne equation (ref. 54) given below

$$C_f = 0.088 \left(\frac{T_\infty}{T'} \right) \frac{\log_{10} \left(R_x \frac{\mu_\infty T_\infty}{\mu' T'} \right) - 2.3686}{\left[\log_{10} \left(R_x \frac{\mu_\infty T_\infty}{\mu' T'} \right) - 1.5 \right]^3} \quad (C10)$$

where

$$\left(\frac{\mu_\infty}{\mu'} \right) \left(\frac{T_\infty}{T'} \right) = \left(\frac{T_\infty}{T'} \right)^{w+1} = \left(\frac{1}{1 + 0.1142 M_\infty^2} \right)^{1.768} \quad (C11)$$

APPENDIX D

C_f DERIVED FROM $d\theta/dx$

In several of the reports for which local skin-friction data are presented in figures 21 through 23, the skin friction was not measured directly but instead the momentum thickness of the boundary layer was measured at various streamwise locations. It was necessary, therefore, to derive the local skin-friction coefficient (C_f) from a differentiation of the equation defining the change in momentum thickness of the boundary layer with streamwise distance. The usual equation for zero pressure gradient relating C_f to momentum thickness given below was used in the calculations

$$C_f = 2 \frac{d\theta}{dx} \quad (D1)$$

Values of C_f from references 46 and 48 had already been derived from measured values of θ . Listed below are the equations relating θ to x_v , the derivative equations ($d\theta/dx$) and the references from which the equations ($\theta = f(x_v)$) were taken. The distance from the virtual origin of the turbulent boundary layer to the point at which θ is measured is x_v .

Reference	Equation for $\theta = F(x_v)$	Equation for $d\theta/dx_v$
44,45	$\theta = \frac{0.0265(x_v)^{0.8}}{(v_\infty/v_0)^{0.2}} \quad (D2)$ <p>where $x_v = x - 1$, in.</p>	$\frac{d\theta}{dx} = \frac{0.0212}{(R_{x,v})^{0.2}} \quad (D5)$
42	$5.85\sqrt{\theta} \log_{10}[(2\theta)(v_\infty/v_0)] = \sqrt{x_v} \quad (D3)$ <p>where $x_v = x$, in.</p>	$\frac{d\theta}{dx} = \frac{\sqrt{\theta}}{\sqrt{x_v}[5.85 \log_{10} R_\theta + 6.842]} \quad (D6)$
47	$\theta = \frac{0.0944x_v}{[\log_{10}(0.0692R_{x,v})]^{2.6}} \quad (D4)$ <p>where $x_v = x - 2$, in.</p>	$\frac{d\theta}{dx} = \frac{0.0944\{[(\log_{10}(0.0692R_{x,v}))^{2.6} - 1.129[\log_{10}(0.0692R_{x,v})]^{1.6}]\}}{[\log_{10}(0.0692R_{x,v})]^{5.2}} \quad (D7)$

REFERENCES

1. Schultz-Grunow, F.: New Frictional Resistance Law for Smooth Plates. NACA TM 986, 1941.
2. Liepmann, Hans W.; and Dhawan, Satish: Direct Measurements of Local Skin Friction in Low Speed and High Speed Flow. U.S. Natl. Congr. of Appl. Mech., First, New York, 1951, pp. 869-874.
3. Dhawan, S.: Direct Measurements of Skin Friction. NACA Rep. 1121, 1953.
4. Smith, Donald W.; and Walker, John H.: Skin-Friction Measurements in Incompressible Flow. NASA TR R-26, 1959.
5. Hakkinen, Raimo J.: Measurements of Turbulent Skin Friction on a Flat Plate at Transonic Speeds. NACA TN 3486, 1955.
6. Stalmach, Charles J., Jr.: Experimental Investigation of the Surface Impact Pressure Probe Method of Measuring Local Skin Friction at Supersonic Speeds. Rep. DRL-410, CF-2675, Defense Res. Lab., Univ. of Texas, 1958.
7. Naleid, J. F.: Experimental Investigation of the Impact Pressure Probe Method of Measuring Local Skin Friction at Supersonic Speeds in Presence of an Adverse Pressure Gradient. Rep. DRL-432, CF-2739, Defense Res. Lab., Univ. of Texas, 1958.
8. Moore, D. R.; and Harkness, J.: Experimental Investigations of the Compressible Turbulent Boundary Layer at Very High Reynolds Numbers. AIAA J., vol. 3, no. 4, April 1965, pp. 631-638.
9. Matting, Fred W.; Chapman, Dean R.; Nyholm, Jack R.; and Thomas, Andrew G.: Turbulent Skin Friction at High Mach Numbers and Reynolds Numbers in Air and Helium. NASA TR R-82, 1961.
10. Coles, Donald: Measurements in the Boundary Layer on a Smooth Flat Plate in Supersonic Flow III. Rep. 20-71, JPL, Calif. Inst. Tech., 1953.
11. Korkegi, Robert H.: Transition Studies and Skin-Friction Measurements on an Insulated Flat Plate at a Mach Number of 5.8. J. Aerospace Sci., vol. 23, no. 2, Feb. 1956, pp. 97-107.
12. Stanton, T. E.; Marshall, D.; and Bryant, C. N.: Boundary Conditions of Fluid in Turbulent Motion. Roy. Soc., Proc. (A), vol. 97, 1920, pp. 413-434.
13. Fage, A.; and Falkner, V. M.: An Experimental Determination of the Intensity of Friction on the Surface of an Aerofoil. Roy. Soc., Proc. (A), vol. 129, 1930, pp. 378-410.
14. Taylor, G. I.: Measurements With a Half-Pitot Tube. Roy. Soc., Proc. (A), vol. 166, 1938, pp. 476-481.

15. Fage, A.; and Sargent, R. F.: Shock-Wave and Boundary-Layer Phenomena Near a Flat Surface. Roy. Soc., Proc. (A), vol. 190, 1947, pp. 1-20.
16. Cope, W. F.: The Measurement of Skin Friction in a Turbulent Boundary Layer at a Mach Number of 2.5, Including the Effect of a Shock Wave. Roy. Soc., Proc. (A), vol. 215, 1952, pp. 84-99.
17. Hakkinen, R. J.: Measurements of Skin Friction in Turbulent Boundary Layers at Transonic Speeds. Ph.D. Thesis, Calif. Inst. Tech., 1954.
18. Trilling, L.; and Hakkinen, R. J.: The Calibration of the Stanton Tube as a Skin-Friction Metre. 50 Jahre Grenzschichtforschung, H. Görtler and W. Tollmien, eds., Friedr. Vieweg and Sohn, 1955, pp. 201-209.
19. Gadd, G. E.: A Note on the Theory of the Stanton Tube. ARC 20, 471, F.M. 2740, T.P. 605, 1958.
20. Bradshaw, P.; and Gregory, N.: The Determination of Local Turbulent Skin Friction From Observations in the Viscous Sub-Layer. ARC 20, 895, F.M. 2802, Perf. 1753, 1959.
21. Abarbanel, S. S.; Hakkinen, R. J.; and Trilling, L.: Use of a Stanton Tube for Skin-Friction Measurements. NASA MEMO 2-17-59W, 1959.
22. Smith, K. G.; Gaudet, L.; and Winter, K. G.: The Use of Surface Pitot Tubes as Skin-Friction Meters at Supersonic Speeds. RAE Aero. 2665, 1962.
23. Smith, K. G.; Gaudet, L.; and Winter, K. G.: The Use of Surface Pitot Tubes as Skin-Friction Meters at Supersonic Speeds. ARC R&M No. 3351, 1964.
24. Edwards, J. B. W.: Measurements of Skin-Friction Using Surface-Pitot Tubes in Free Flight at Supersonic Speeds. Tech. Note Aero. 2891, 1963.
25. Preston, J. H.: The Determination of Turbulent Skin Friction by Means of Pitot Tubes. ARC No. 15, 758, F.M. 1883, 1953.
26. Hsu, E. Y.: The Measurement of Local Turbulent Skin Friction by Means of Surface Pitot Tubes. Rep. 957, David Taylor Model Basin, 1955.
27. Fenter, F. W.; and Stalmach, C. J.: The Measurement of Local Turbulent Skin Friction at Supersonic Speeds by Means of Surface Impact Pressure Probes. DRL 392, CM 878, Univ. of Texas, 1957.
28. Wilson, R. E.: Characteristics of Turbulent Boundary Layer Flow Over a Smooth Thermally Insulated Flat Plate at Supersonic Speeds. CM-712, DRL-301, Univ. of Texas, 1952.
29. Fenter, Felix W.; and Stalmach, Charles J.: The Measurement of Turbulent-Boundary-Layer Shear Stress by Means of Surface Impact-Pressure Probes. Reader's Forum of J. Aero/Space Sci., vol. 25, no. 12, Dec. 1958, pp. 793-794.

30. Coles, Donald: The Law of the Wall in Turbulent Shear Flow. 50 Jahre Grenzschichtforschung, H. Görtler and W. Tollmien, eds., Heinrich-Braun-schweig, F. Vieweg., 1955, pp. 153-163.
31. Staff of Aerodynamics Division, NPL: On the Measurement of Local Surface Friction on a Flat Plate by Means of Preston Tubes. ARC R&M 3185, 1961.
32. Head, M. R.; and Rechenberg, I.: The Preston Tube as a Means of Measuring Skin Friction. Dept. of Eng., Univ. of Cambridge, 1962.
33. Rechenberg, Ingo: Messung Der Turbuleten Wandschubspannung. Zeitschrift Für Flugwissenschaften, vol. 11, no. 11, Nov. 1963, pp. 429-438.
34. Rechenberg, Ingo: Zur Messung Der Turbulenten Wandreibung Mit Dem Prestonrohr. Wissenschaftliche Gessellschaft für Luft-und Raumfahrt, Hermann Blenk, ed., vol. 9, no. 12, Oct. 1962, pp. 151-159.
35. Wilson, R. E.: Turbulent Boundary-Layer Characteristics at Supersonic Speeds - Theory and Experiment. J. Aerospace Sci., vol. 17, no. 9, Sept. 1950, pp. 585-594.
36. Sommer, S. C.; and Short, B. J.: Free-Flight Measurements of Turbulent-Boundary-Layer Skin Friction in the Presence of Severe Aerodynamic Heating at Mach Numbers From 2.8 to 7.0. NACA TN 3391, 1955. (Also J. Aerospace Sci., vol. 23, no. 6, June 1956.)
37. Ames Research Staff: Equations, Tables, and Charts for Compressible Flow. NACA Rep. 1135, 1953. (Supersedes NACA TN 1428.)
38. Nothwang, George J.: An Evaluation of Four Experimental Methods for Measuring Mean Properties of a Supersonic Turbulent Boundary Layer. NACA TR 1320, 1957.
39. Sigalla, Armand: Calibration of Preston Tubes in Supersonic Flow. AIAA J., vol. 3, no. 8, Aug. 1965, p. 1531.
40. Moeckel, W. E.: Some Effects of Bluntness on Boundary-Layer Transition and Heat Transfer at Supersonic Speeds. NACA Rep. 1312, 1957.
41. Jillie, Don W.; and Hopkins, Edward J.: Effects of Mach Number, Leading-Edge Bluntness, and Sweep on Boundary-Layer Transition on a Flat Plate. NACA TN D-1071, 1961.
42. Ashkenas, Harry; and Riddell, Frederick R.: Investigation of the Turbulent Boundary Layer on a Yawed Flat Plate. NACA TN 3383, 1955.
43. Shutts, W. H.; Hartwig, W. H.; and Weiler, J. E.: Final Report on Turbulent Boundary-Layer and Skin-Friction Measurements on a Smooth, Thermally Insulated Flat Plate at Supersonic Speeds. Defense Res. Lab., Univ. of Texas, Rep. DRL-364, CM-823, 1955.

44. Monaghan, R. J.; and Cooke, J. R.: The Measurement of Heat Transfer and Skin Friction at Supersonic Speeds. Part III: Measurements of Overall Heat Transfer and of the Associated Boundary Layers on a Flat Plate at $M_1 = 2.43$. RAE TN No. Aero. 2129, 1951.
45. Monaghan, R. J.; and Johnson, J. E.: The Measurement of Heat Transfer and Skin Friction at Supersonic Speeds. Part II. Boundary Layer Measurements on a Flat Plate at $M = 2.5$ and Zero Heat Transfer. ARC CP No. 64 (13,064), TN No. Aero. 2031, 1949.
46. Spivack, H. M.: Experiments in the Turbulent Boundary Layer of a Supersonic Flow. North American Aviation, Aerophysics Laboratory, Rep. CM-615, 1950.
47. Monaghan, R. J.; and Cooke, J. R.: The Measurement of Heat Transfer and Skin Friction at Supersonic Speeds. Part IV. Tests on a Flat Plate at $M = 2.82$. ARC TR CP No. 140 (15,400), 1953.
48. Brinich, Paul F.; and Diaconis, Nick S.: Boundary-Layer Development and Skin Friction at Mach Number 3.05. NACA TN 2742, 1952.
49. Lobb, R. Kenneth; Winkler, Eva M.; and Persh, Jerome: Experimental Investigation of Turbulent Boundary Layers in Hypersonic Flow. J. Aero. Sci., vol. 22, no. 1, Jan. 1955, pp. 1-9.
50. Peterson, John B., Jr.: A Comparison of Experimental and Theoretical Results for the Compressible Turbulent-Boundary-Layer Skin Friction With Zero Pressure Gradient. NASA TN D-1795, 1963.
51. Locke, F. W. S., Jr.: Recommended Definition of Turbulent Friction in Incompressible Fluid. Navy Dept., Bureau of Aeronautics, Research Div., DR Rep. 1415, June 1952.
52. Bertram, Mitchel H.: Calculations of Compressible Average Turbulent Skin Friction. NASA TR R-123, 1962.
53. Prandtl L.: Zur Turbulenten Strömung in Rohren und Längs Platten. Ergebn. d. Aerodyn. Versuchsanst, Göttingen, IV, Lieferung, 1932, p. 18.
54. Sivells, J. C.; and Payne, R. G.: A Method of Calculating Turbulent-Boundary-Layer Growth at Hypersonic Mach Numbers. AEEDC-TR-59-3, Arnold Eng. Dev. Center, March 1959, DDC, AD-208774.
55. Wilson, R. E.; Young, E. C.; and Thompson, M. J.: Experimentally Determined Turbulent Boundary Layer Characteristics at Supersonic Speeds. Second Interim Report DRL-196 CM-501, Univ. of Texas, 1949.

TABLE I.-- CALIBRATION FACTORS AND FLOW CONDITIONS FOR THE PRESENT DATA

M_∞	q_∞ , lb/ft ²	T_∞ , °R	$(T_w)_{ad}$, °R	$(T_w)_{mess}$, °R	V_∞/V_{ref} , $\times 10^{-6}$ per ft	C_p	Type tube	Tube height, in.	Stanton tube position	C_f	M_B	$f_2(T_w)R_d^2C_p$	$f_2(T_w)R_d^2C_f$	$f_2(T_w)R_d^2\left(\frac{M_B}{M_\infty}\right)^2$	$f_2(T_w)R_d^2\left(\frac{M_B}{M_\infty}\right)^2$	$f_2(T_w)R_d^2C_f$	$f_1(T_w) \frac{R_d}{\sqrt{\sigma_\infty}} \sin^{-1}\left(\sqrt{\frac{V_B}{V_\infty}}\right)^2$
2.419	189	540	505	527	1.015	0.1983	Preston	0.061	-	0.00142	0.962	7.676x10 ⁵	5.506x10 ⁵	6.121x10 ⁵	1.021x10 ⁵	9.178x10 ⁵	5.688x10 ⁵
↓	↓	↓	↓	↓	↓	↓	↓	↓	↓	↓	1.006	1.865x10 ⁵	1.200x10 ⁵	1.459x10 ⁵	2.432x10 ⁵	2.001x10 ⁵	1.339x10 ⁵
↓	↓	↓	↓	↓	↓	↓	↓	↓	↓	↓	1.040	3.975x10 ⁵	2.352x10 ⁵	3.056x10 ⁵	5.095x10 ⁵	3.922x10 ⁵	2.779x10 ⁵
↓	↓	↓	↓	↓	↓	↓	↓	↓	↓	↓	1.037	9.885x10 ⁵	5.239x10 ⁵	7.436x10 ⁵	1.240x10 ⁷	8.734x10 ⁴	6.672x10 ⁵
2.432	193	547	512	532	1.020	↓	Stanton	0.189	Rearward	↓	↓	8.72	5.821x10 ⁵	5.285x10 ⁵	4.827x10 ⁵	8.811x10 ⁵	4.592x10 ⁵
↓	↓	↓	↓	↓	↓	↓	↓	↓	↓	↓	↓	803	1.277x10 ⁵	1.418x10 ⁵	1.090x10 ⁵	1.821x10 ⁵	2.369x10 ⁵
↓	↓	↓	↓	↓	↓	↓	↓	↓	↓	↓	↓	1.002	1.825x10 ⁵	1.195x10 ⁵	1.431x10 ⁵	1.998x10 ⁵	1.313x10 ⁵
↓	↓	↓	↓	↓	↓	↓	↓	↓	↓	↓	↓	1.056	4.083x10 ⁵	2.343x10 ⁵	3.115x10 ⁵	5.204x10 ⁵	2.819x10 ⁵
↓	↓	↓	↓	↓	↓	↓	↓	↓	↓	↓	↓	1.157	2.020x10 ⁷	9.224x10 ⁴	1.472x10 ⁷	2.459x10 ⁷	1.541x10 ⁵
2.438	296	558	521	533	1.523	↓	Stanton	0.189	Forward	↓	↓	990	7.807x10 ⁵	5.265x10 ⁵	6.152x10 ⁵	1.028x10 ⁷	8.796x10 ⁴
↓	↓	↓	↓	↓	↓	↓	↓	↓	↓	↓	↓	882	3.524x10 ⁵	2.885x10 ⁵	2.919x10 ⁵	4.869x10 ⁵	5.669x10 ⁵
↓	↓	↓	↓	↓	↓	↓	↓	↓	↓	↓	↓	1.037	4.413x10 ⁵	2.432x10 ⁵	3.397x10 ⁵	5.673x10 ⁵	4.062x10 ⁴
↓	↓	↓	↓	↓	↓	↓	↓	↓	↓	↓	↓	1.101	1.006x10 ⁷	4.766x10 ⁴	7.510x10 ⁵	1.254x10 ⁷	7.961x10 ⁴
↓	↓	↓	↓	↓	↓	↓	↓	↓	↓	↓	↓	1.208	4.981x10 ⁷	1.876x10 ⁵	3.557x10 ⁷	5.941x10 ⁷	3.094x10 ⁵
2.445	284	544	508	521	1.516	↓	Stanton	0.189	Forward	↓	↓	1.005	1.797x10 ⁵	1.071x10 ⁵	1.406x10 ⁷	2.348x10 ⁷	3.075x10 ⁷
↓	↓	↓	↓	↓	↓	↓	↓	↓	↓	↓	↓	997	1.778x10 ⁵	1.065x10 ⁴	1.396x10 ⁵	1.789x10 ⁵	1.286x10 ⁵
↓	↓	↓	↓	↓	↓	↓	↓	↓	↓	↓	↓	1.022	4.121x10 ⁵	2.320x10 ⁴	3.199x10 ⁵	5.361x10 ⁵	2.929x10 ⁵
↓	↓	↓	↓	↓	↓	↓	↓	↓	↓	↓	↓	1.093	9.556x10 ⁵	4.548x10 ⁴	7.168x10 ⁵	1.202x10 ⁷	6.426x10 ⁵
↓	↓	↓	↓	↓	↓	↓	↓	↓	↓	↓	↓	1.140	2.366x10 ⁷	1.013x10 ⁵	1.737x10 ⁷	2.912x10 ⁷	1.534x10 ⁵
2.446	386	554	517	521	2.011	↓	Stanton	0.189	Rearward	↓	↓	878	1.254x10 ⁷	1.022x10 ⁵	1.040x10 ⁷	1.698x10 ⁵	9.872x10 ⁵
↓	↓	↓	↓	↓	↓	↓	↓	↓	↓	↓	↓	996	3.136x10 ⁵	1.918x10 ⁴	2.460x10 ⁵	4.118x10 ⁵	3.211x10 ⁴
↓	↓	↓	↓	↓	↓	↓	↓	↓	↓	↓	↓	1.058	7.927x10 ⁵	4.180x10 ⁴	6.048x10 ⁵	1.013x10 ⁷	2.268x10 ⁵
↓	↓	↓	↓	↓	↓	↓	↓	↓	↓	↓	↓	1.133	1.845x10 ⁷	8.192x10 ⁴	1.359x10 ⁷	2.277x10 ⁷	5.471x10 ⁵
↓	↓	↓	↓	↓	↓	↓	↓	↓	↓	↓	↓	1.183	4.584x10 ⁷	1.825x10 ⁵	3.301x10 ⁷	5.528x10 ⁷	1.203x10 ⁷
2.441	402	568	531	533	2.014	↓	Stanton	0.189	Rearward	↓	↓	874	2.193x10 ⁷	1.841x10 ⁵	3.044x10 ⁷	3.082x10 ⁵	5.880x10 ⁷
↓	↓	↓	↓	↓	↓	↓	↓	↓	↓	↓	↓	920	6.831x10 ⁵	5.143x10 ⁵	9.259x10 ⁵	8.582x10 ⁵	1.720x10 ⁷
↓	↓	↓	↓	↓	↓	↓	↓	↓	↓	↓	↓	1.057	8.099x10 ⁵	4.335x10 ⁴	6.173x10 ⁵	1.030x10 ⁷	5.588x10 ⁵
↓	↓	↓	↓	↓	↓	↓	↓	↓	↓	↓	↓	1.120	1.835x10 ⁷	8.496x10 ⁴	1.359x10 ⁷	2.268x10 ⁷	1.418x10 ⁵
↓	↓	↓	↓	↓	↓	↓	↓	↓	↓	↓	↓	1.255	9.583x10 ⁷	3.344x10 ⁵	6.714x10 ⁷	1.120x10 ⁸	5.723x10 ⁷
2.441	395	562	525	533	2.017	↓	Stanton	0.189	Forward	↓	↓	1.024	3.295x10 ⁷	1.909x10 ⁵	2.551x10 ⁷	4.258x10 ⁷	5.581x10 ⁵
↓	↓	↓	↓	↓	↓	↓	↓	↓	↓	↓	↓	0.911	6.654x10 ⁵	5.123x10 ⁵	5.430x10 ⁵	3.186x10 ⁵	2.333x10 ⁷
↓	↓	↓	↓	↓	↓	↓	↓	↓	↓	↓	↓	1.054	8.009x10 ⁵	4.318x10 ⁴	6.125x10 ⁵	9.074x10 ⁵	8.559x10 ⁵
↓	↓	↓	↓	↓	↓	↓	↓	↓	↓	↓	↓	1.111	1.795x10 ⁷	8.464x10 ⁴	1.334x10 ⁷	2.229x10 ⁷	5.117x10 ⁵
↓	↓	↓	↓	↓	↓	↓	↓	↓	↓	↓	↓	1.260	9.659x10 ⁷	3.332x10 ⁵	6.755x10 ⁷	1.129x10 ⁸	5.541x10 ⁵
2.445	498	566	529	532	2.511	↓	Stanton	0.625	Rearward	↓	↓	822	2.121x10 ⁵	2.082x10 ⁴	1.795x10 ⁵	3.002x10 ⁵	5.747x10 ⁷
↓	↓	↓	↓	↓	↓	↓	↓	↓	↓	↓	↓	1.027	5.319x10 ⁵	2.945x10 ⁴	4.112x10 ⁵	5.566x10 ⁵	1.737x10 ⁵
↓	↓	↓	↓	↓	↓	↓	↓	↓	↓	↓	↓	1.083	1.322x10 ⁷	6.419x10 ⁴	9.972x10 ⁵	3.479x10 ⁴	3.756x10 ⁵
↓	↓	↓	↓	↓	↓	↓	↓	↓	↓	↓	↓	1.143	2.966x10 ⁷	1.258x10 ⁵	2.176x10 ⁷	1.073x10 ⁵	8.958x10 ⁵
↓	↓	↓	↓	↓	↓	↓	↓	↓	↓	↓	↓	1.188	7.278x10 ⁷	2.802x10 ⁵	5.237x10 ⁷	3.637x10 ⁷	1.920x10 ⁷
2.442	506	575	537	533	2.496	↓	Stanton	0.189	Rearward	↓	↓	878	3.488x10 ⁷	2.827x10 ⁵	2.885x10 ⁷	4.821x10 ⁷	4.556x10 ⁷
↓	↓	↓	↓	↓	↓	↓	↓	↓	↓	↓	↓	943	1.114x10 ⁵	7.628x10 ⁵	8.960x10 ⁵	1.418x10 ⁵	2.744x10 ⁷
↓	↓	↓	↓	↓	↓	↓	↓	↓	↓	↓	↓	1.067	1.273x10 ⁷	6.429x10 ⁴	9.663x10 ⁵	1.272x10 ⁴	8.370x10 ⁵
↓	↓	↓	↓	↓	↓	↓	↓	↓	↓	↓	↓	1.151	3.018x10 ⁷	1.260x10 ⁵	2.204x10 ⁷	1.612x10 ⁷	8.714x10 ⁵
↓	↓	↓	↓	↓	↓	↓	↓	↓	↓	↓	↓	1.265	1.501x10 ⁸	4.961x10 ⁵	3.676x10 ⁷	1.072x10 ⁵	1.941x10 ⁵
↓	↓	↓	↓	↓	↓	↓	↓	↓	↓	↓	↓	1.038	5.228x10 ⁷	2.832x10 ⁵	1.048x10 ⁸	8.273x10 ⁵	9.900x10 ⁷
2.447	500	571	533	533	2.498	↓	Stanton	0.189	Forward	↓	↓	938	1.088x10 ⁵	7.781x10 ⁵	6.718x10 ⁷	4.723x10 ⁵	3.663x10 ⁷
↓	↓	↓	↓	↓	↓	↓	↓	↓	↓	↓	↓	1.059	1.237x10 ⁷	6.558x10 ⁴	8.774x10 ⁵	1.465x10 ⁵	8.208x10 ⁵
↓	↓	↓	↓	↓	↓	↓	↓	↓	↓	↓	↓	1.143	2.932x10 ⁷	1.285x10 ⁵	2.151x10 ⁷	1.096x10 ⁵	8.520x10 ⁵
↓	↓	↓	↓	↓	↓	↓	↓	↓	↓	↓	↓	1.290	1.558x10 ⁸	5.060x10 ⁵	1.078x10 ⁸	3.593x10 ⁷	1.898x10 ⁷
↓	↓	↓	↓	↓	↓	↓	↓	↓	↓	↓	↓	832	3.328x10 ⁴	3.162x10 ⁴	2.804x10 ⁵	5.283x10 ⁴	9.090x10 ⁷
2.468	671	582	544	548	3.270	↓	Stanton	0.625	Rearward	↓	↓	1.061	9.422x10 ⁵	4.944x10 ⁴	7.174x10 ⁵	1.802x10 ⁵	2.699x10 ⁵
↓	↓	↓	↓	↓	↓	↓	↓	↓	↓	↓	↓	1.085	2.178x10 ⁷	1.078x10 ⁵	1.636x10 ⁷	8.285x10 ⁴	6.492x10 ⁵
↓	↓	↓	↓	↓	↓	↓	↓	↓	↓	↓	↓	1.167	5.111x10 ⁷	2.112x10 ⁵	3.709x10 ⁷	6.216x10 ⁷	1.472x10 ⁷
↓	↓	↓	↓	↓	↓	↓	↓	↓	↓	↓	↓	1.221	1.273x10 ⁸	4.704x10 ⁵	9.044x10 ⁷	3.540x10 ⁵	3.252x10 ⁷
↓	↓	↓	↓	↓	↓	↓	↓	↓	↓	↓	↓	875	5.654x10 ⁷	4.747x10 ⁵	4.685x10 ⁷	7.883x10 ⁵	7.795x10 ⁷
↓	↓	↓	↓	↓	↓	↓	↓	↓	↓	↓	↓	↓	↓	↓	↓	↓	4.461x10 ⁷

TABLE I.- CALIBRATION FACTORS AND FLOW CONDITIONS FOR THE PRESENT DATA - Concluded

M_∞	q_∞ , lb/ft. ²	T_t , °R	$(T_w)_{ad}$, °R	$(T_w)_{meas}$, °R	$V_\infty/V_{\infty,0}$, x10 ⁻⁶ per ft	C_p	Type tube	Tube height, in.	Stanton tube position	C_f	M_s	$f_2(T_w)R_d^2 C_p$	$f_2(T_w)R_d^2 C_f$	$f_2(T_w)R_d^2 \left(\frac{M_s}{M_\infty}\right)^2$	$f_2(T')R_d^2 \left(\frac{M_s}{M_\infty}\right)^2$	$f_2(T')R_d^2 C_f$	$f_1(T_w) \frac{R_d}{\sqrt{\sigma_\infty}} \sin^{-1} \left(\sqrt{\sigma_\infty} \frac{V_s}{V_\infty} \right)^2$
2.978	606	611	564	537	3.157	0.2066	Preston	0.061	-	0.00110	1.156	4.097x10 ⁶	2.183x10 ⁴	2.988x10 ⁶	5.546x10 ⁶	4.053x10 ⁴	2.680x10 ⁶
						.2176					1.181	9.406x10 ⁶	4.759x10 ⁴	6.787x10 ⁶	1.260x10 ⁷	8.834x10 ⁴	6.042x10 ⁶
						.2492					1.247	2.112x10 ⁷	9.328x10 ⁴	1.486x10 ⁷	2.758x10 ⁷	1.731x10 ⁵	1.295x10 ⁷
						.3080					1.360	5.812x10 ⁷	2.077x10 ⁵	3.935x10 ⁷	7.306x10 ⁷	3.856x10 ⁵	3.311x10 ⁷
						.1238	Stanton	.189	Rearward	.00129 ^a	.940	2.356x10 ⁷	2.096x10 ⁵	1.896x10 ⁷	3.520x10 ⁷	3.891x10 ⁵	1.806x10 ⁷
3.232	70	550	505	537	.464	.0409	Preston	.061	-	(.00086)	.623	1.224x10 ⁴	2.959x10 ²	1.112x10 ⁴	2.186x10 ⁴	5.816x10 ²	1.143x10 ⁴
						.0692					.788	4.512x10 ⁴	6.451x10 ²	3.876x10 ⁴	1.268x10 ⁵	3.846x10 ⁴	
						.1096					.957	1.400x10 ⁵	1.265x10 ³	1.120x10 ⁵	2.201x10 ⁵	1.068x10 ⁵	
						.1488					1.082	4.235x10 ⁵	2.815x10 ³	3.190x10 ⁵	6.269x10 ⁵	5.534x10 ⁵	
						.0667	Stanton	.189	Rearward	.00111 ^a	.775	1.915x10 ⁵	2.841x10 ³	1.651x10 ⁵	3.244x10 ⁵	2.946x10 ⁵	
3.376	137	547	501	529	.959	.0969	Preston	.061	-	(.00090)	.943	1.033x10 ⁵	1.181x10 ³	8.317x10 ⁴	1.676x10 ⁵	2.377x10 ³	7.986x10 ⁴
						.1232					1.039	2.863x10 ⁵	2.574x10 ³	2.201x10 ⁵	5.584x10 ³	2.063x10 ⁵	
						.1469					1.115	6.692x10 ⁵	5.044x10 ³	4.969x10 ⁵	1.001x10 ⁶	4.562x10 ⁵	
						.1848					1.223	1.875x10 ⁶	1.123x10 ⁴	1.331x10 ⁶	2.683x10 ⁶	1.184x10 ⁶	
						.0945	Stanton	.189	Rearward	.00101 ^a	.933	9.677x10 ⁵	1.133x10 ⁴	7.822x10 ⁵	1.576x10 ⁶	2.283x10 ⁴	7.533x10 ⁵
3.463	258	570	521	531	1.463	.1263	Preston	.061	-	(.00089)	1.071	2.884x10 ⁵	2.317x10 ³	2.184x10 ⁵	4.441x10 ⁵	2.032x10 ⁵	2.032x10 ⁵
						.1488					1.144	7.405x10 ⁵	5.049x10 ³	5.430x10 ⁵	1.104x10 ⁶	1.027x10 ⁴	4.952x10 ⁵
						.1749					1.221	1.705x10 ⁶	9.895x10 ³	1.213x10 ⁶	2.466x10 ⁶	2.012x10 ⁴	1.082x10 ⁶
						.2037					1.299	4.425x10 ⁶	2.205x10 ⁴	3.056x10 ⁶	6.214x10 ⁶	2.660x10 ⁶	
						.1020	Stanton	.189	Rearward	.00097 ^a	.903	2.235x10 ⁶	2.224x10 ⁴	1.765x10 ⁶	3.590x10 ⁶	4.522x10 ⁴	1.662x10 ⁶
3.474	296	561	531	531	1.954	.1452	Preston	.061	-	(.00090)	1.136	5.881x10 ⁵	3.946x10 ³	4.331x10 ⁵	8.800x10 ⁵	8.022x10 ³	3.958x10 ⁵
						.1613					1.184	1.425x10 ⁶	8.602x10 ³	1.026x10 ⁶	2.085x10 ⁶	1.748x10 ⁴	9.256x10 ⁵
						.1823					1.244	3.155x10 ⁶	1.686x10 ⁴	2.219x10 ⁶	4.511x10 ⁶	3.427x10 ⁴	1.966x10 ⁶
						.2162					1.335	8.333x10 ⁶	3.754x10 ⁴	5.692x10 ⁶	1.157x10 ⁷	7.633x10 ⁴	4.902x10 ⁶
						.1044	Stanton	.189	Rearward	.00096 ^a	.995	4.062x10 ⁶	3.789x10 ⁴	3.192x10 ⁶	6.488x10 ⁶	7.702x10 ⁴	3.031x10 ⁶
3.443	377	590	540	531	2.399	.1548	Preston	.061	-	(.00091)	1.157	9.910x10 ⁵	6.119x10 ³	7.228x10 ⁵	1.460x10 ⁶	1.236x10 ⁴	6.563x10 ⁵
						.1692					1.199	2.360x10 ⁶	1.334x10 ⁴	1.691x10 ⁶	3.415x10 ⁶	2.693x10 ⁴	3.011x10 ⁶
						.1971					1.275	5.389x10 ⁶	2.614x10 ⁴	3.749x10 ⁶	7.569x10 ⁶	5.279x10 ⁴	1.518x10 ⁶
						.2334					1.367	1.421x10 ⁷	5.823x10 ⁴	9.597x10 ⁶	1.938x10 ⁷	1.176x10 ⁵	3.291x10 ⁶
						.1068	Stanton	.189	Rearward	.00094 ^a	.997	6.561x10 ⁶	5.875x10 ⁴	5.151x10 ⁶	1.040x10 ⁷	1.187x10 ⁵	4.889x10 ⁶
3.451	370	564	534	534	2.403	.1023	Preston	.031	-	(.00093)	.982	1.673x10 ⁵	1.538x10 ³	1.324x10 ⁵	2.680x10 ⁵	3.113x10 ³	1.260x10 ⁵
						.1726					1.211	2.360x10 ⁶	1.296x10 ⁴	1.698x10 ⁶	3.436x10 ⁶	2.623x10 ⁴	1.518x10 ⁶
						.1910					1.262	5.161x10 ⁶	2.541x10 ⁴	3.614x10 ⁶	7.317x10 ⁶	5.141x10 ⁴	3.179x10 ⁶
						.2586					1.430	2.751x10 ⁷	9.998x10 ⁴	1.827x10 ⁷	3.697x10 ⁷	2.024x10 ⁵	1.526x10 ⁷
						.1576	Stanton	.189	Forward		1.167	9.569x10 ⁶	5.709x10 ⁴	6.943x10 ⁶	1.405x10 ⁷	1.156x10 ⁵	6.290x10 ⁶

^aThese skin-friction coefficients were computed by the Sommer and Short T' theory (ref. 36) from the measured values of R_d in order to improve the accuracy of $f_2(T_w)R_d^2 C_f$ and $f_2(T')R_d^2 C_f$ for the low pressure flow conditions. See equation (A4) and the accuracy section. All other skin-friction coefficients listed including those in parentheses were measured directly by the skin-friction balance.

TABLE II.- CALIBRATION FACTORS^a FOR DATA FROM REFERENCE 6

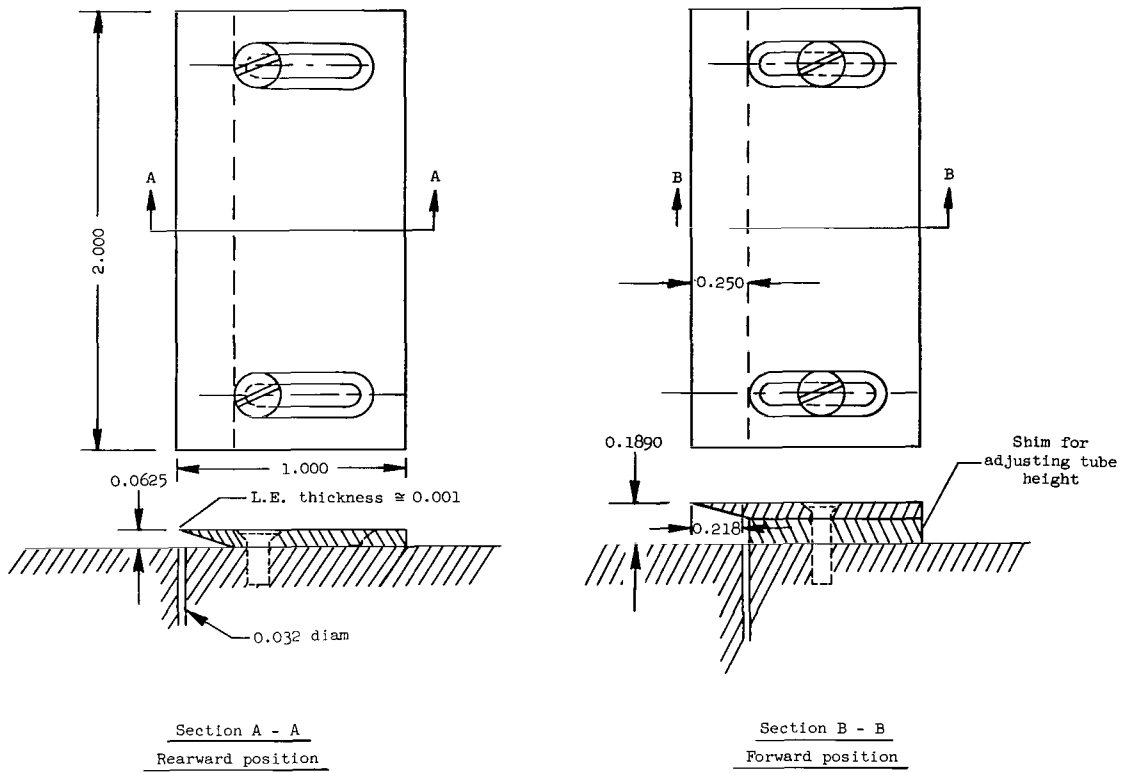
M_{∞}	T_t , OR	M_S	Tube height, in.	$f_2(T_W)R_d^2C_f$	$\left[f_1(T_W) \frac{R_d}{\sqrt{\sigma_{\infty}}} \sin^{-1} \left(\sqrt{\sigma_{\infty}} \frac{V_S}{V_{\infty}} \right) \right]^2$	$f_2(T')R_d^2C_f$	$f_2(T')R_d^2 \left(\frac{M_S}{M_{\infty}} \right)^2$
2.480	546	1.100	0.012	1.028×10^4	9.633×10^5	1.737×10^4	1.753×10^6
2.468	↓	1.065	↓	3.481×10^3	2.390×10^5	5.865×10^3	4.386×10^5
2.737	↓	1.167	↓	2.519×10^4	2.742×10^6	4.504×10^4	5.352×10^6
2.719	547	1.126	↓	7.635×10^3	6.792×10^7	1.360×10^4	1.325×10^6
2.711	↓	1.085	↓	2.506×10^3	1.741×10^5	4.456×10^3	3.117×10^5
2.981	↓	1.236	↓	1.696×10^4	1.722×10^6	3.189×10^4	3.655×10^6
2.966	540	1.180	↓	5.032×10^3	4.223×10^5	9.437×10^3	8.684×10^5
2.941	↓	1.096	↓	1.662×10^3	9.890×10^4	3.102×10^3	1.994×10^5
3.196	↓	1.261	↓	1.341×10^4	1.316×10^6	2.623×10^4	2.917×10^6
3.159	542	1.185	↓	5.014×10^3	4.056×10^5	9.744×10^3	8.733×10^5
3.135	↓	1.036	↓	1.360×10^3	7.069×10^4	2.632×10^3	1.420×10^5
3.375	↓	1.224	↓	1.021×10^4	9.434×10^5	2.060×10^4	2.117×10^6
3.372	539	1.195	↓	4.111×10^3	3.283×10^5	8.292×10^3	7.334×10^5
3.368	↓	1.075	↓	1.020×10^3	4.977×10^4	2.055×10^3	1.085×10^5
2.490	546	1.250	.020	9.343×10^4	1.240×10^7	1.582×10^5	2.388×10^7
2.483	↓	1.219	↓	2.824×10^4	3.147×10^6	4.775×10^4	5.902×10^6
2.484	↓	1.262	↓	9.212×10^3	8.417×10^5	1.558×10^4	1.609×10^6
2.739	547	1.298	↓	7.133×10^4	9.264×10^6	1.276×10^5	1.885×10^7
2.728	↓	1.253	↓	1.641×10^4	1.689×10^6	2.928×10^4	3.530×10^6
2.729	↓	1.295	↓	7.140×10^3	6.388×10^5	1.275×10^4	1.281×10^6
2.949	540	1.339	↓	5.044×10^4	6.012×10^6	9.427×10^4	1.304×10^7
2.949	↓	1.337	↓	1.492×10^4	1.564×10^6	2.789×10^4	3.332×10^6
2.958	↓	1.374	↓	4.794×10^3	4.132×10^5	8.977×10^3	9.093×10^5
3.161	541	1.389	↓	3.796×10^4	4.045×10^6	7.379×10^4	1.018×10^7
3.168	↓	1.331	↓	1.482×10^4	1.475×10^6	2.885×10^4	3.285×10^6
3.166	↓	1.412	↓	3.376×10^3	2.792×10^5	6.568×10^3	6.463×10^5
3.389	539	1.424	↓	2.645×10^4	3.085×10^6	5.350×10^4	7.322×10^6
3.402	↓	1.351	↓	1.141×10^4	1.102×10^6	2.313×10^4	2.587×10^6
3.400	↓	1.386	↓	2.636×10^3	1.927×10^5	5.341×10^3	4.528×10^5
2.502	546	1.407	.035	2.939×10^5	4.725×10^7	4.991×10^5	9.508×10^7

^aSee footnote, page 44.

TABLE II.- CALIBRATION FACTORS^a FOR DATA FROM REFERENCE 6 - Concluded

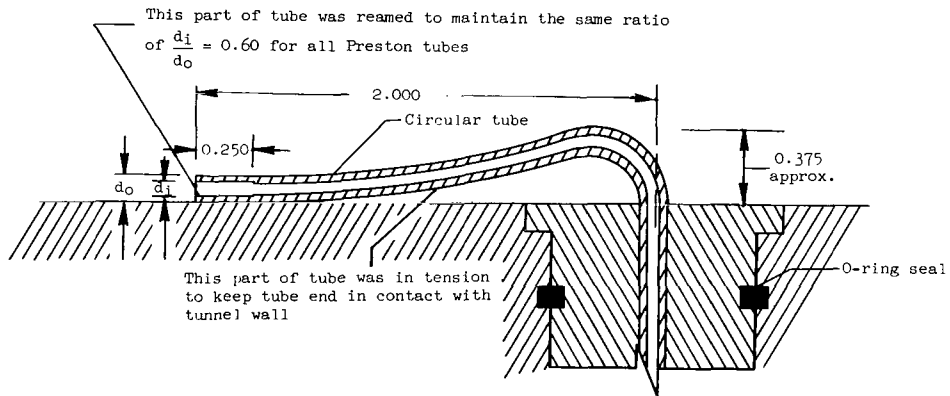
M_{∞}	T_{OR}	M_S	Tube height, in.	$f_2(T_w)R_d^2C_f$	$\left[f_1(T_w) \frac{R_d}{\sqrt{\sigma_{\infty}}} \sin^{-1} \left(\sqrt{\frac{\sigma_{\infty}}{V_S}} \frac{V_S}{V_{\infty}} \right) \right]^2$	$f_2(T')R_d^2C_f$	$f_2(T')R_d^2 \left(\frac{M_S}{M_{\infty}} \right)^2$
2.486	546	1.341	0.035	9.096×10^4	1.190×10^7	1.539×10^5	2.308×10^7
2.482	↓	1.462	↓	3.021×10^4	3.561×10^6	5.106×10^4	7.232×10^6
2.729	547	1.461	↓	2.187×10^5	3.487×10^7	3.903×10^5	7.360×10^7
2.719	↓	1.386	↓	6.696×10^4	8.469×10^6	1.193×10^5	1.761×10^7
2.704	↓	1.410	↓	2.215×10^4	2.307×10^6	3.933×10^4	4.731×10^6
2.978	540	1.579	↓	1.402×10^5	2.113×10^7	2.634×10^5	4.937×10^7
2.882	↓	1.441	↓	5.079×10^4	6.325×10^6	9.368×10^4	1.370×10^7
2.968	↓	1.556	↓	1.334×10^4	1.379×10^6	2.503×10^4	3.156×10^6
3.205	542	1.617	↓	1.063×10^5	1.537×10^7	2.082×10^5	3.786×10^7
3.162	↓	1.532	↓	4.038×10^4	4.909×10^6	7.852×10^4	1.174×10^7
3.122	↓	1.538	↓	1.146×10^4	1.142×10^6	2.212×10^4	2.644×10^6
3.399	539	1.601	↓	8.013×10^4	1.116×10^7	1.623×10^5	2.792×10^7
3.383	↓	1.550	↓	3.681×10^4	4.639×10^6	7.437×10^4	1.107×10^7
3.385	↓	1.630	↓	8.104×10^3	7.637×10^5	1.638×10^4	1.938×10^6
2.498	546	1.564	0.065	9.809×10^5	1.864×10^8	1.664×10^6	3.906×10^8
2.477	↓	1.501	↓	2.996×10^5	4.688×10^7	5.059×10^5	9.526×10^7
2.471	↓	1.592	↓	1.011×10^5	1.356×10^7	1.705×10^5	2.831×10^7
2.713	547	1.616	↓	7.757×10^5	1.462×10^8	1.380×10^6	3.242×10^8
2.702	↓	1.559	↓	2.331×10^5	3.584×10^7	4.137×10^5	7.819×10^7
2.700	↓	1.579	↓	7.689×10^4	9.612×10^6	1.364×10^5	2.064×10^7
2.962	540	1.715	↓	5.018×10^5	8.723×10^7	9.401×10^5	2.101×10^8
2.898	↓	1.609	↓	1.689×10^5	2.456×10^7	3.126×10^5	5.635×10^7
2.935	↓	1.857	↓	4.987×10^4	6.873×10^6	9.295×10^4	1.731×10^7
3.158	542	1.727	↓	4.062×10^5	6.693×10^7	7.892×10^5	1.686×10^8
3.155	↓	1.683	↓	1.388×10^5	2.329×10^7	2.696×10^5	1.955×10^7
3.142	↓	1.728	↓	3.789×10^4	4.404×10^6	7.339×10^4	1.088×10^7
3.414	539	1.800	↓	2.680×10^5	4.403×10^7	5.443×10^5	1.173×10^8
3.402	↓	1.713	↓	1.098×10^5	1.513×10^7	2.225×10^5	3.945×10^7
3.403	↓	1.875	↓	2.681×10^4	3.063×10^6	5.434×10^4	8.374×10^6

^aSutherland's formula was used instead of the approximate viscosity formula for computing the viscosity in the calibration factors; therefore, the values shown in table II differ somewhat from those presented in reference 6. See equations (B13) and (B14) for the corrections that were applied.



Stanton tube

Note: All dimensions are in inches



Preston tube

Figure 1.- Geometry of the Stanton tube and the Preston tube.

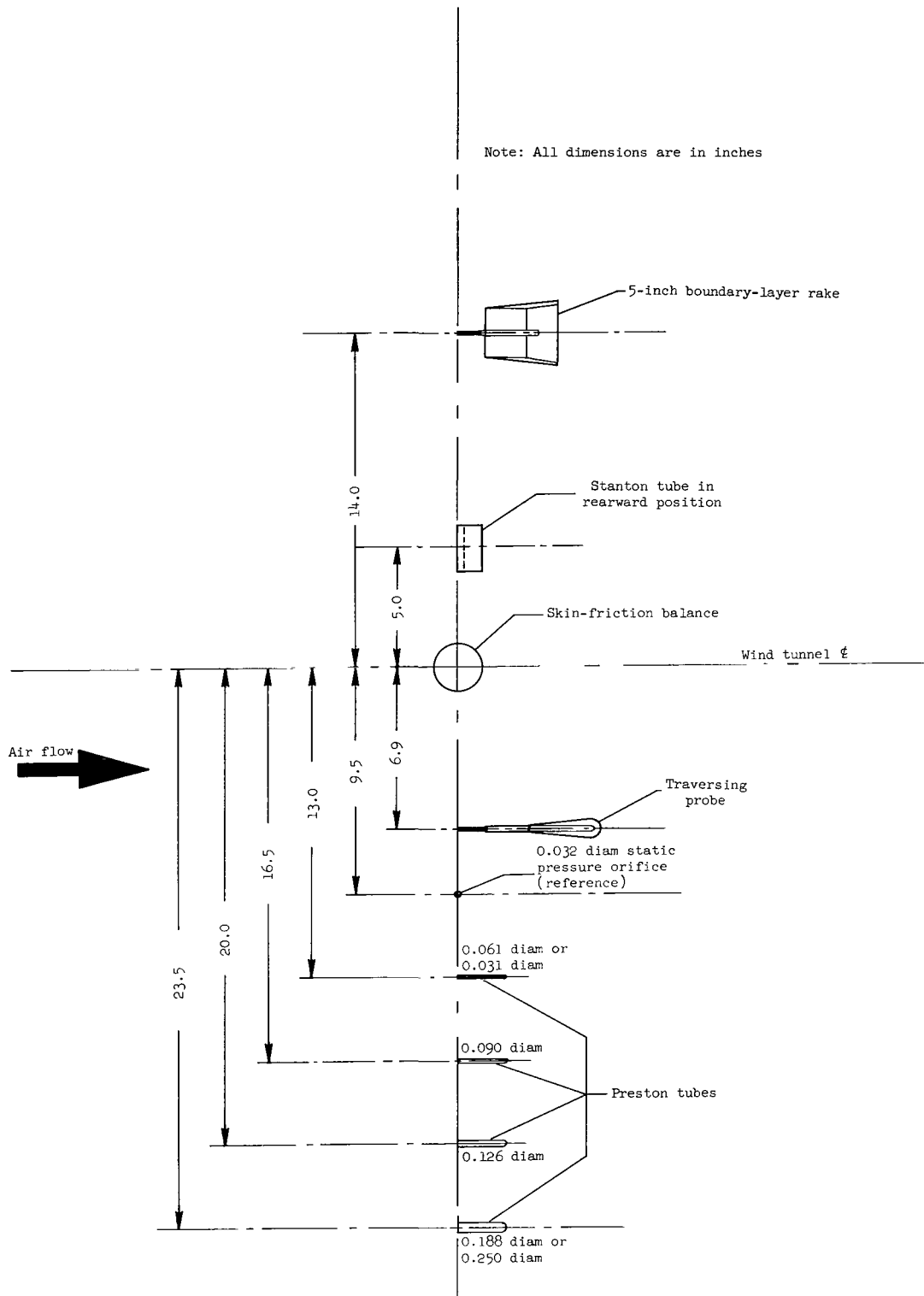
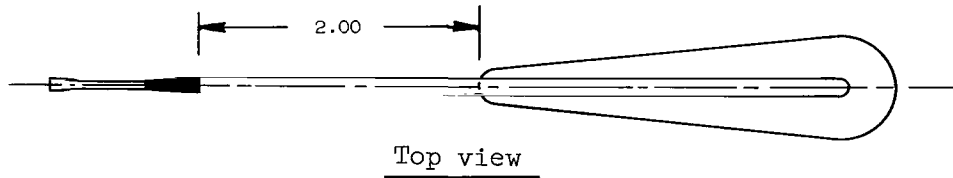


Figure 2.- Relative locations of the boundary-layer probes and the skin-friction balance mounted on the side wall of the Ames 8- by 7-Foot Supersonic Wind Tunnel.



Note: All dimensions are in inches

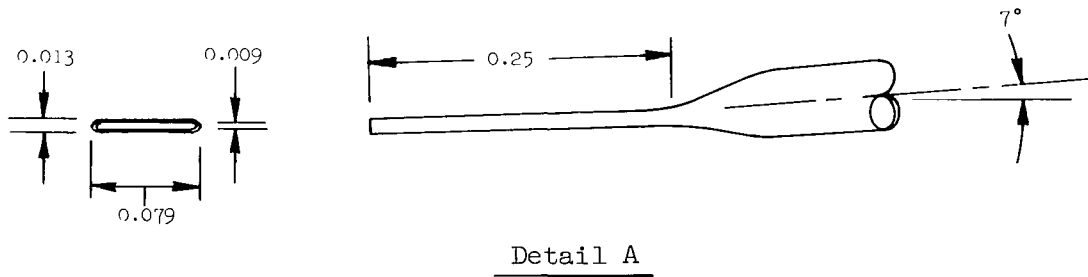
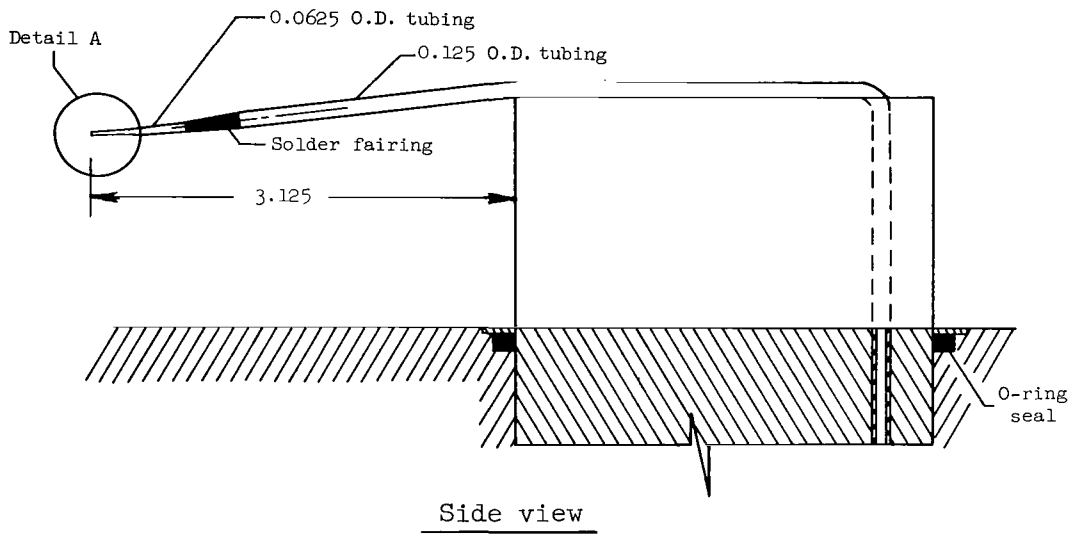


Figure 3.- Geometry of traversing probe.

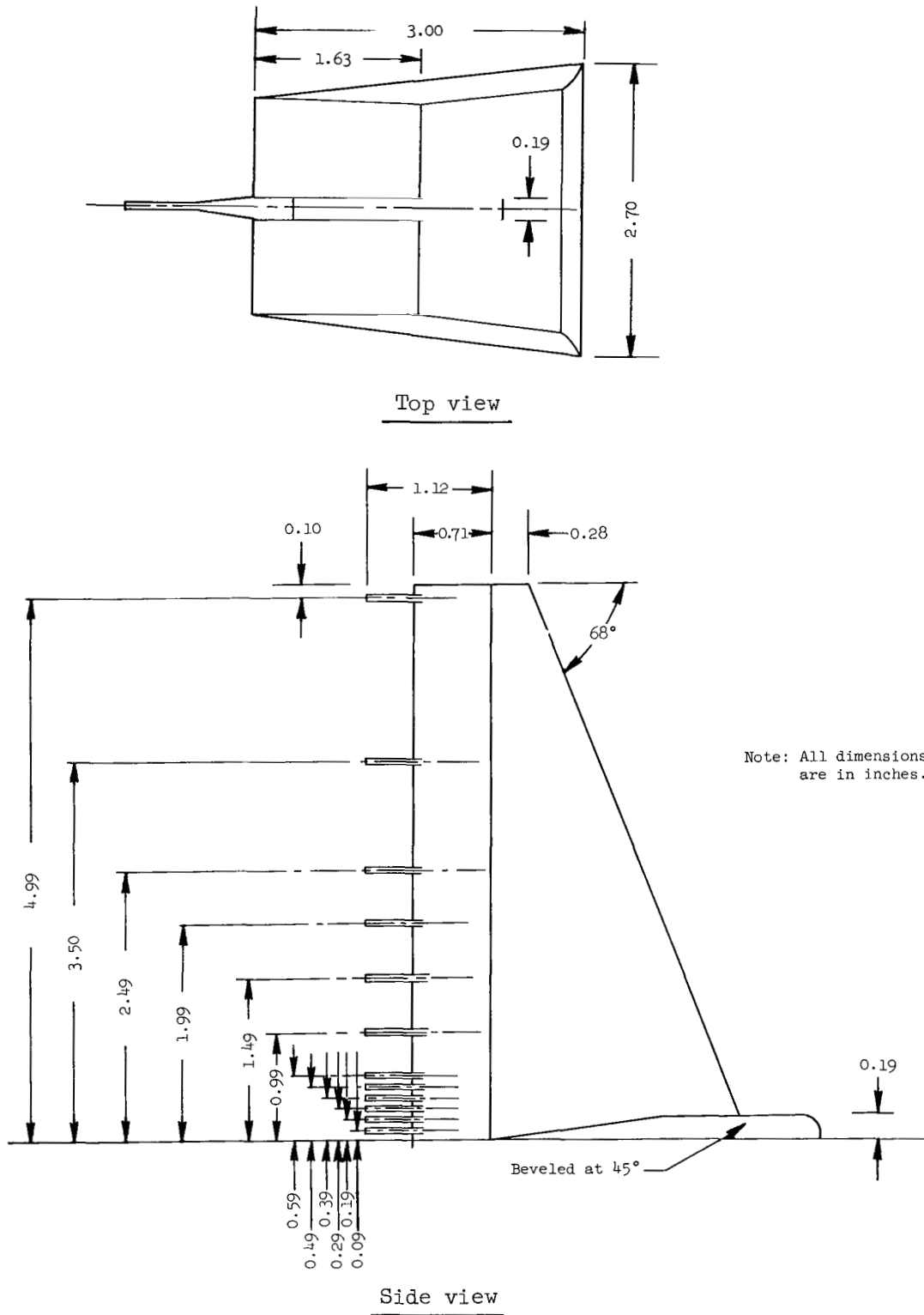
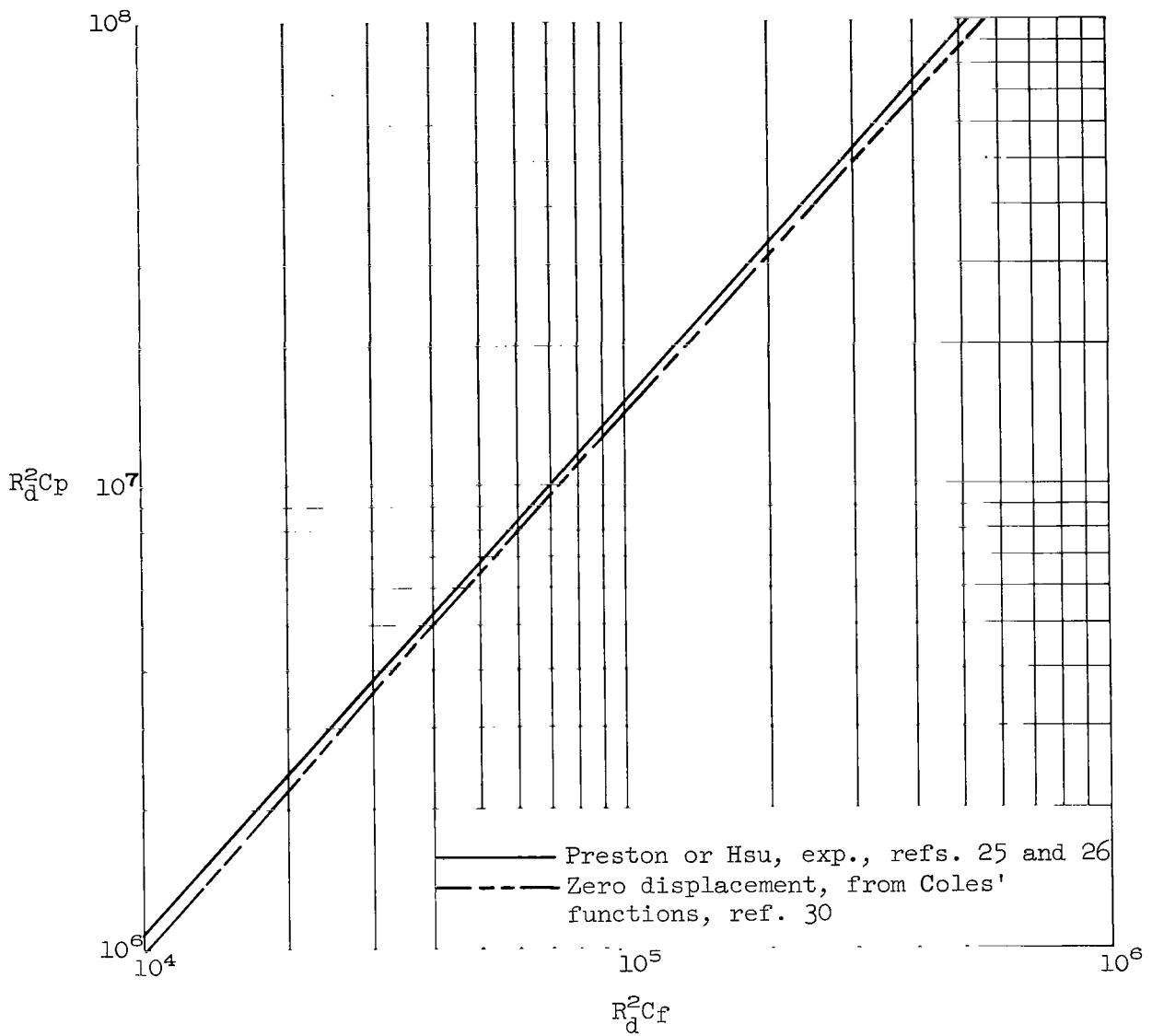
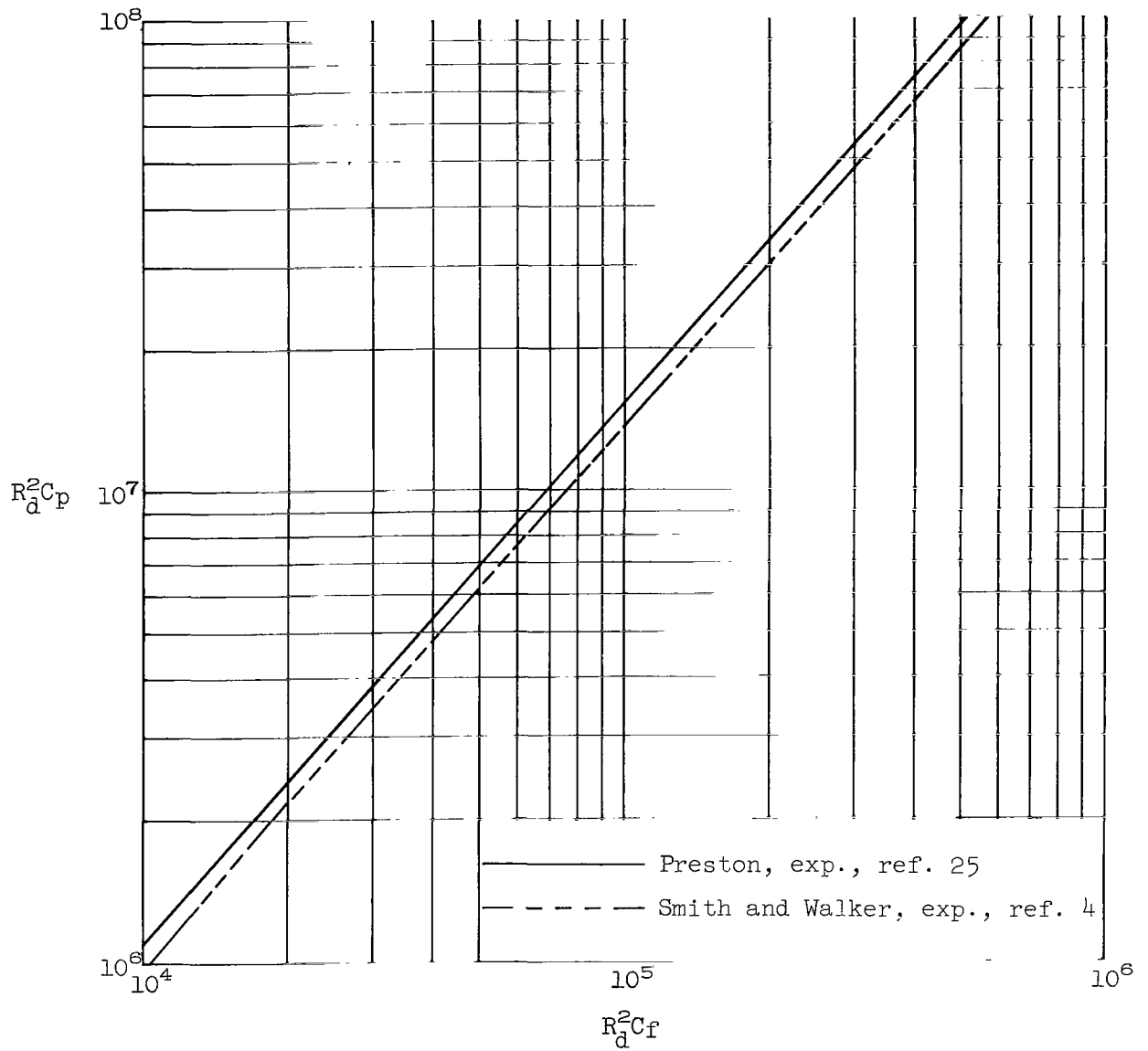


Figure 4.- Geometry of the 5-inch boundary-layer rake.



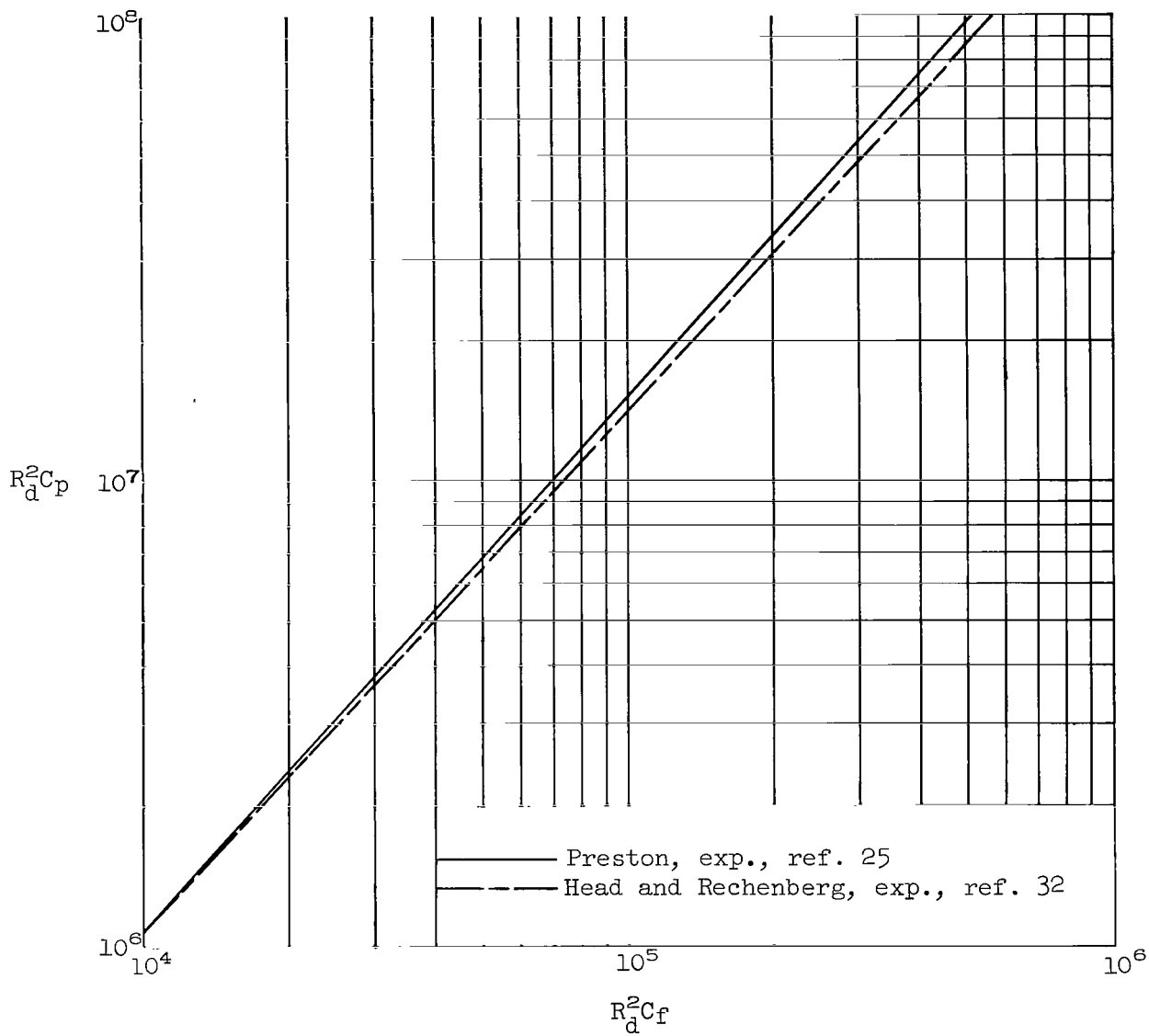
(a) Preston or Hsu (exp.) and Coles' functions.

Figure 5.- Incompressible calibration curves for Preston tubes.



(b) Preston (exp.), and Smith and Walker (exp.).

Figure 5.- Continued.



(c) Preston (exp.), and Head and Rechenberg (exp.).

Figure 5.- Concluded.

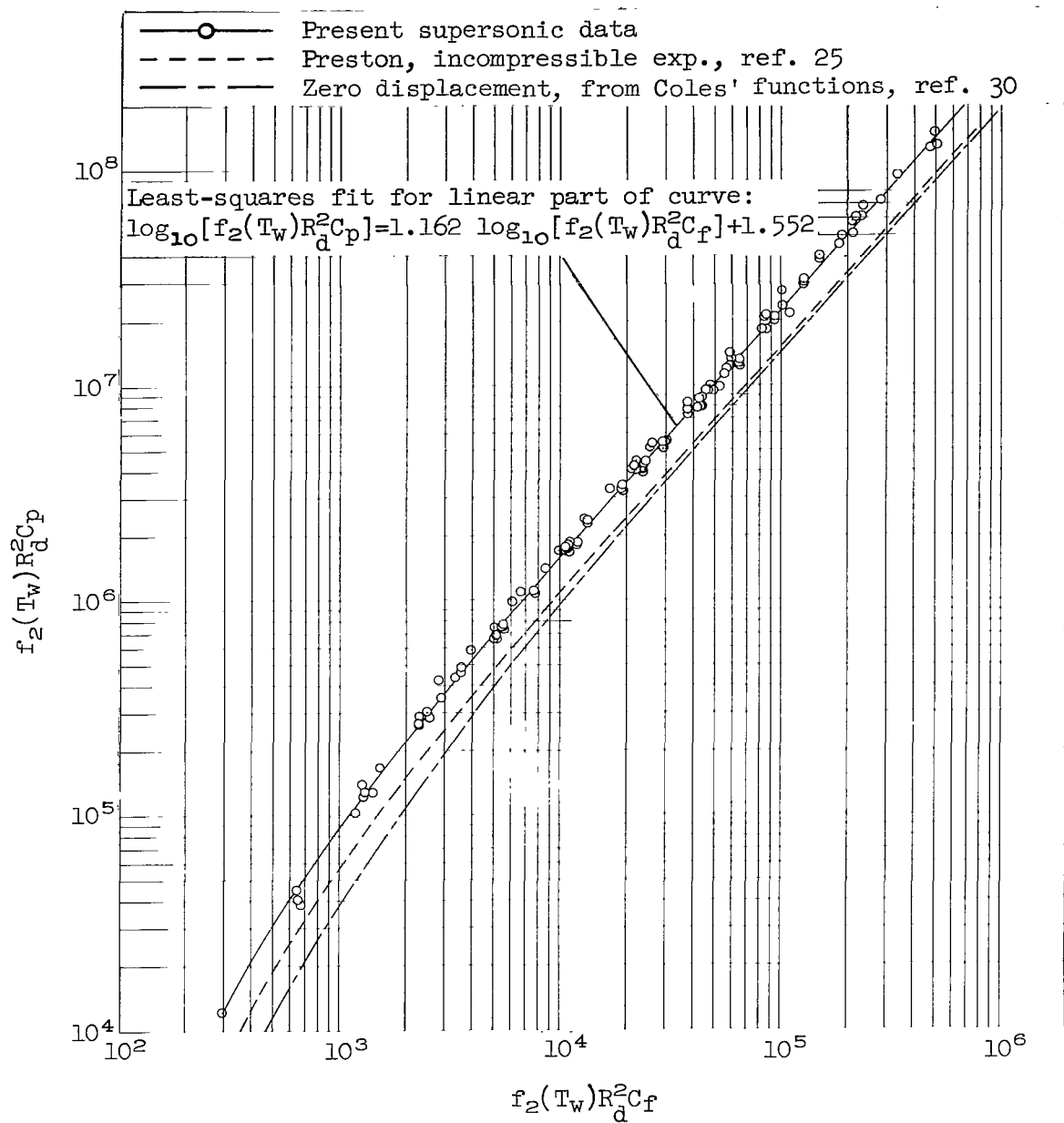


Figure 6.- Preston tube calibration based on the functional equation (B6). Present supersonic data.

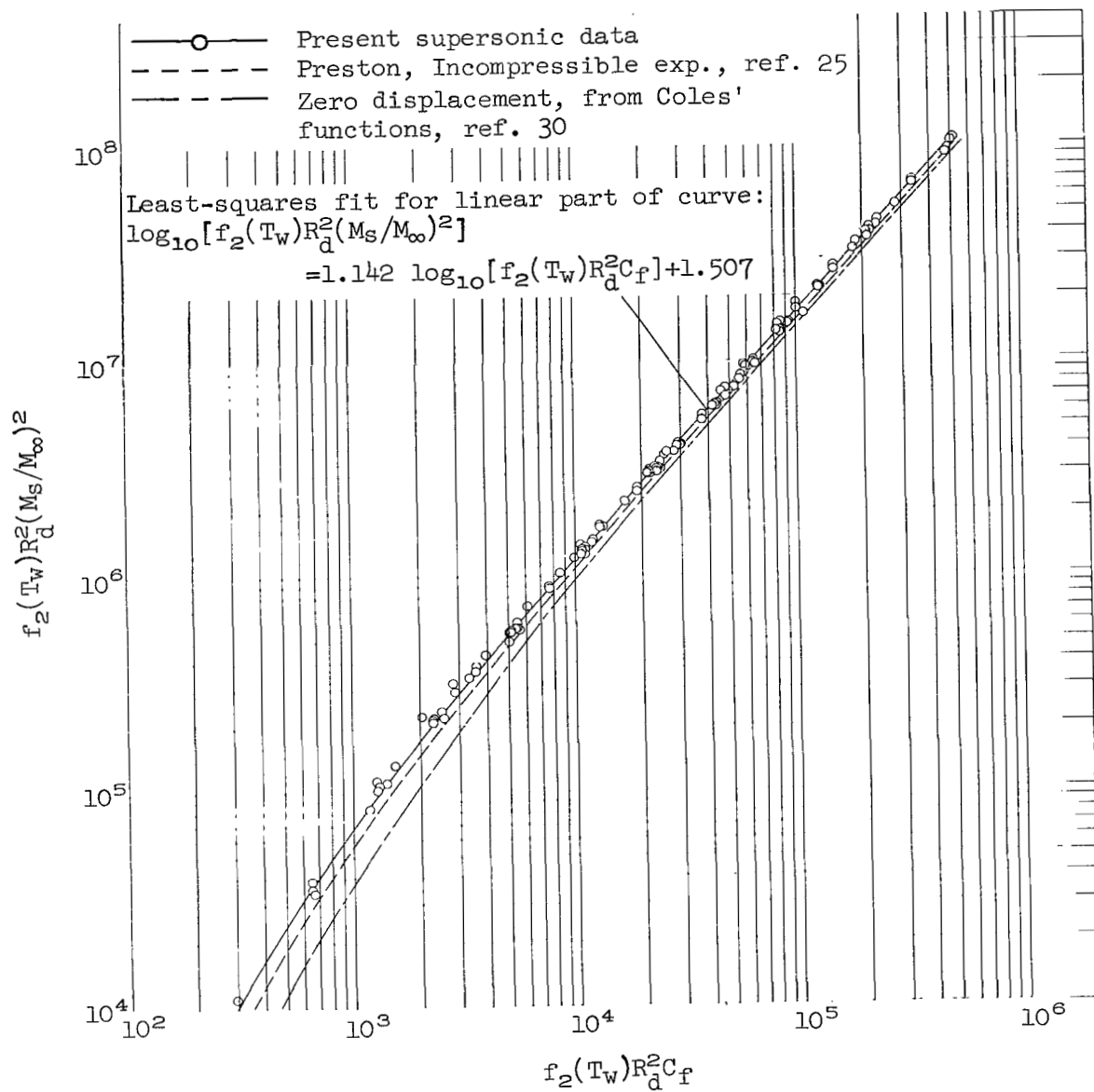
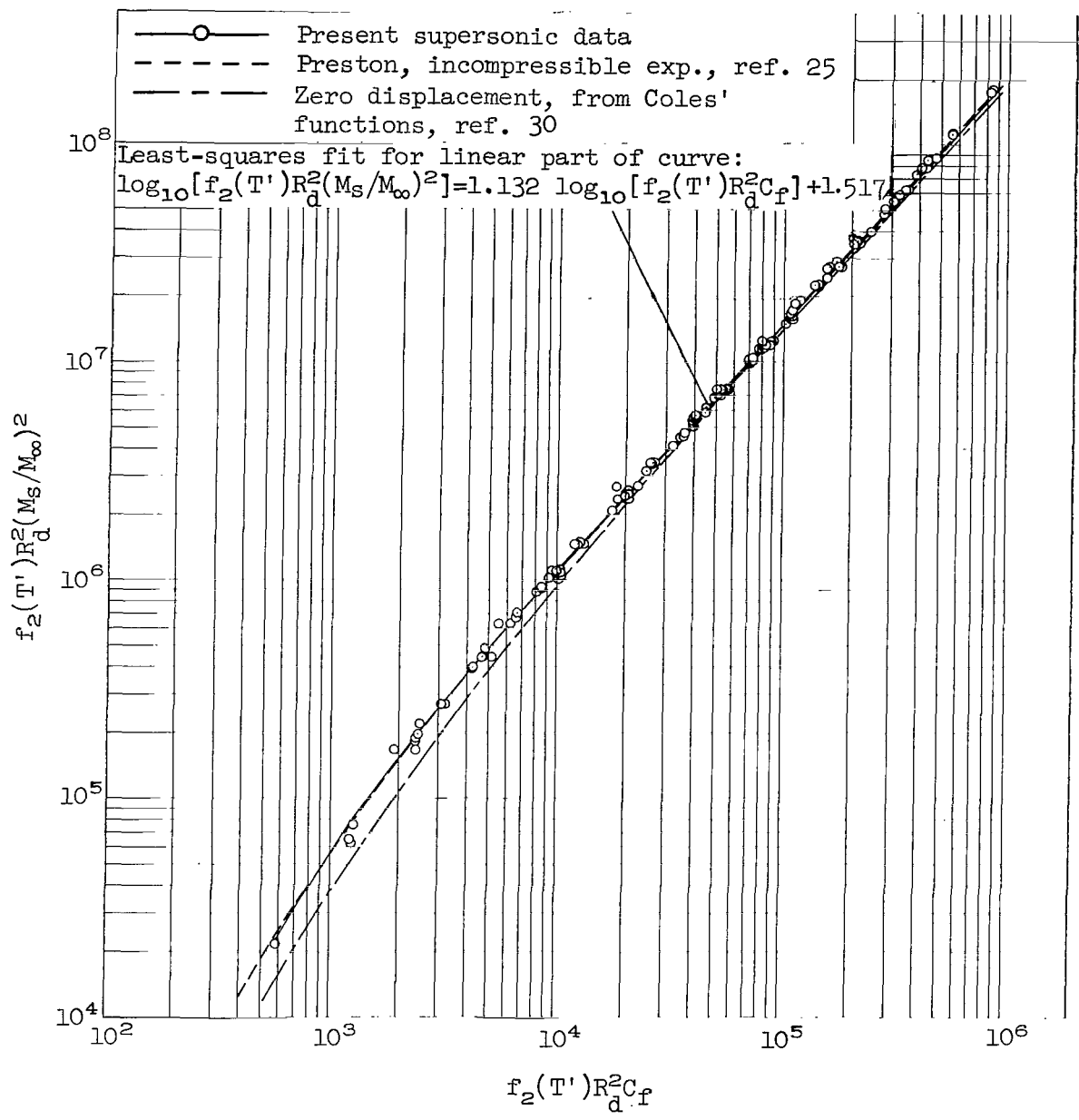
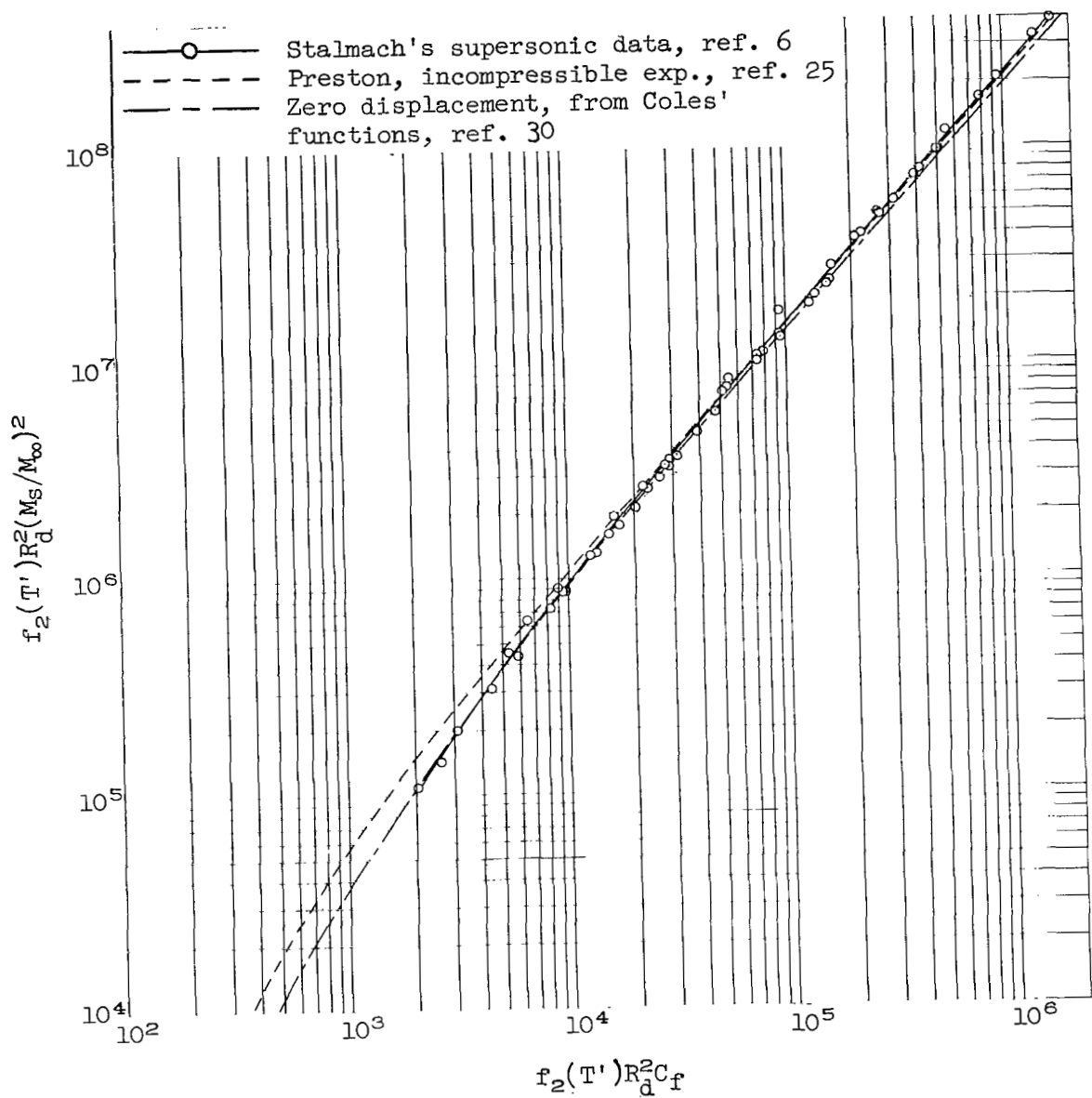


Figure 7.- Preston-tube calibration based on the functional equation (2). Present supersonic data.



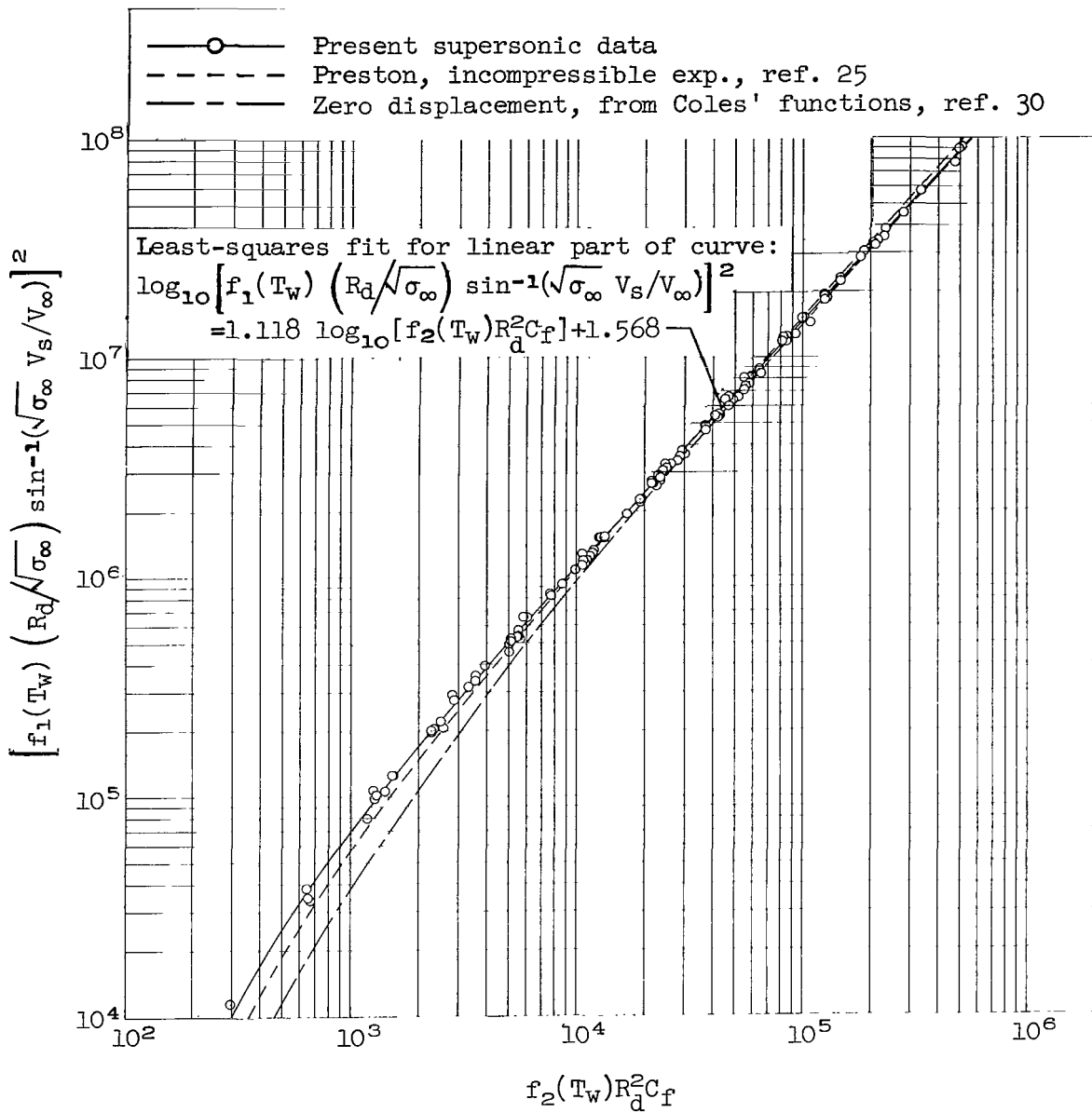
(a) Present supersonic data.

Figure 8.- Preston tube calibration based on the new functional equation developed herein (eq. (4)).



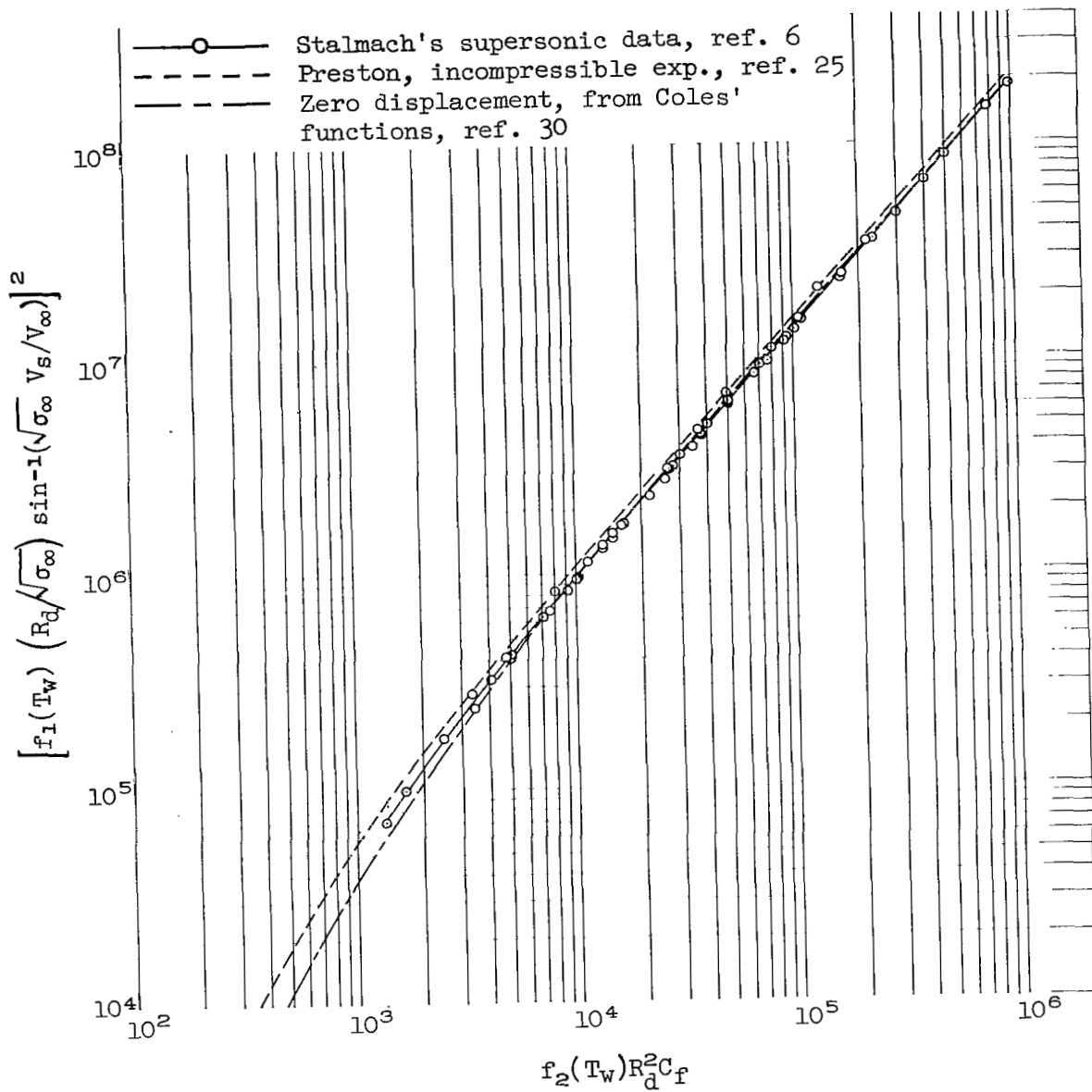
(b) Stalmach's supersonic data.

Figure 8.- Concluded.



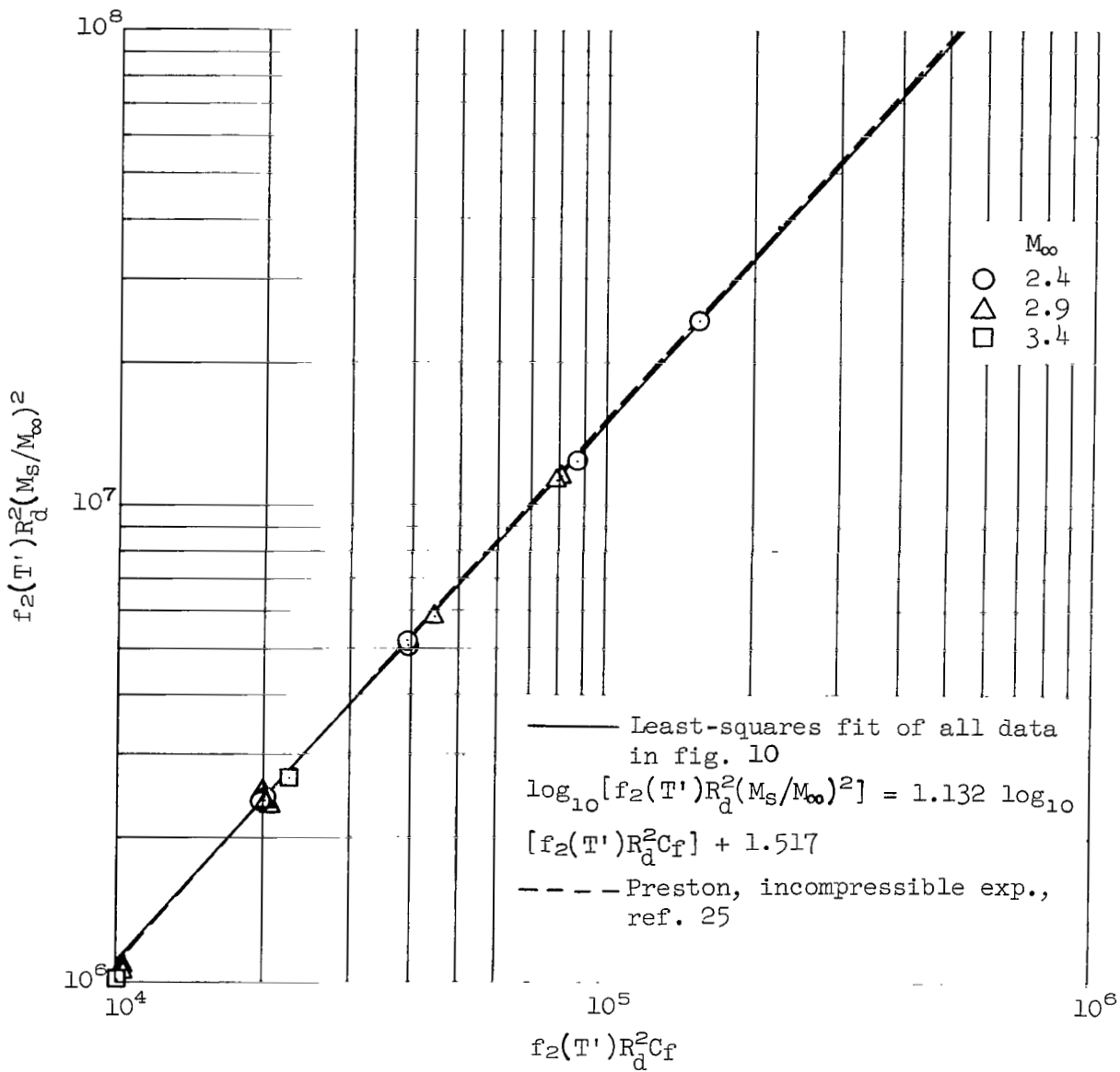
(a) Present supersonic data.

Figure 9.- Preston tube calibration based on the functional equation (B11).



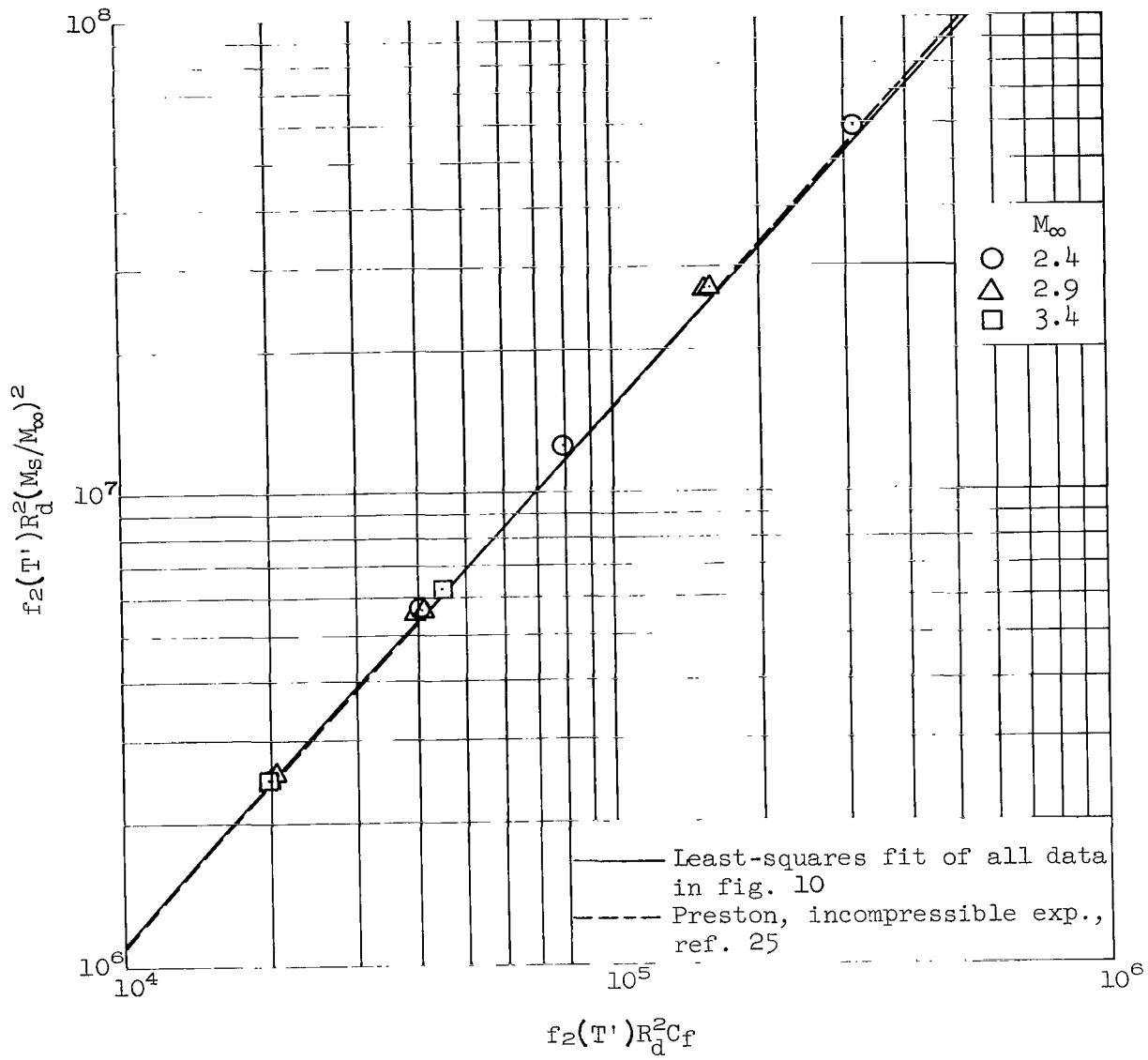
(b) Stalmach's supersonic data.

Figure 9.- Concluded.



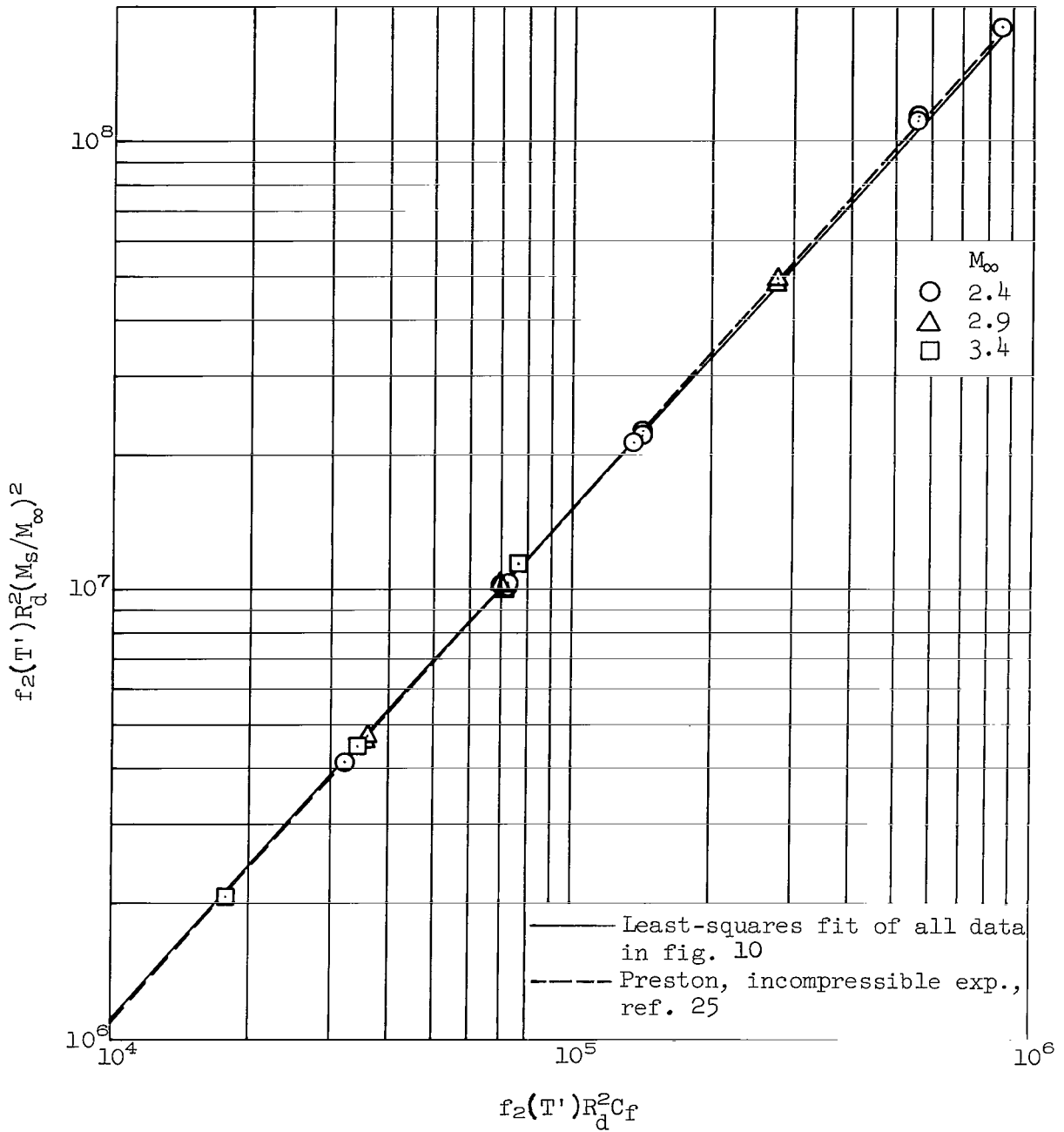
(a) $V_\infty/\nu_\infty = 1.0 \times 10^6$ per foot.

Figure 10.- Reynolds number and Mach number effects on the linear portion of the Preston tube calibration based on the new functional equation developed herein (eq. (4)). Present supersonic data.



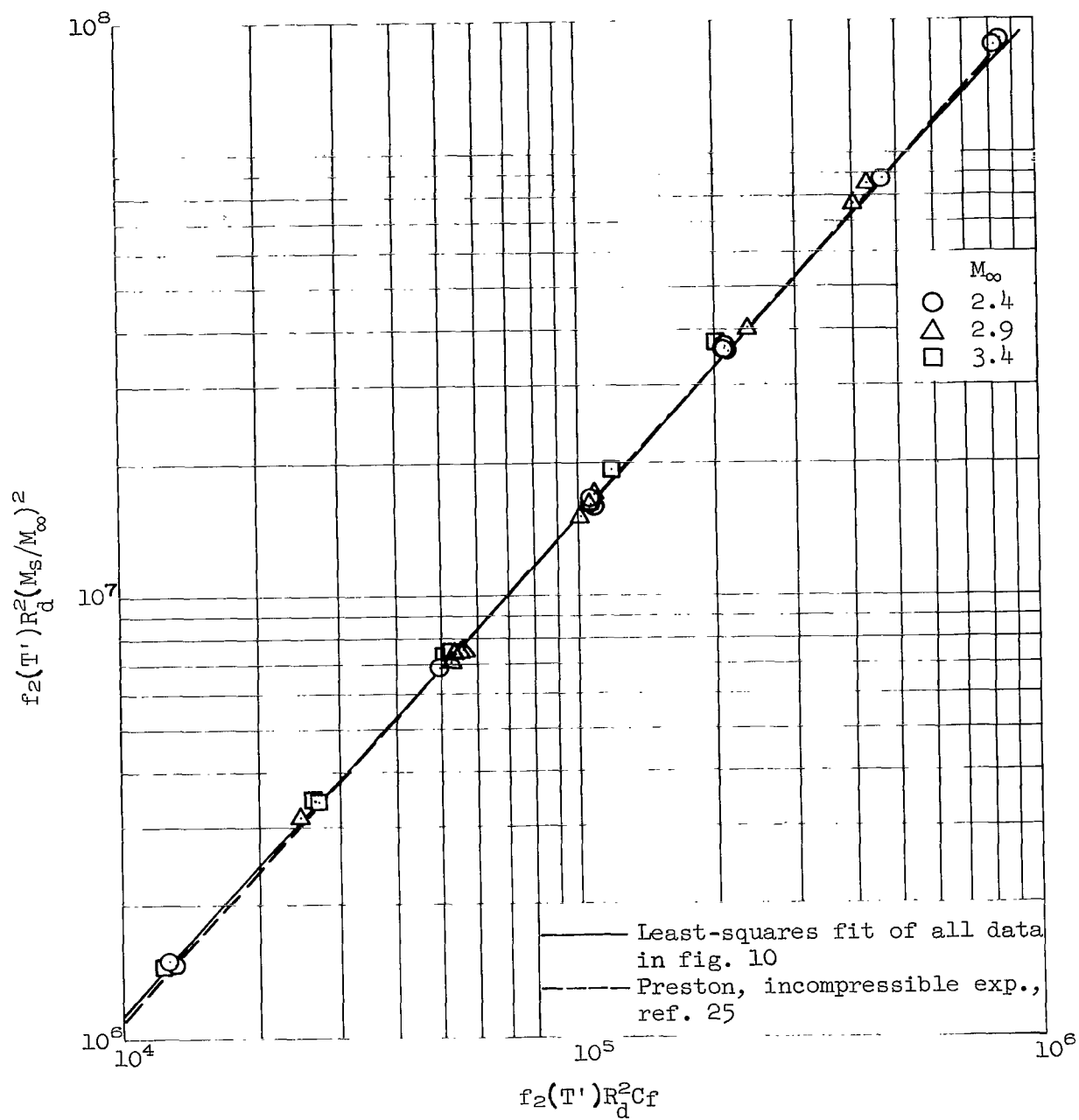
(b) $V_\infty/\nu_\infty = 1.5 \times 10^6$ per foot.

Figure 10.- Continued.



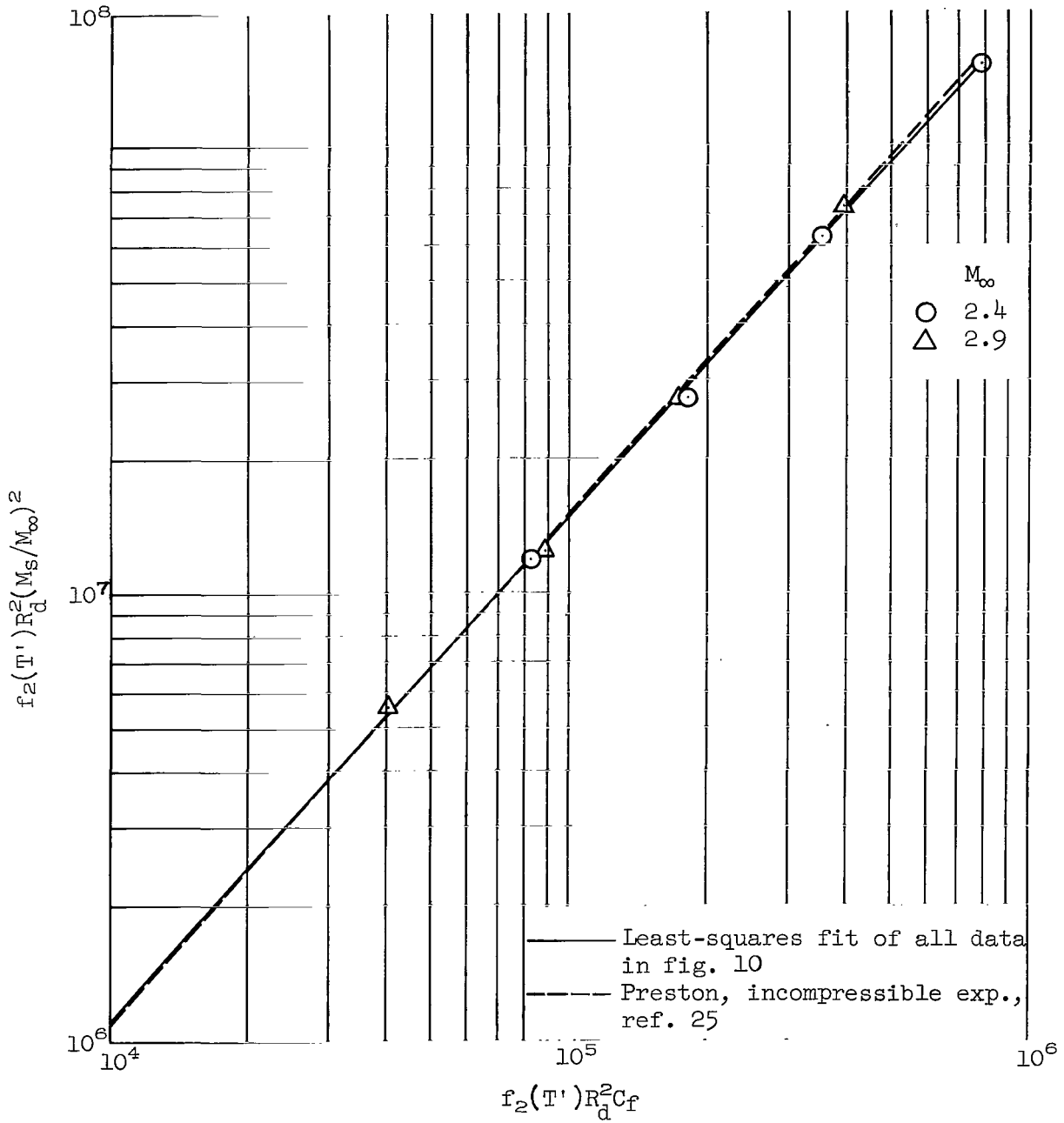
(c) $V_\infty/\nu_\infty = 2.0 \times 10^6$ per foot.

Figure 10.- Continued.



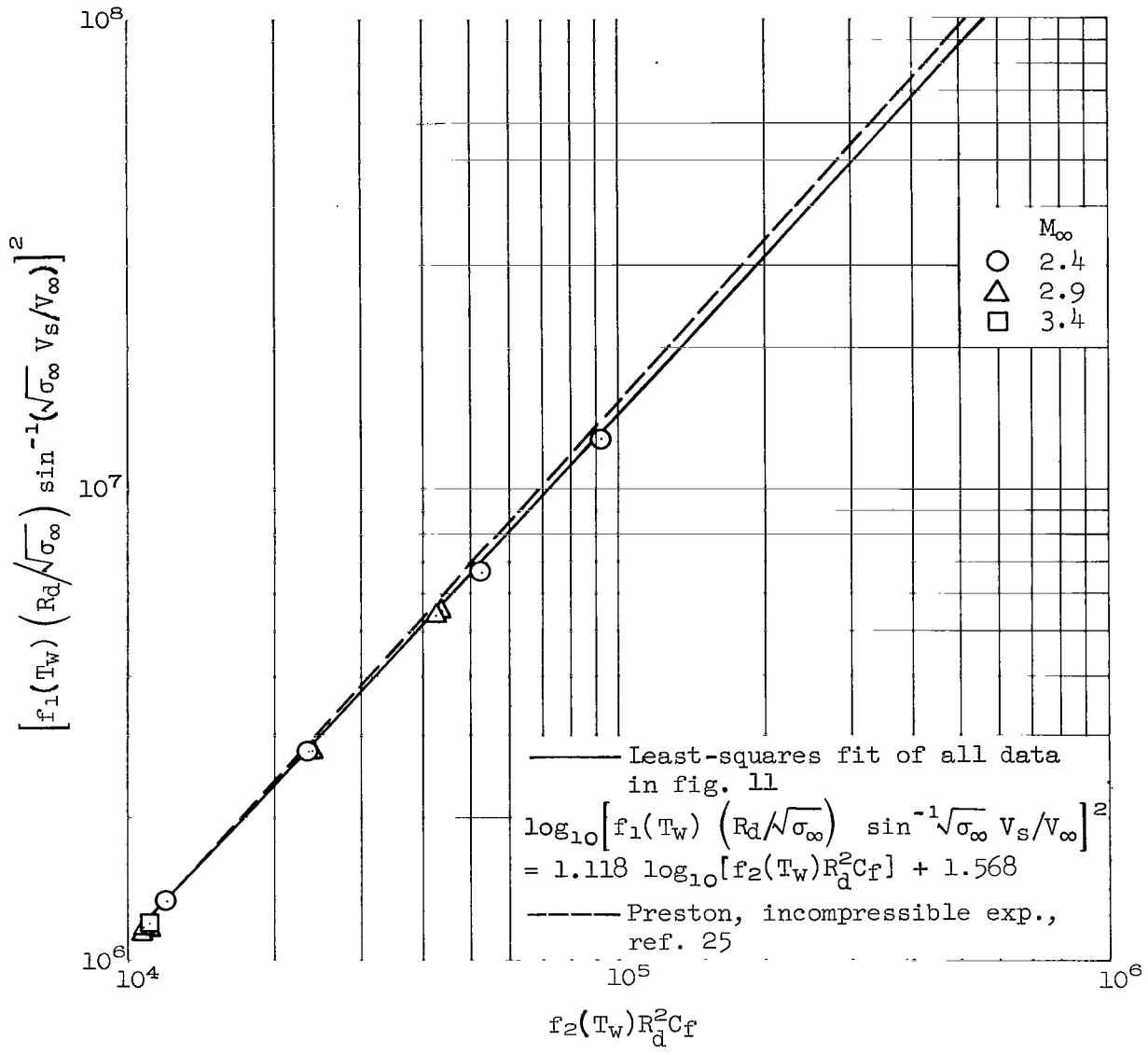
(d) $V_\infty/\nu_\infty = 2.5 \times 10^6$ per foot.

Figure 10.- Continued.



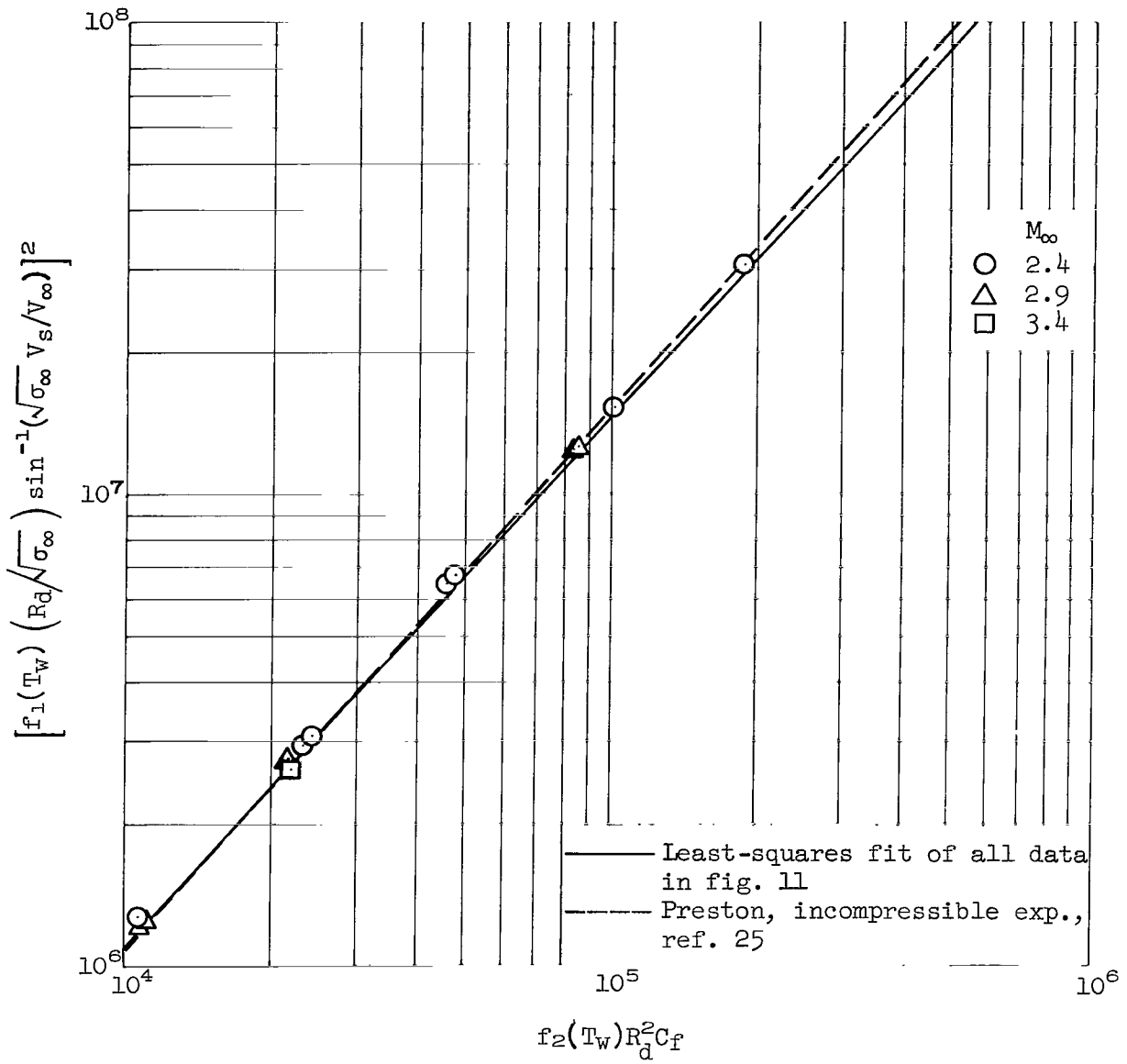
(e) $v_\infty/\nu_\infty = 3.2 \times 10^6$ per foot.

Figure 10.- Concluded.



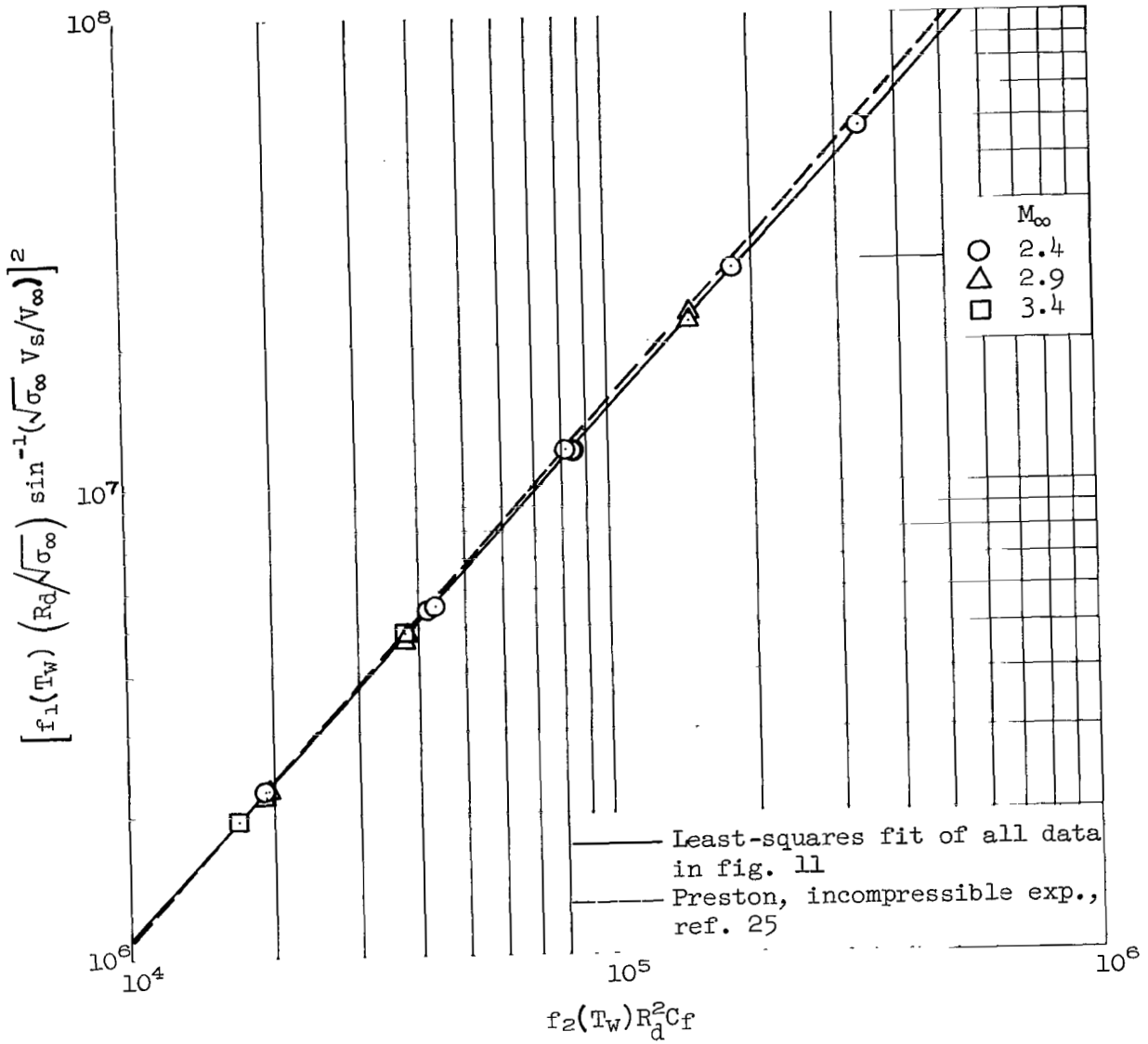
(a) $V_\infty/\nu_\infty = 1 \times 10^6$ per foot.

Figure 11.- Reynolds number and Mach number effects on the linear portion of the Preston tube calibration based on the functional equation (B11). Present supersonic data.



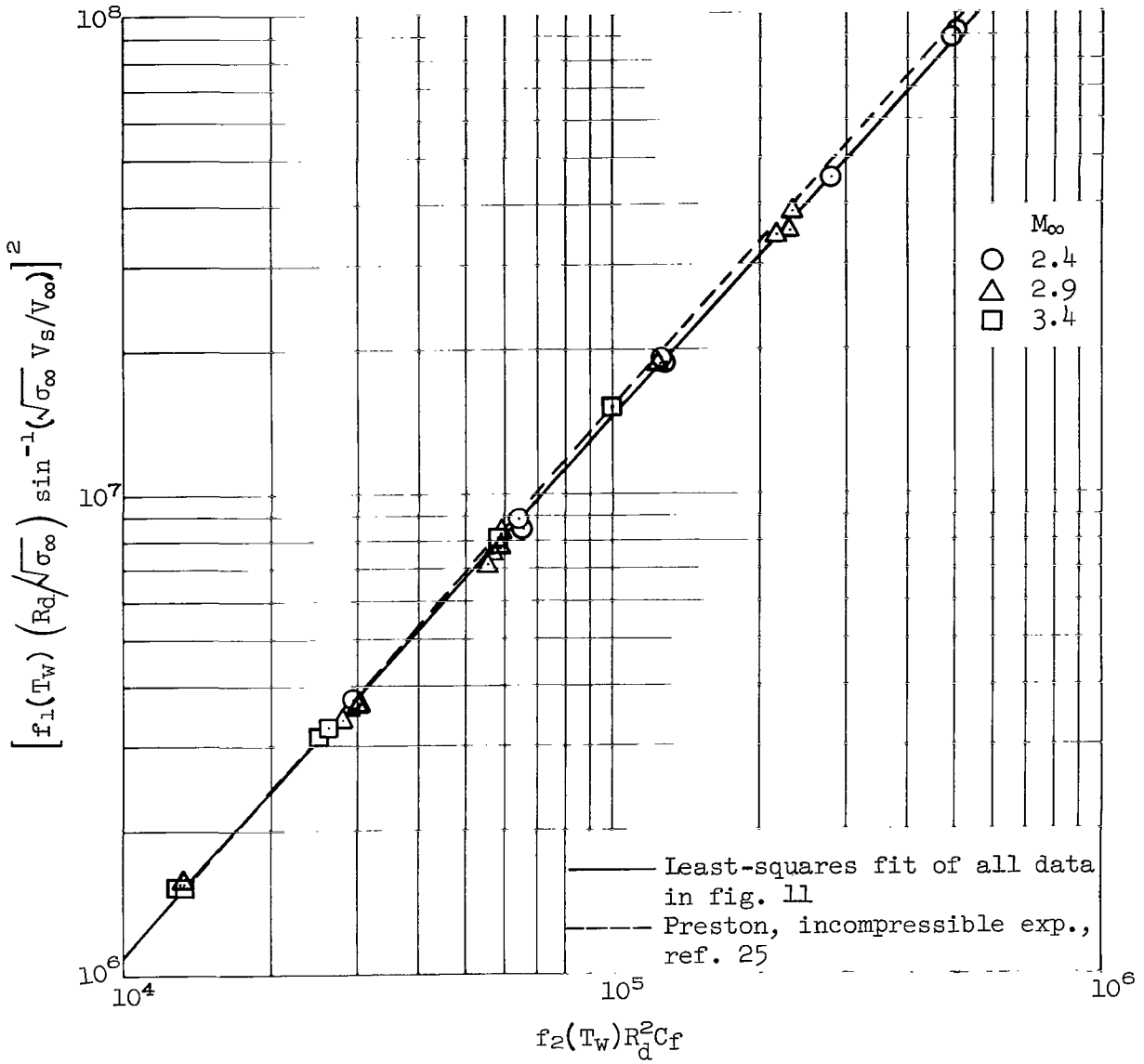
(b) $V_{\infty}/\nu_{\infty} = 1.5 \times 10^6$ per foot.

Figure 11.- Continued.



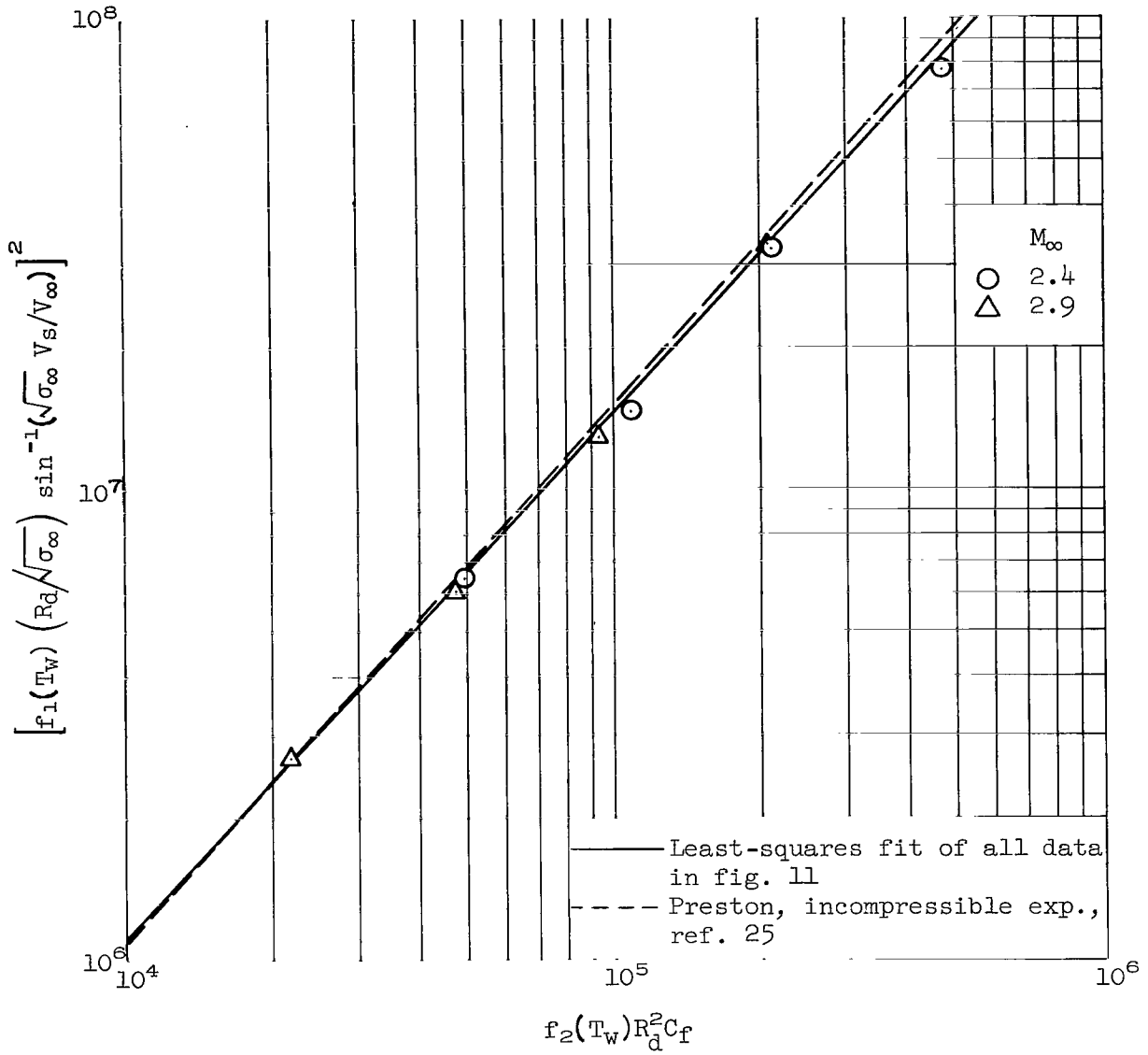
(c) $V_\infty/\nu_\infty = 2.0 \times 10^6$ per foot.

Figure 11.- Continued.



(d) $V_\infty/\nu_\infty = 2.5 \times 10^6$ per foot.

Figure 11.- Continued.



(e) $V_\infty/\nu_\infty = 3.2 \times 10^6$ per foot.

Figure 11.- Concluded.

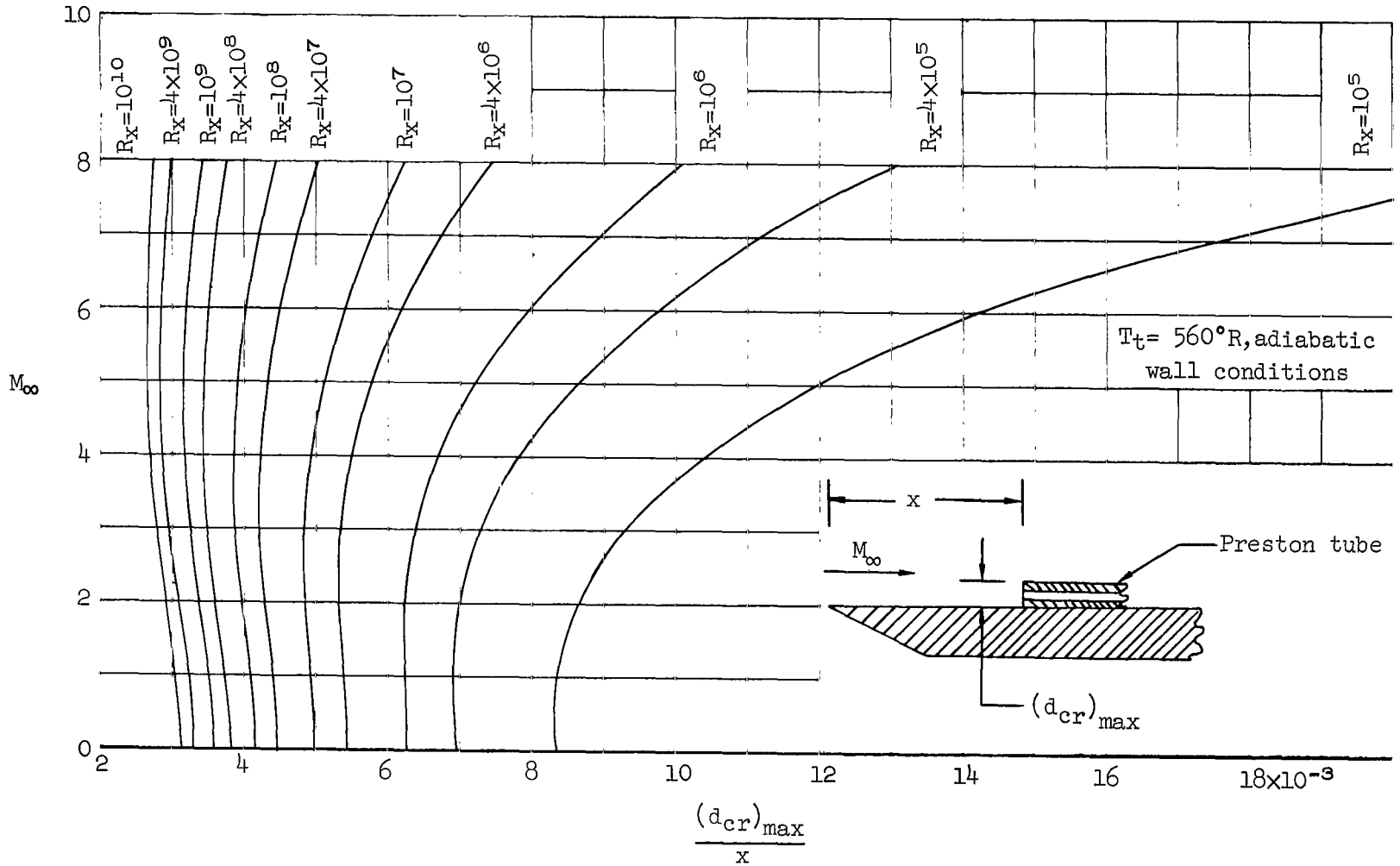


Figure 12.- Effect of Mach number and Reynolds number on the maximum critical tube diameter for which the Preston tube calibration is expected to be valid.

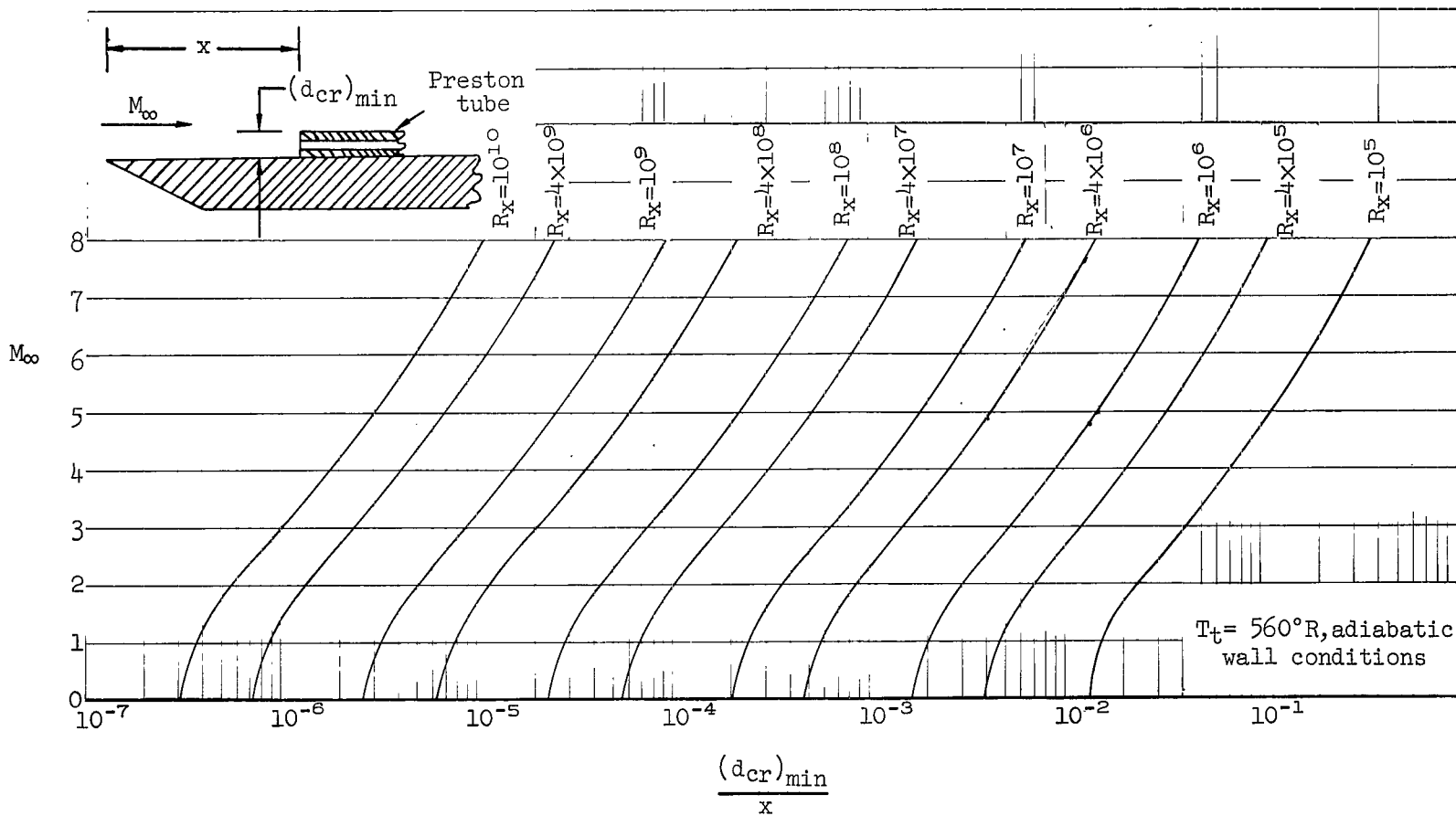


Figure 13.- Effect of Mach number and Reynolds number on the minimum critical tube diameter for which the Preston tube calibration is linear.

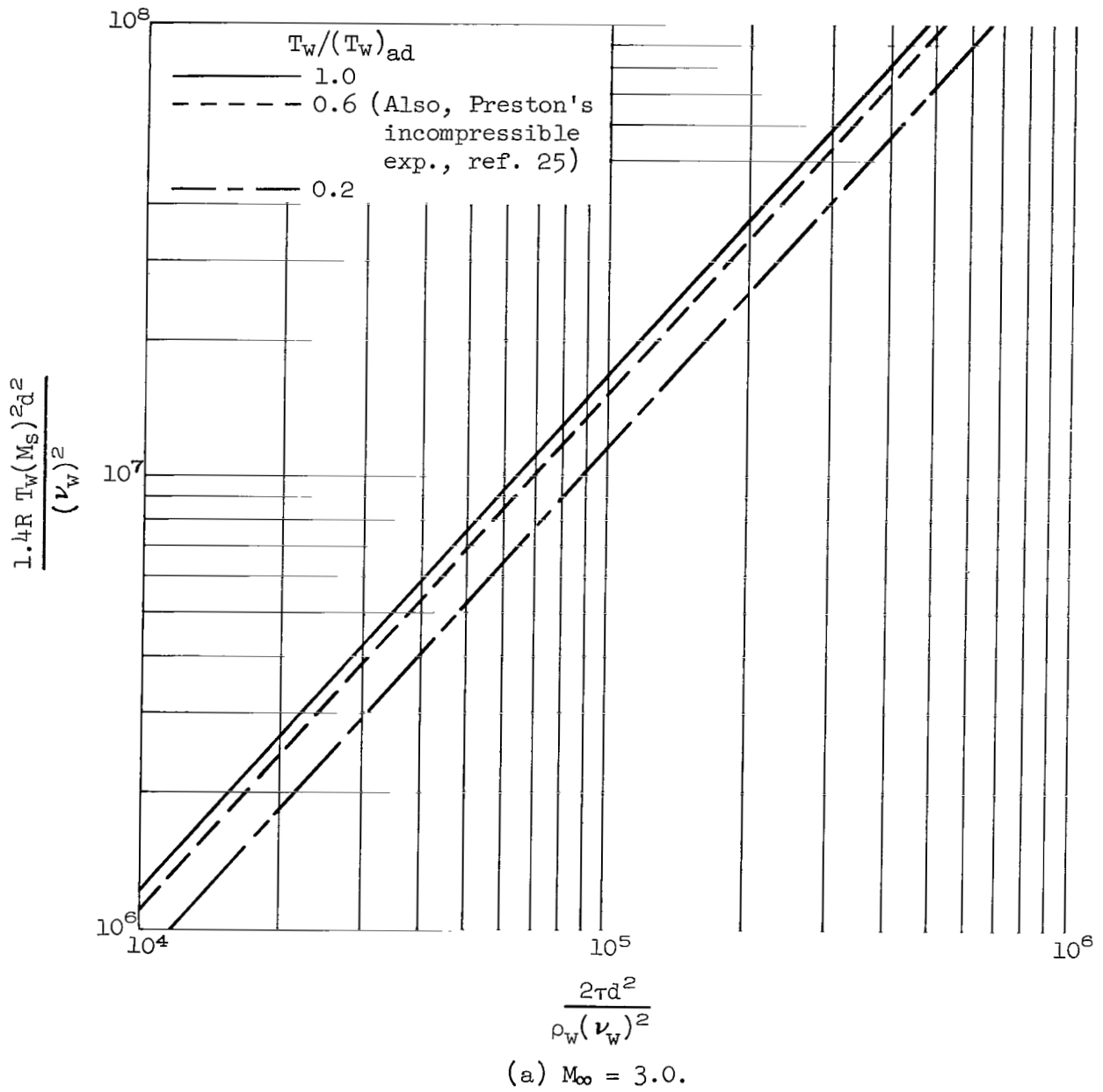
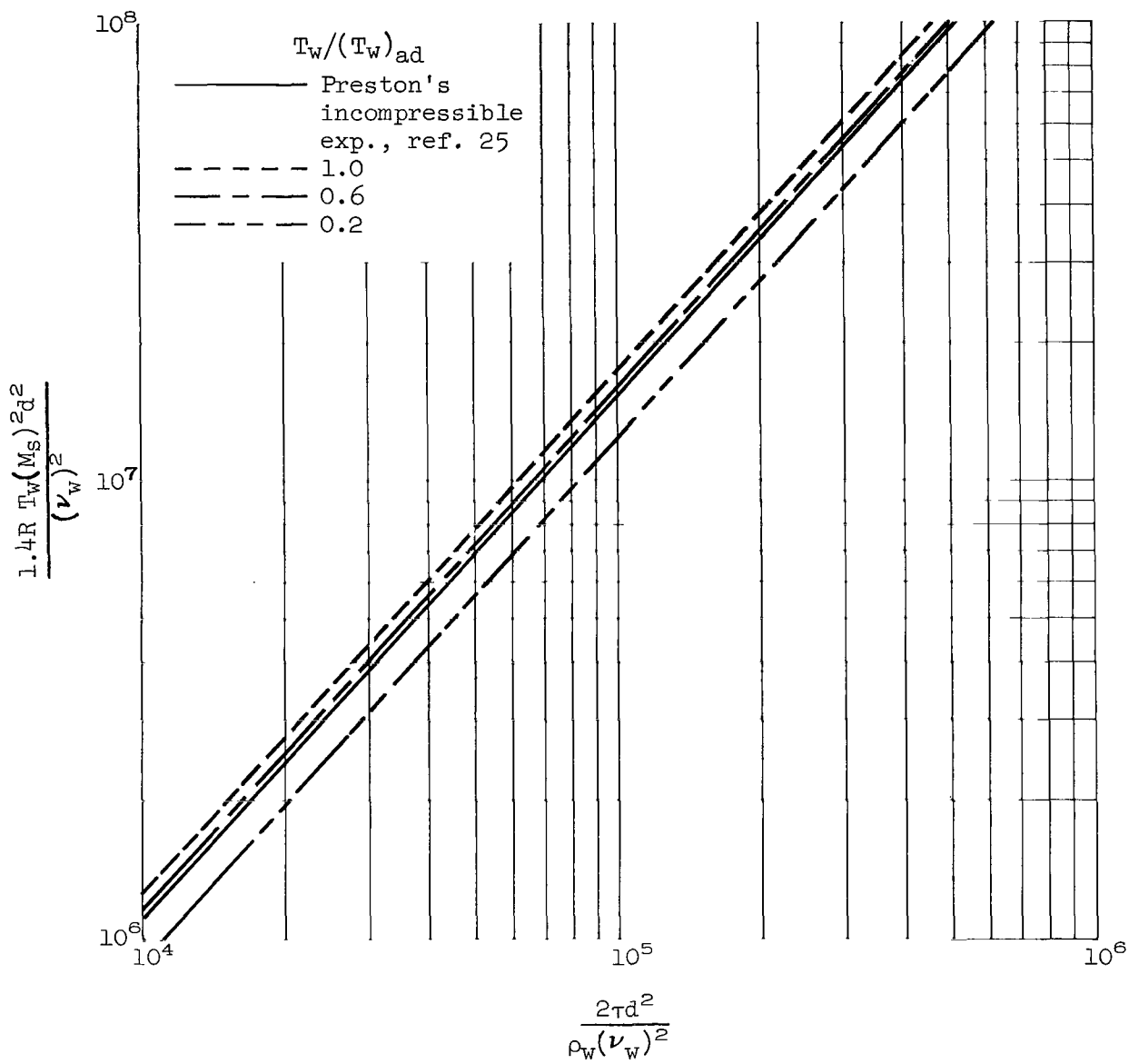


Figure 14.- Estimated effect of heat transfer on the Preston tube calibration at several Mach numbers when the calibration factors are based on wall conditions; sharp leading edge.



(b) $M_\infty = 5.0$.

Figure 14.- Continued.

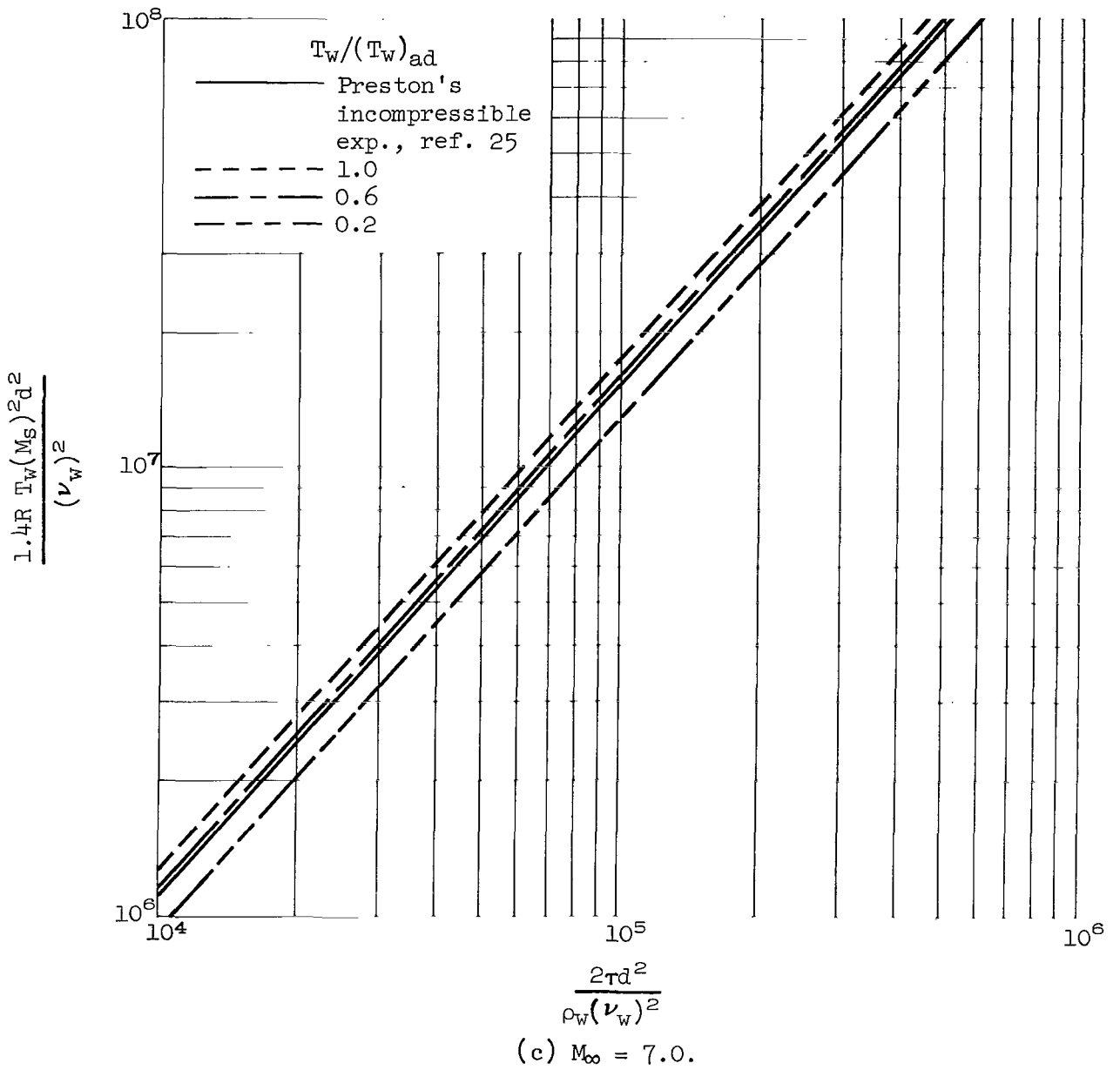
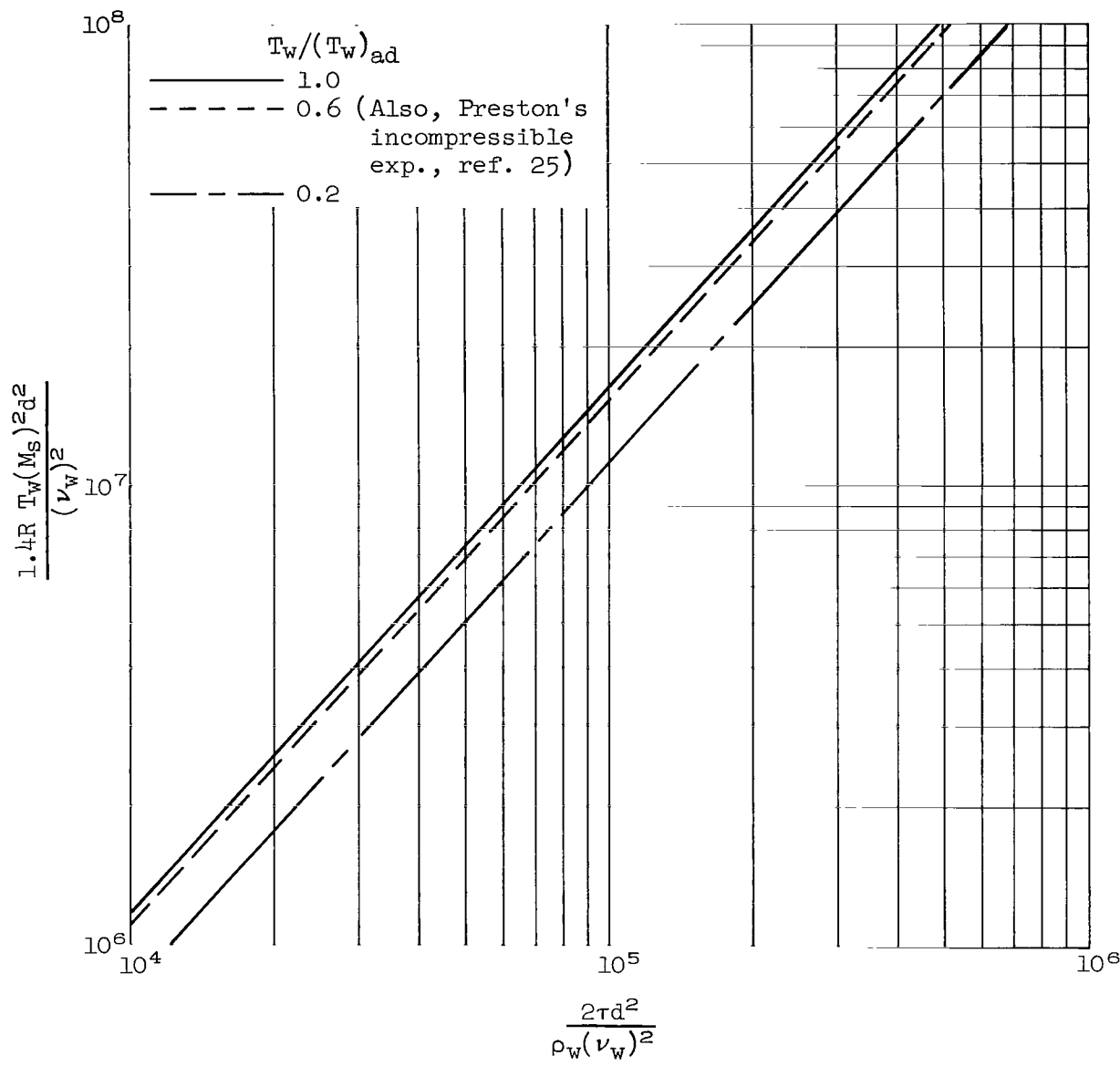
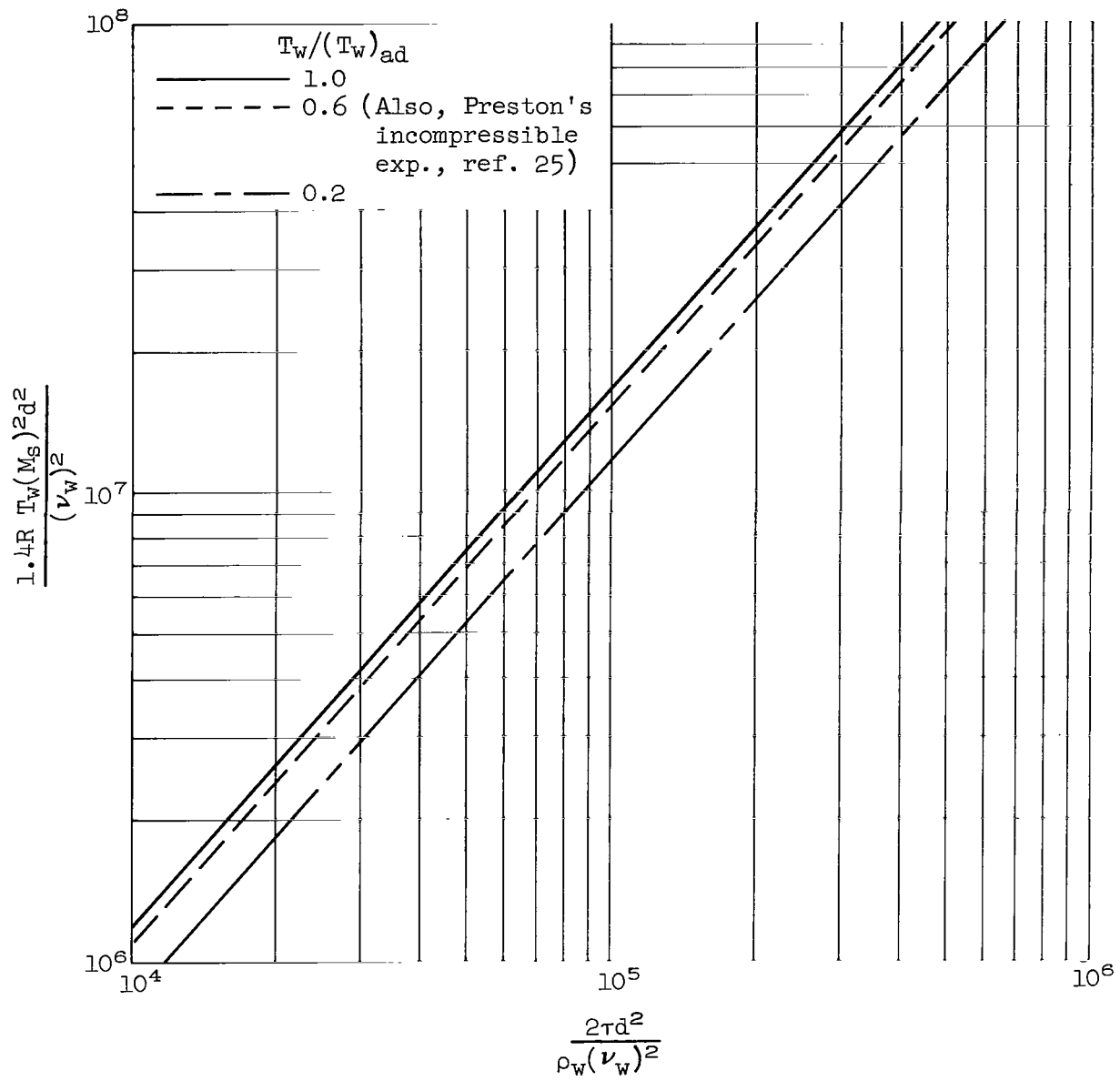


Figure 14.- Concluded.



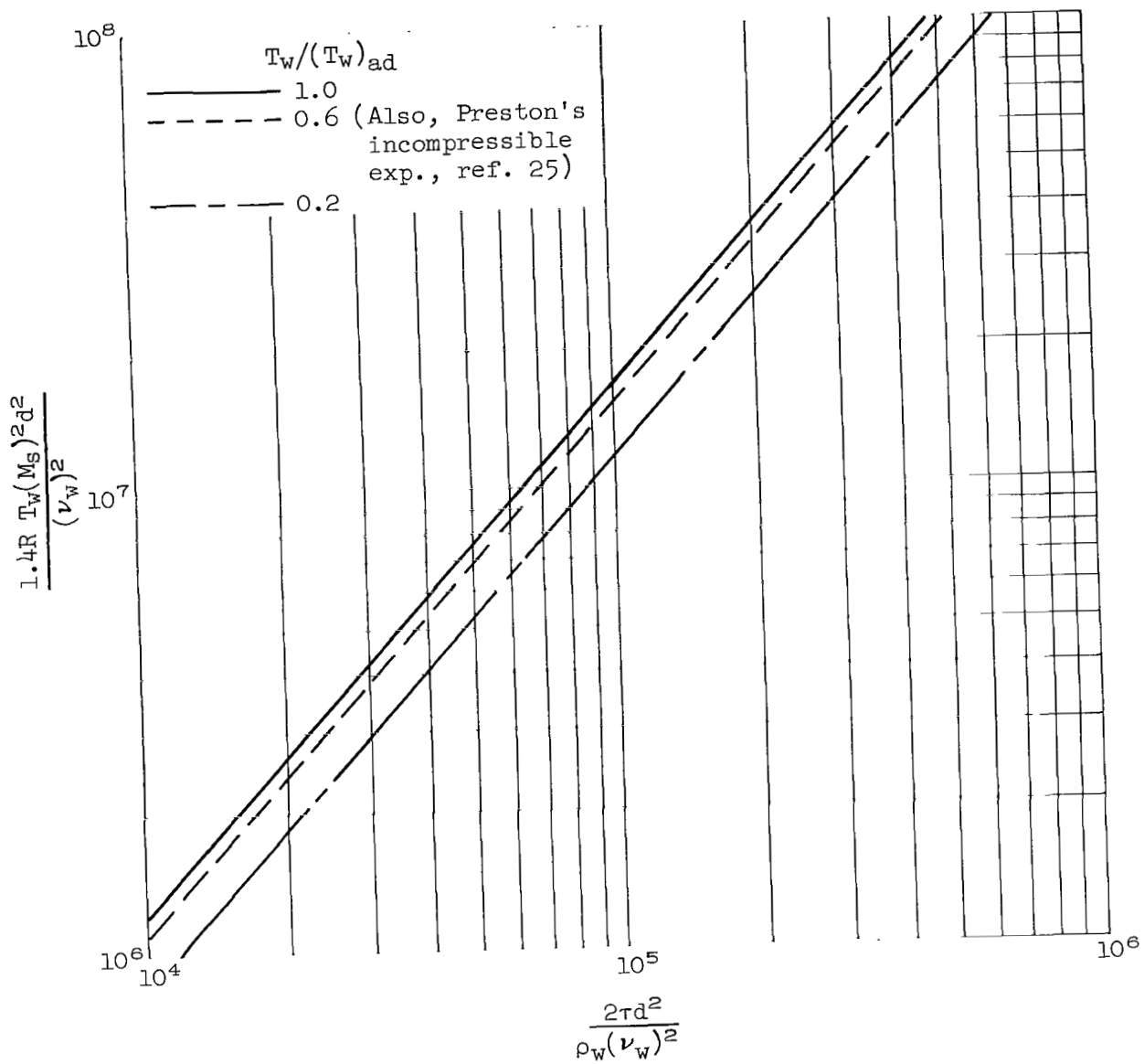
(a) $M_\infty = 3.0$.

Figure 15.- Estimated effect of heat transfer on the Preston tube calibration at several Mach numbers when the calibration factors are based on wall conditions; blunt leading edge.



(b) $M_\infty = 5.0$.

Figure 15.- Continued.



(c) $M_\infty = 7.0$.

Figure 15.- Concluded.

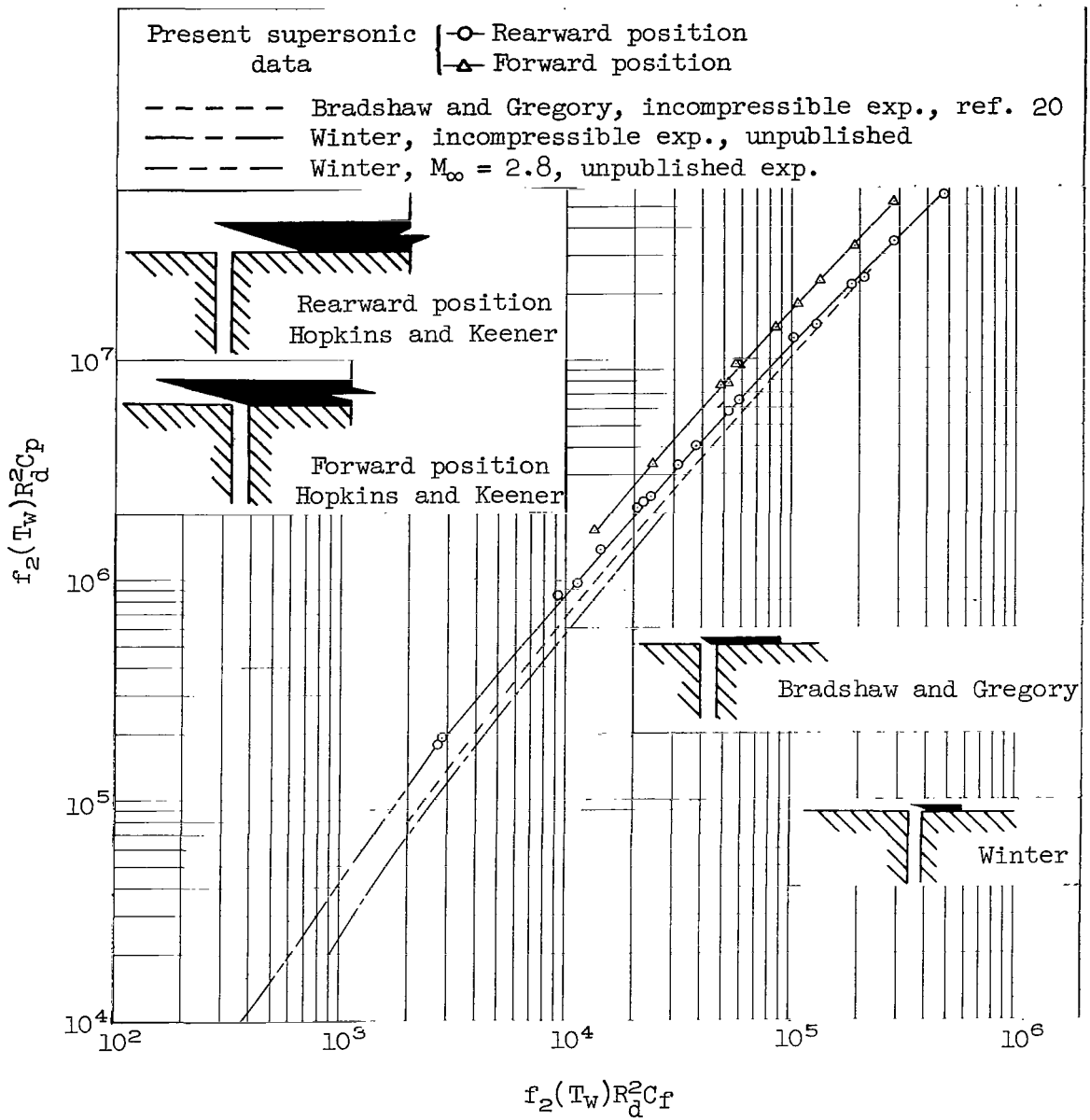


Figure 16.- Stanton tube calibration based on the functional equation (B6).
Present supersonic data.

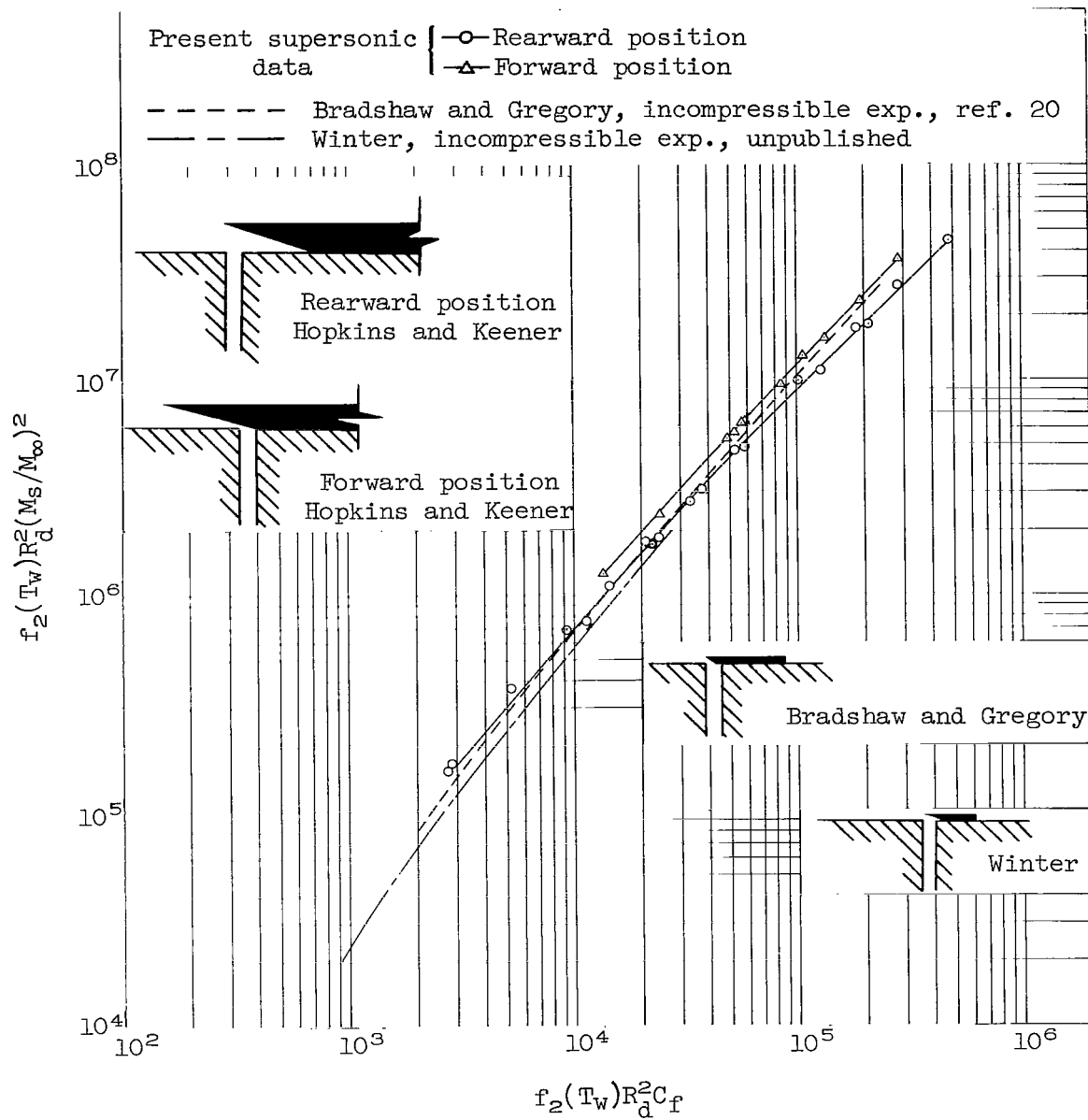


Figure 17.- Stanton tube calibration based on the functional equation (2).
Present supersonic data.

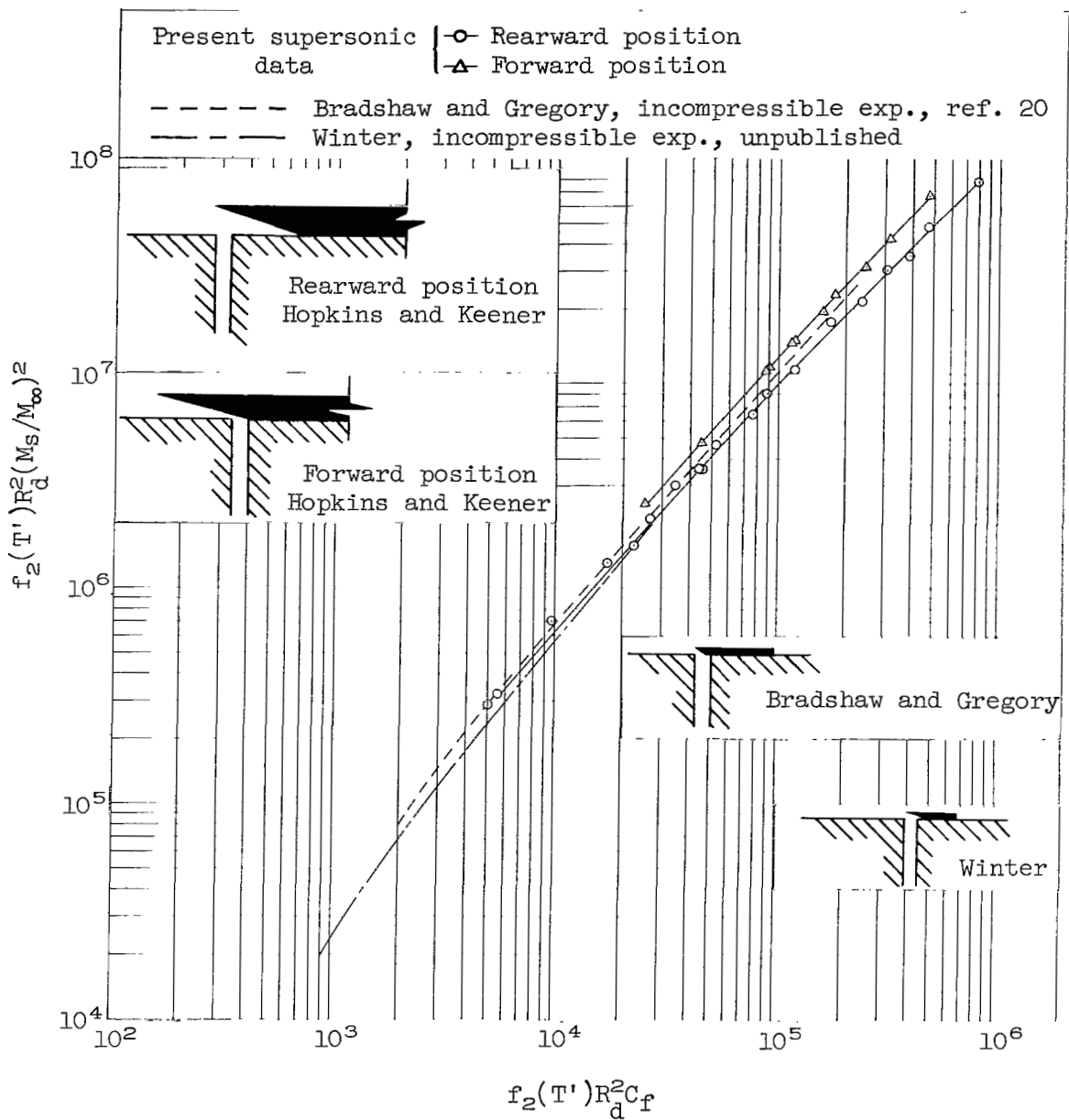


Figure 18.- Stanton tube calibration based on the new functional equation developed herein (eq. (4)). Present supersonic data

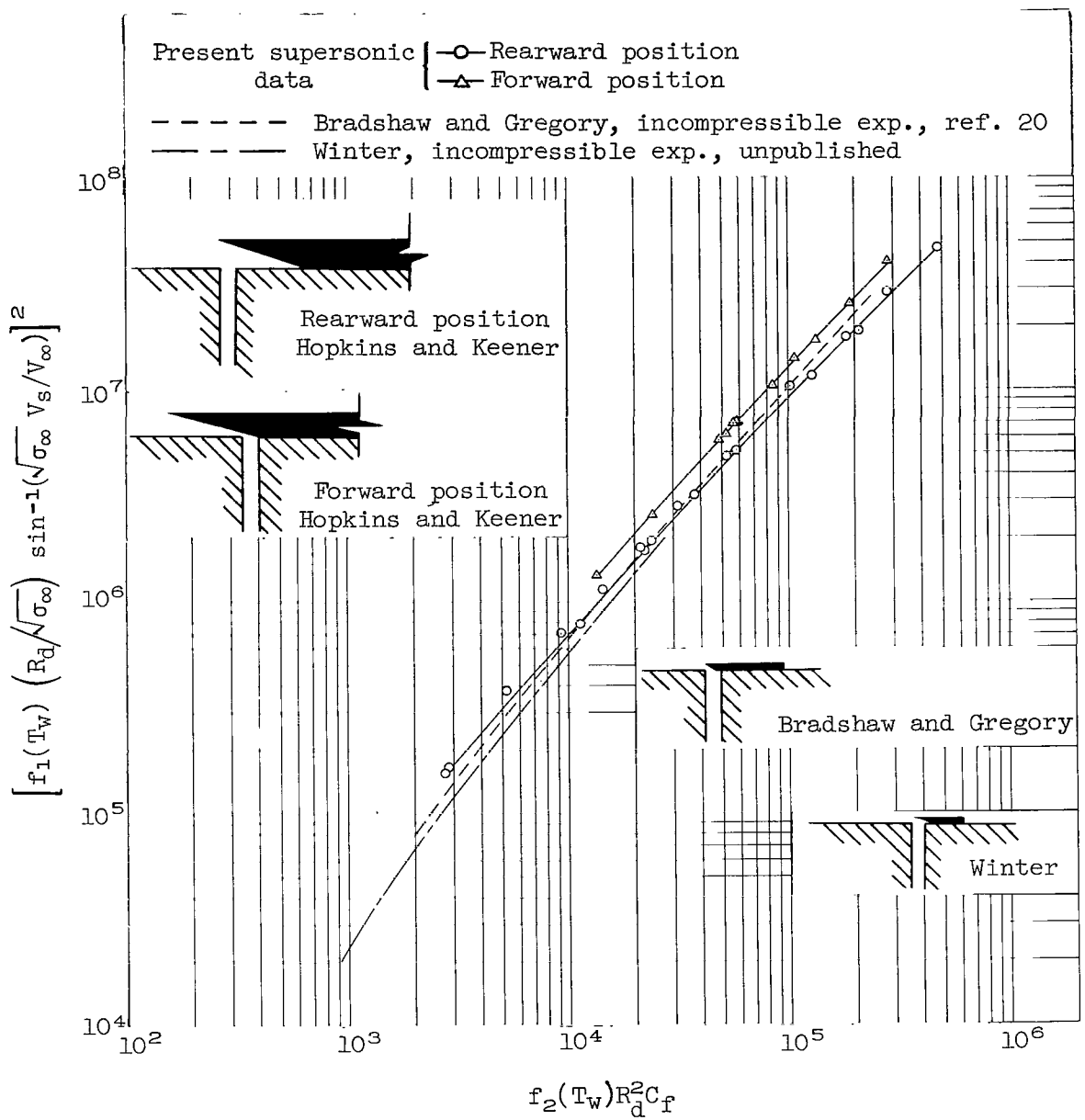


Figure 19.- Stanton tube calibration based on the functional equation (B11). Present supersonic data.

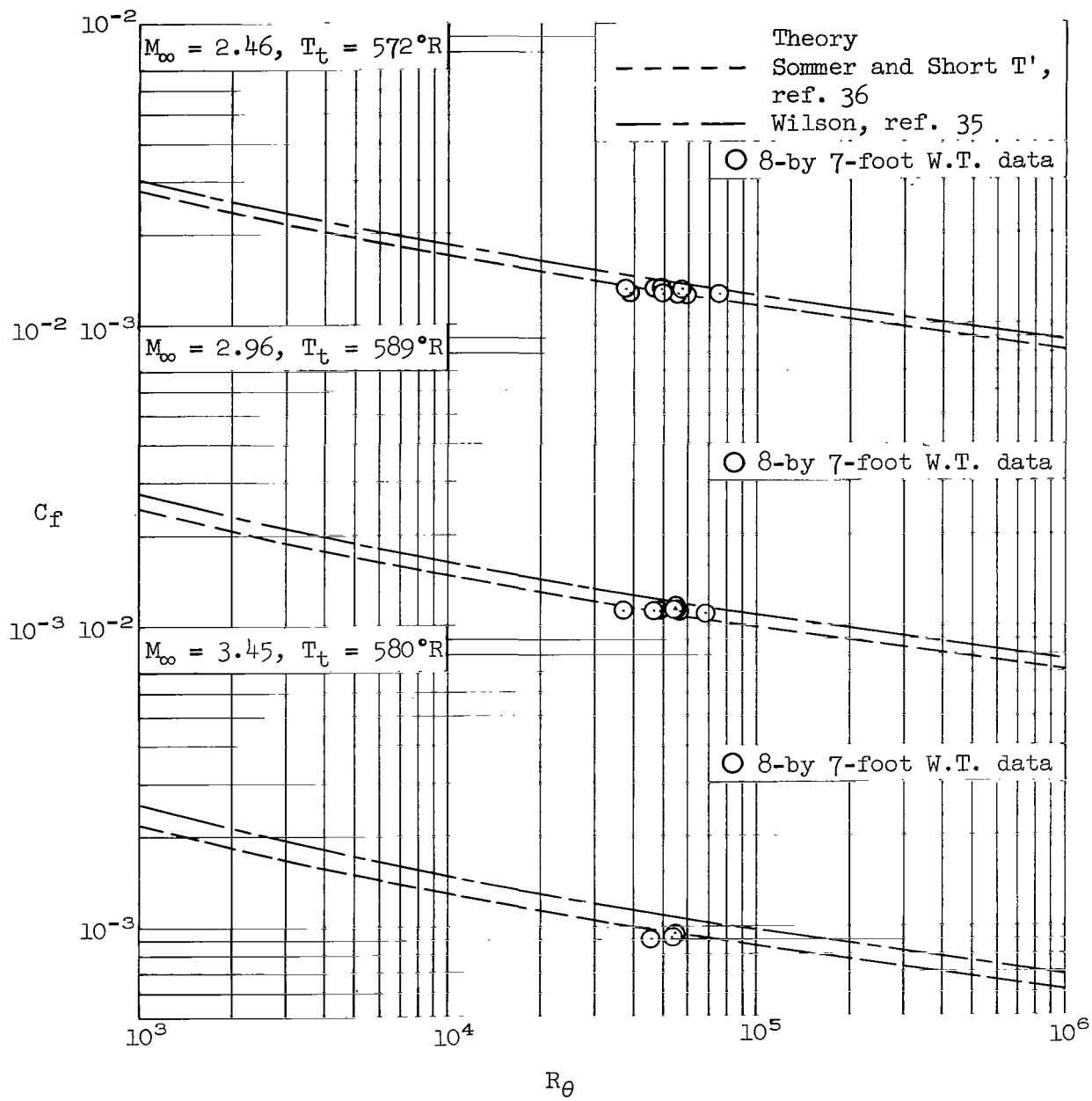
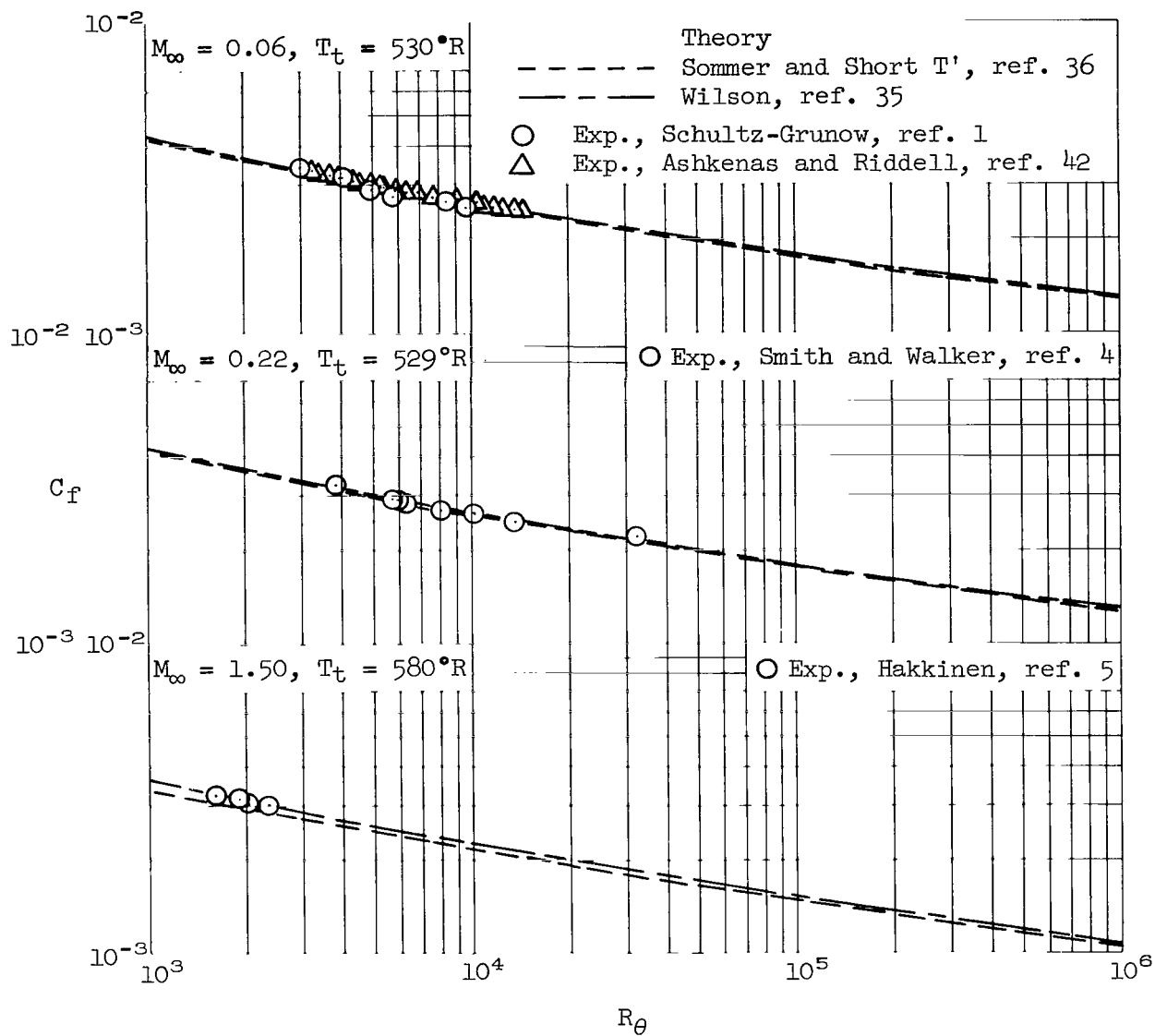
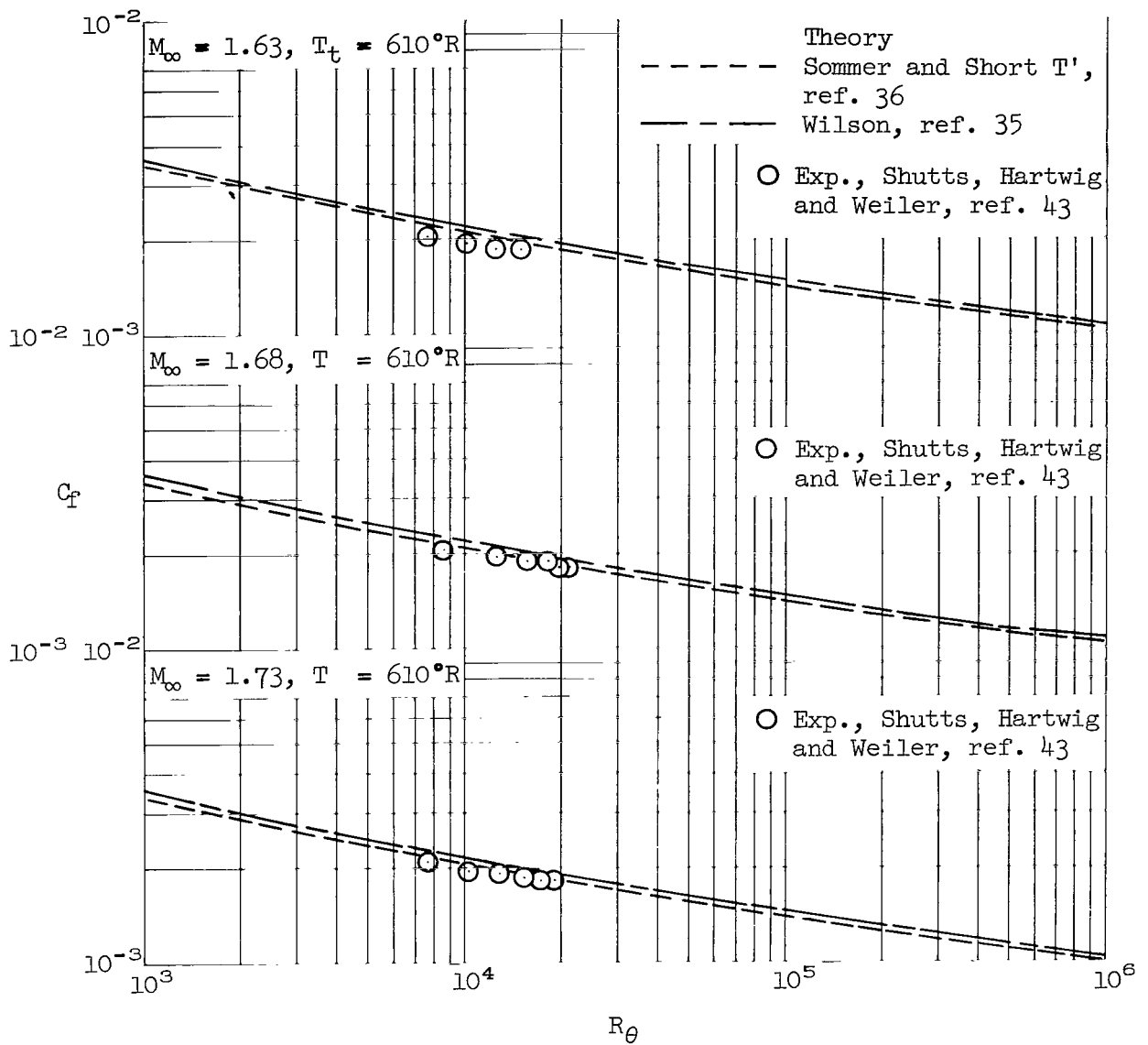


Figure 20.- Variation of local skin-friction coefficient with Reynolds number based on momentum thickness. Present data.



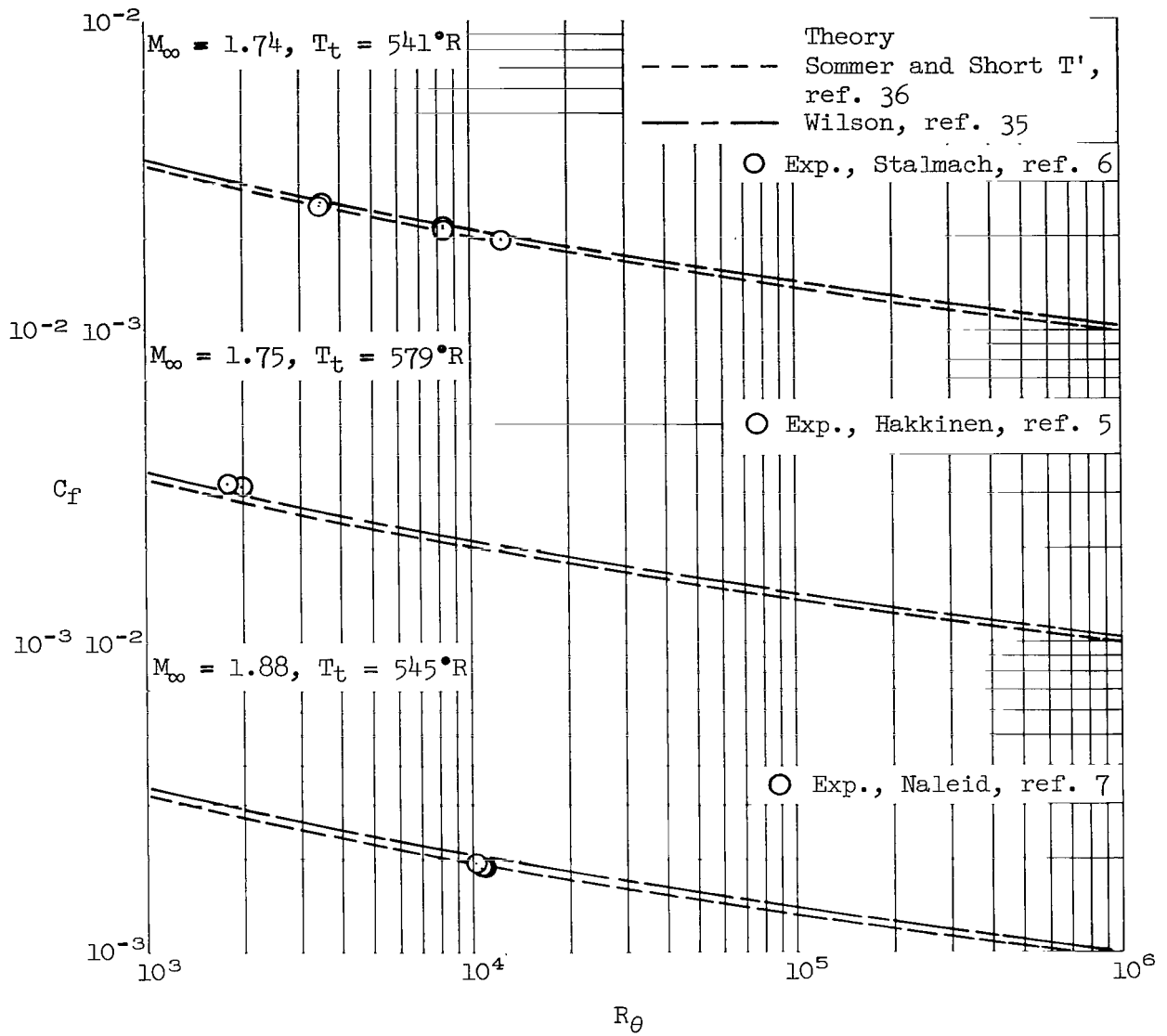
(a) $M_\infty = 0.06, 0.22$ and 1.50 .

Figure 21.- Variation of local skin-friction coefficient with Reynolds number based on momentum thickness. Data from other sources.



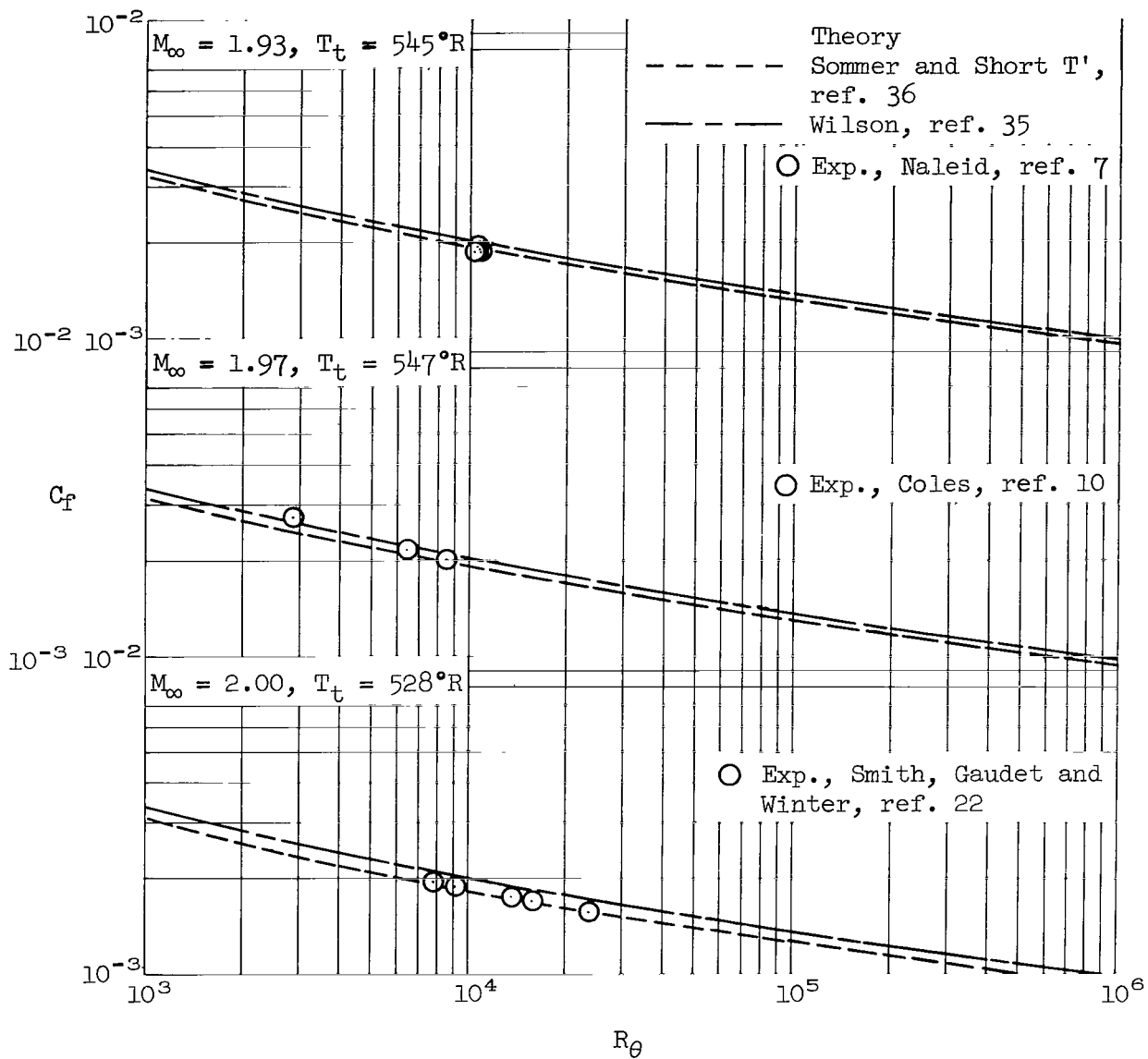
(b) $M_\infty = 1.63, 1.68$ and 1.73 .

Figure 21.- Continued.



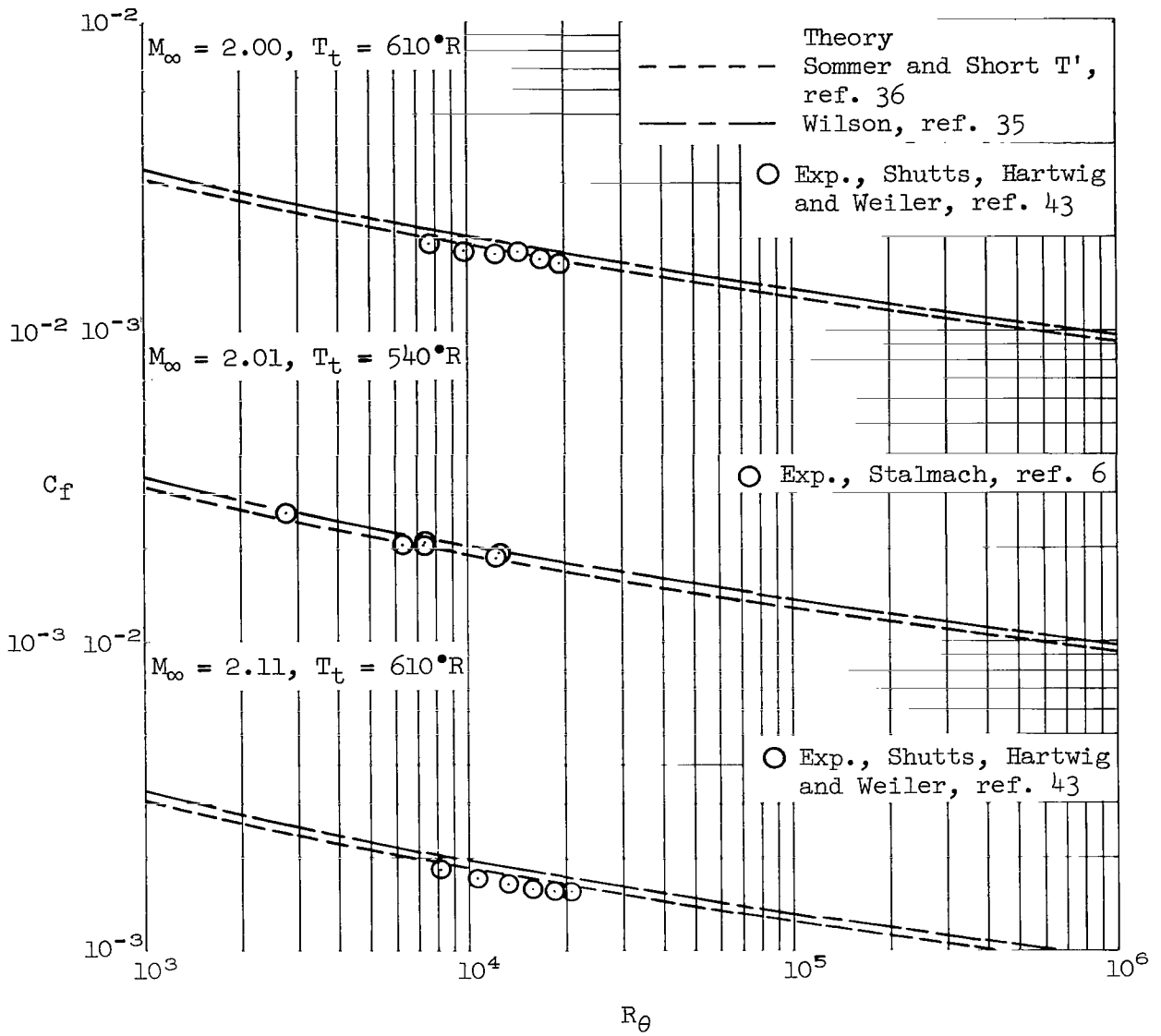
(c) $M_\infty = 1.74, 1.75$ and 1.88 .

Figure 21.- Continued.



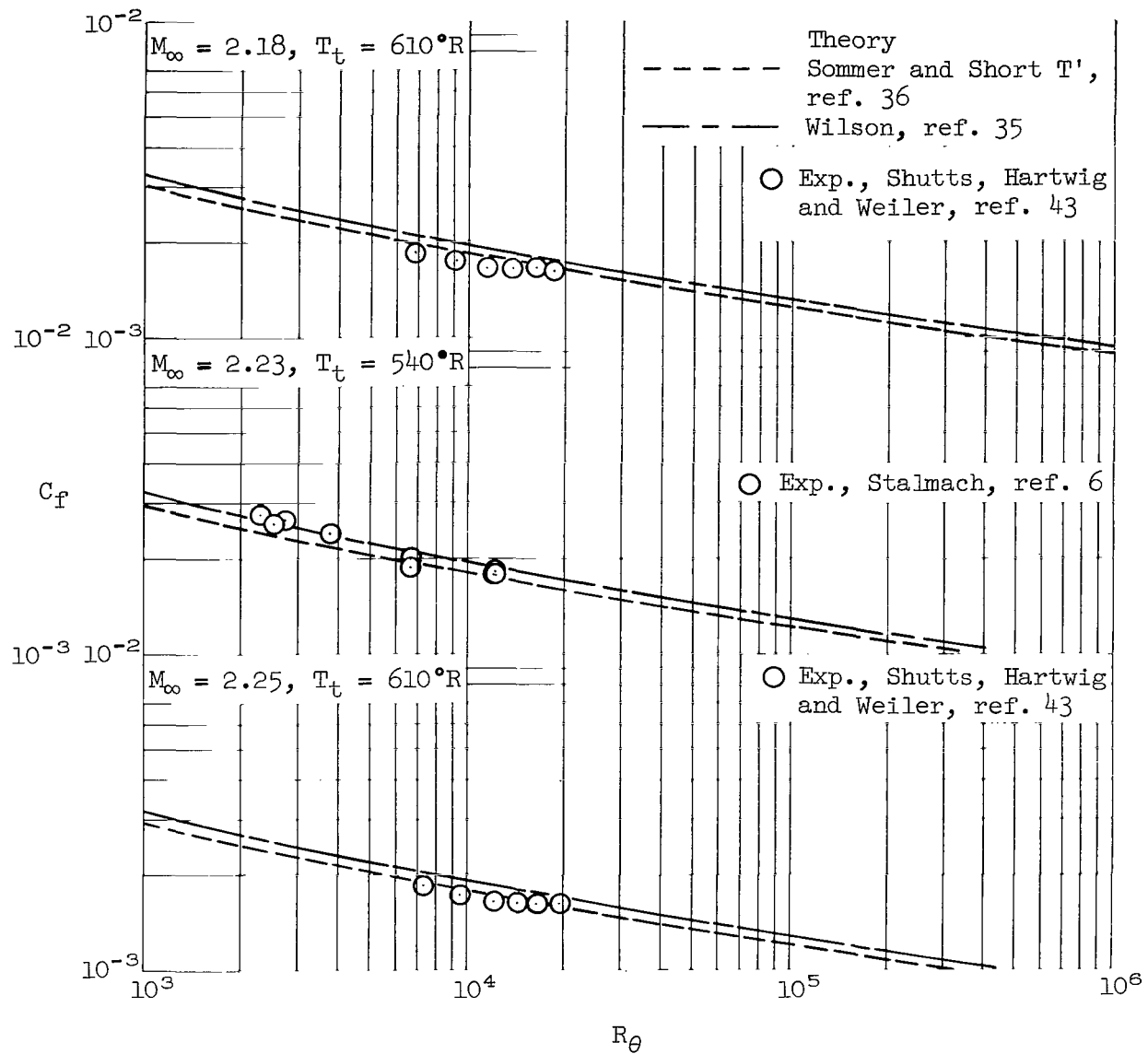
(d) $M_\infty = 1.93, 1.97$ and 2.00 .

Figure 21.- Continued.



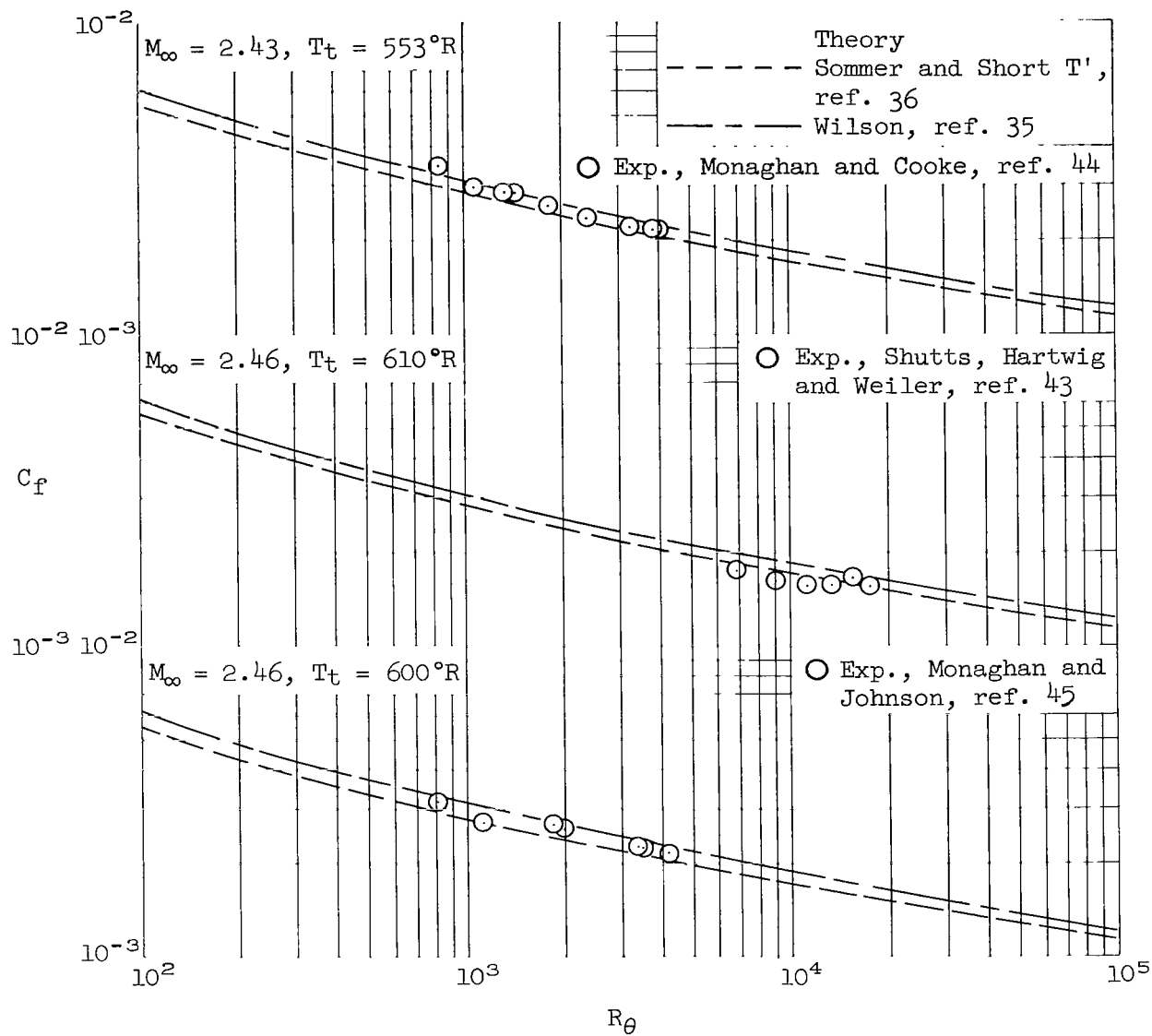
(e) $M_\infty = 2.00, 2.01$ and 2.11 .

Figure 21.- Continued.



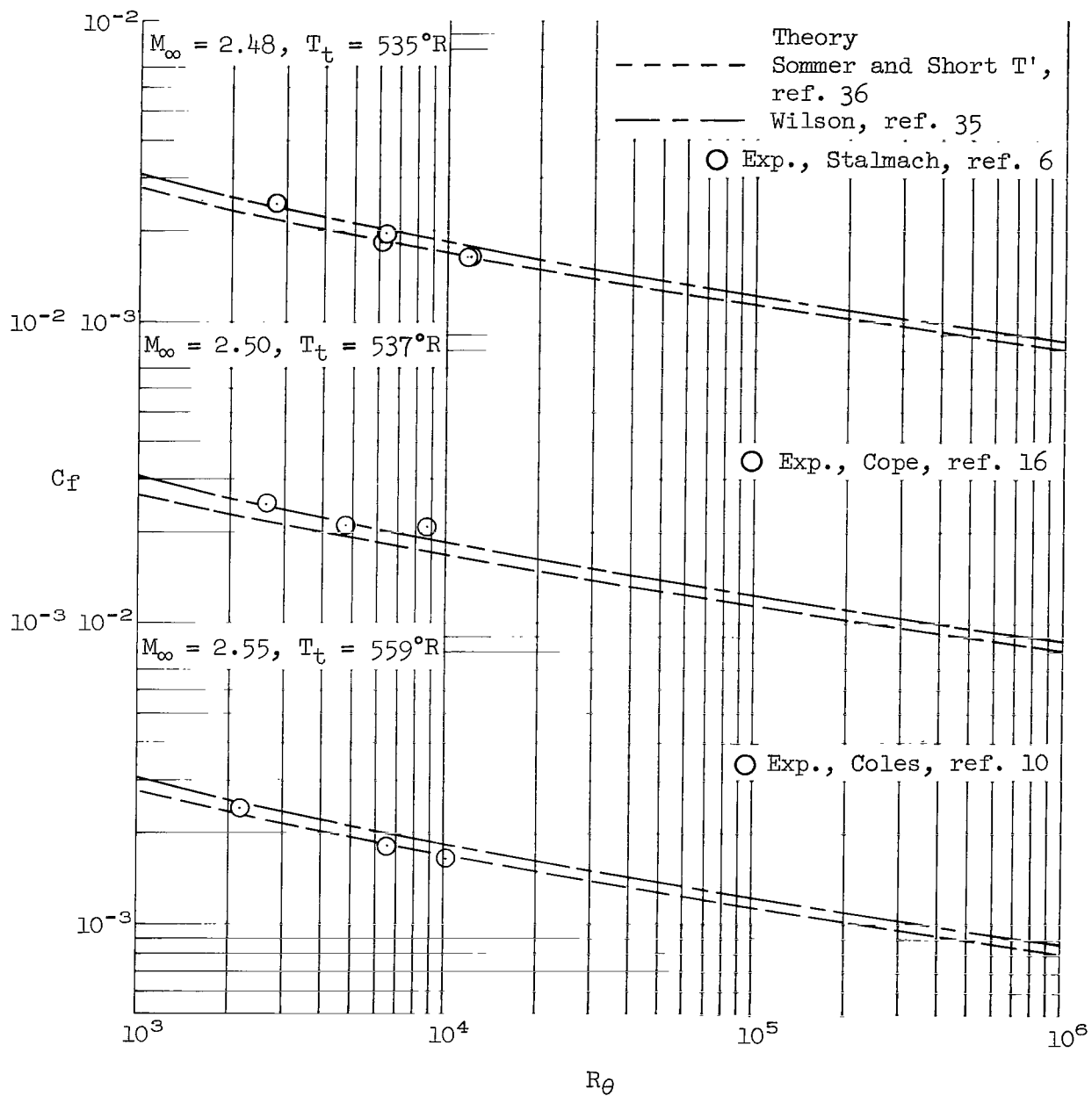
(f) $M_\infty = 2.18, 2.23$ and 2.25 .

Figure 21.- Continued.



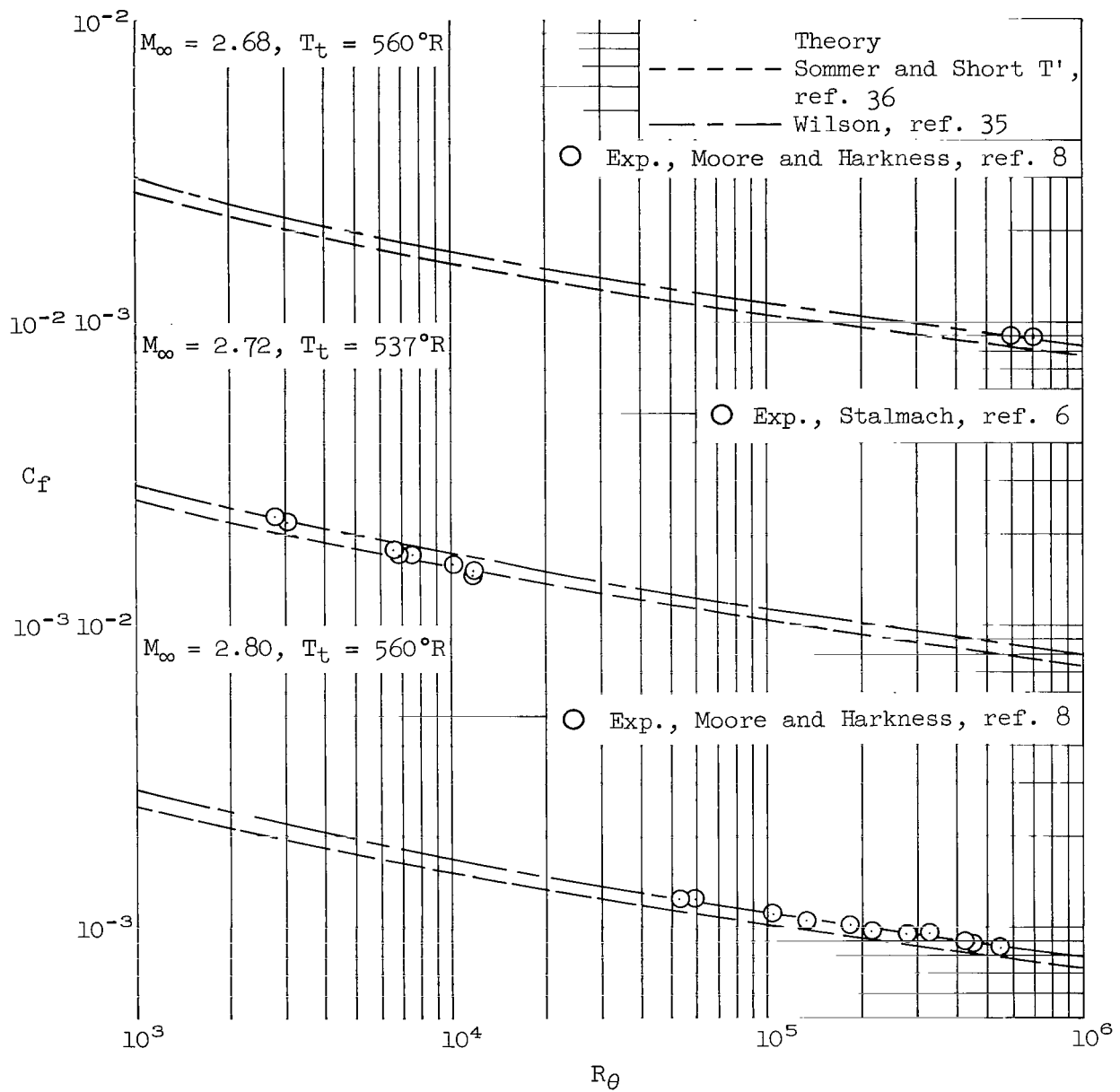
(g) $M = 2.43$ and 2.46 .

Figure 21. Continued.



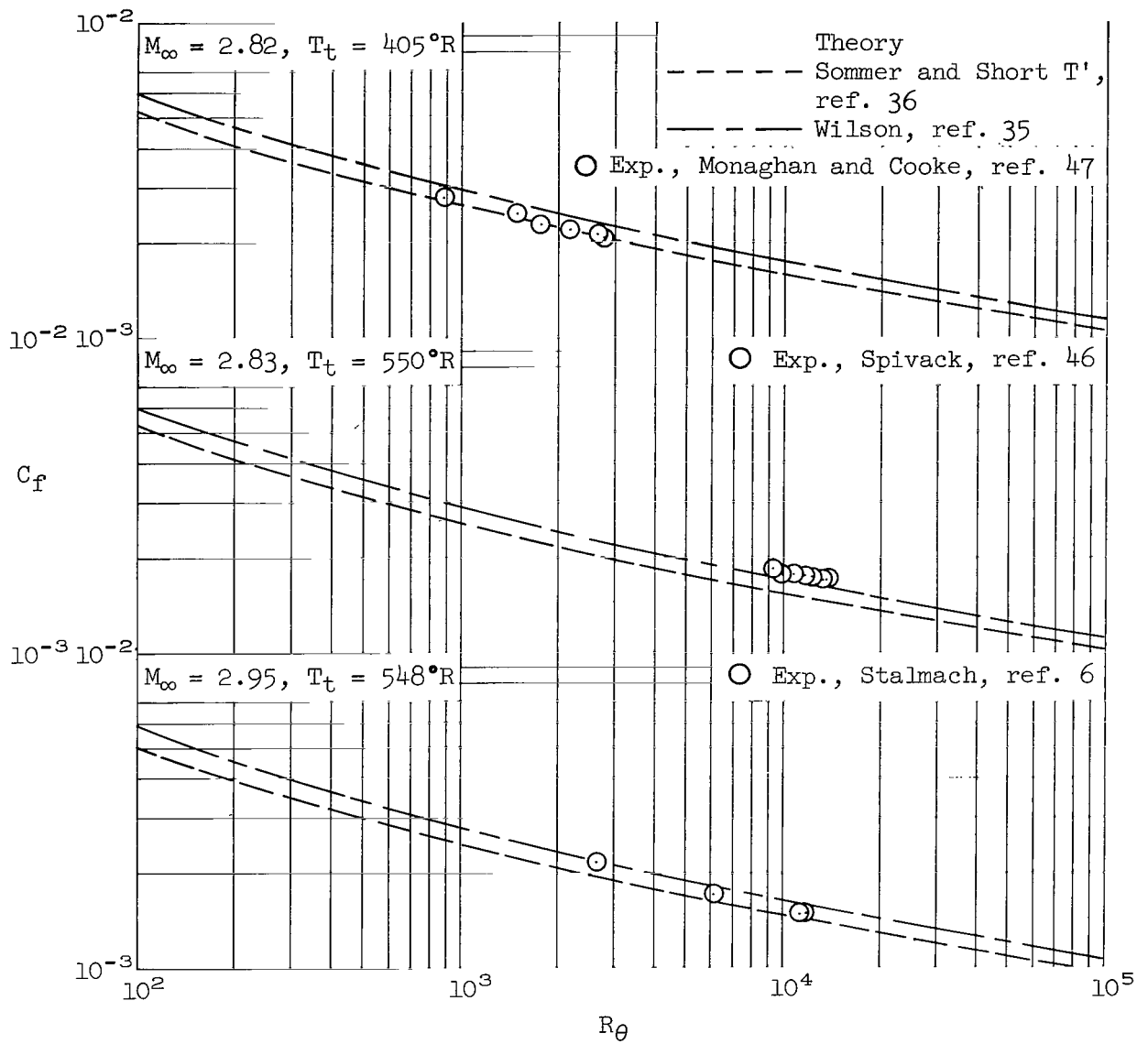
(h) $M_\infty = 2.48, 2.50$ and 2.55 .

Figure 21.- Continued.



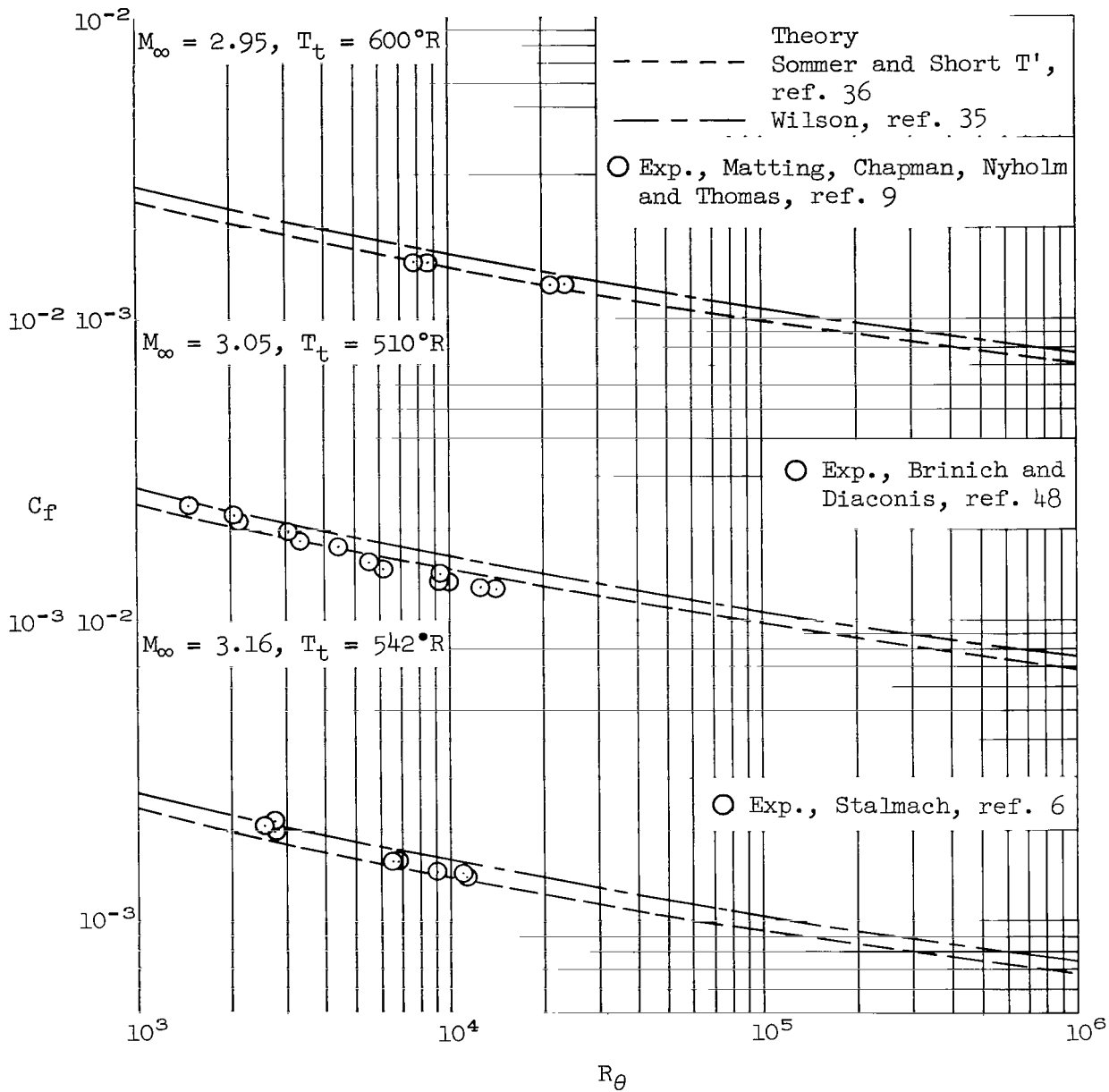
(i) $M_\infty = 2.68, 2.72$ and 2.80 .

Figure 21.- Continued.



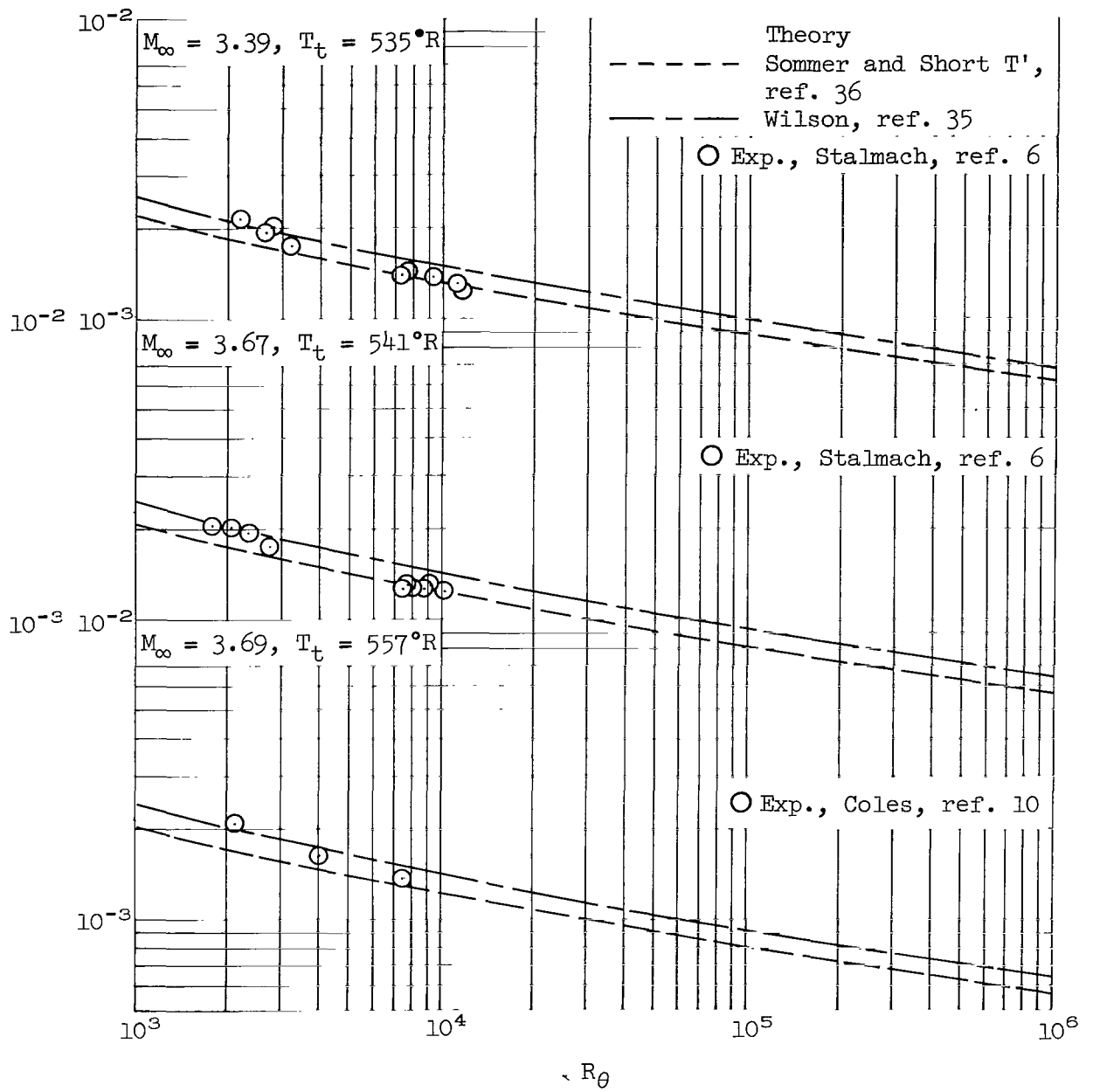
(j) $M_\infty = 2.82, 2.83$ and 2.95 .

Figure 21.- Continued.



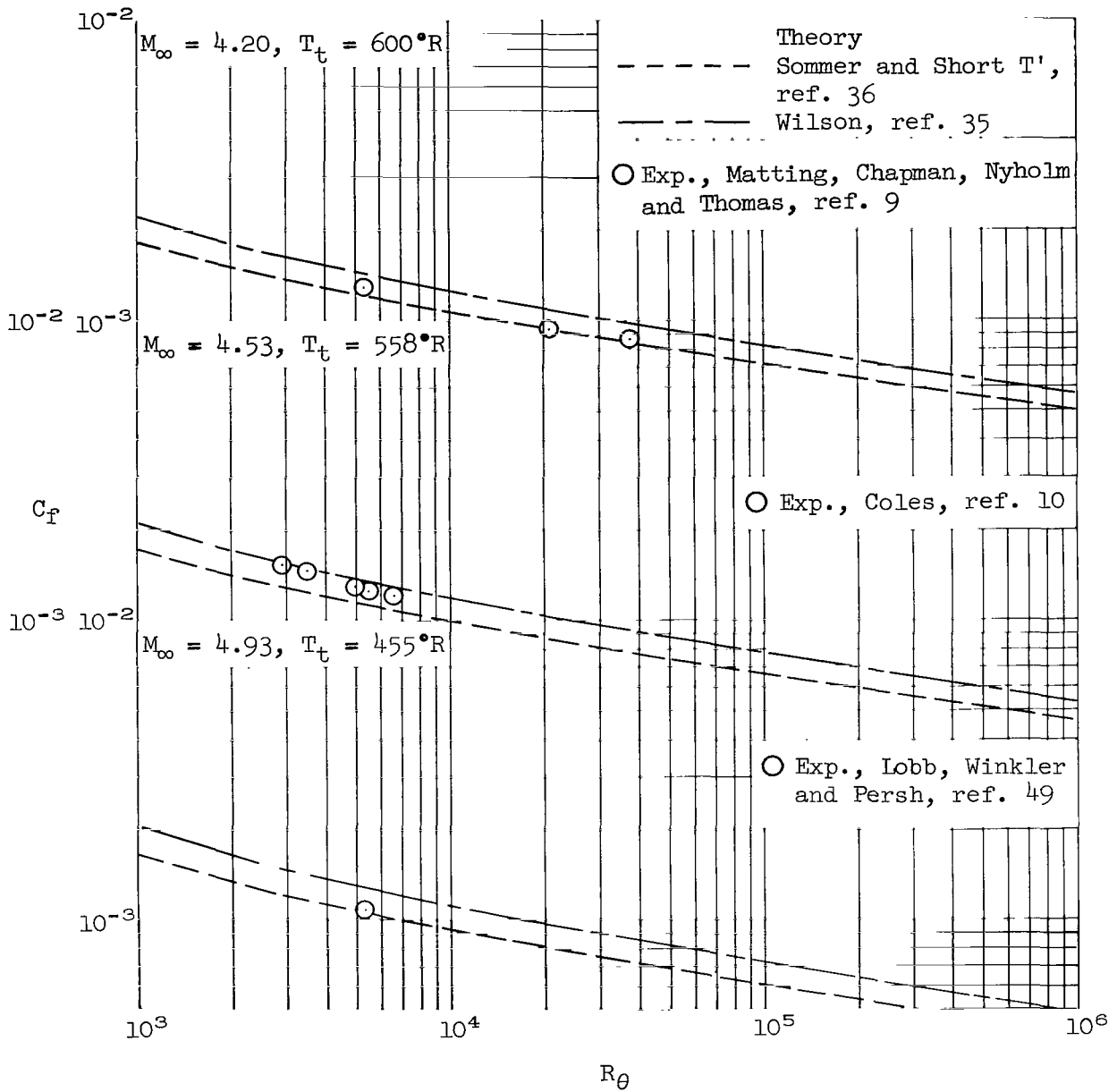
(k) $M_\infty = 2.95, 3.05$ and 3.16 .

Figure 21.- Continued.



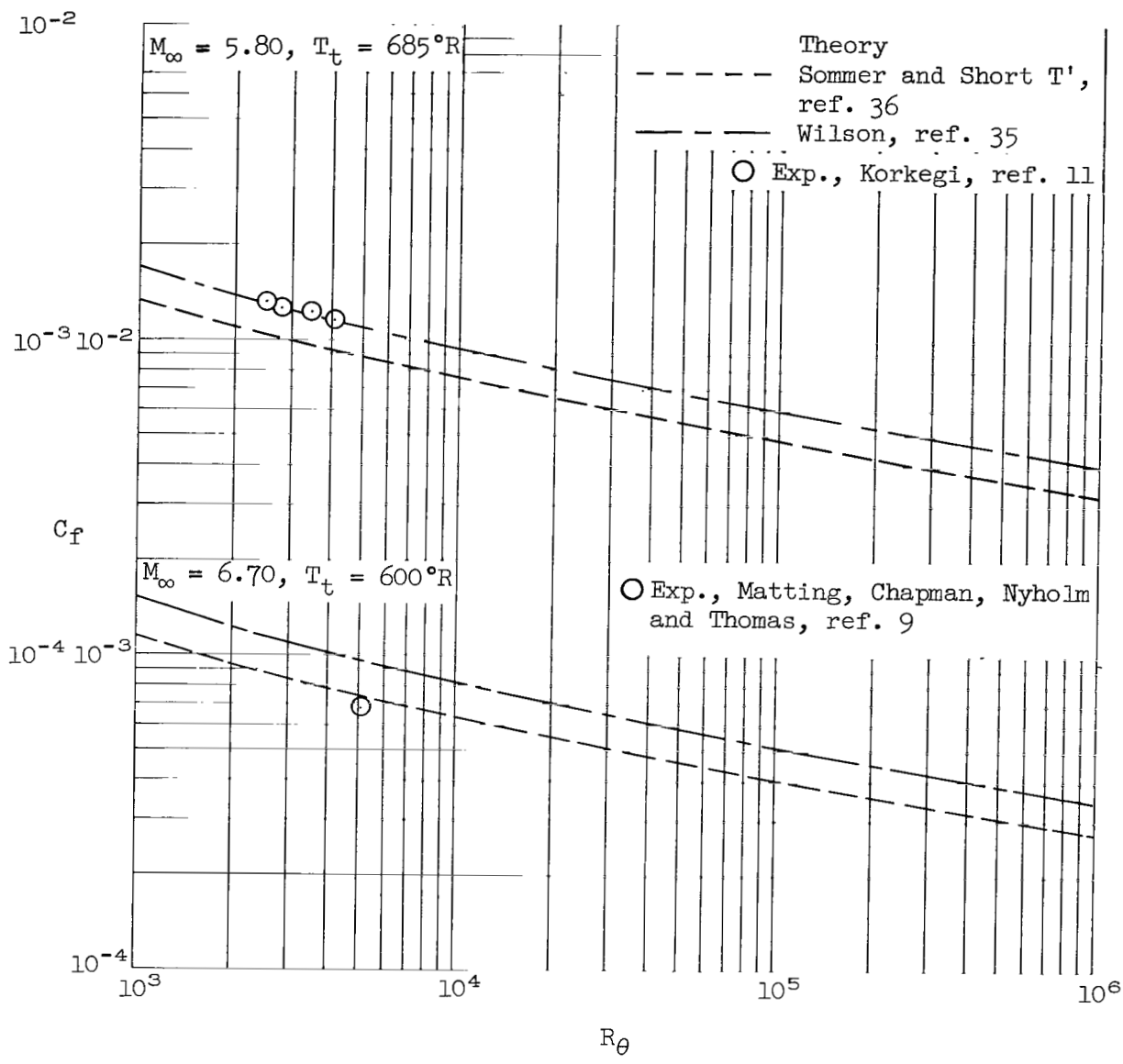
(1) $M_\infty = 3.39, 3.67$ and 3.69 .

Figure 21.- Continued.



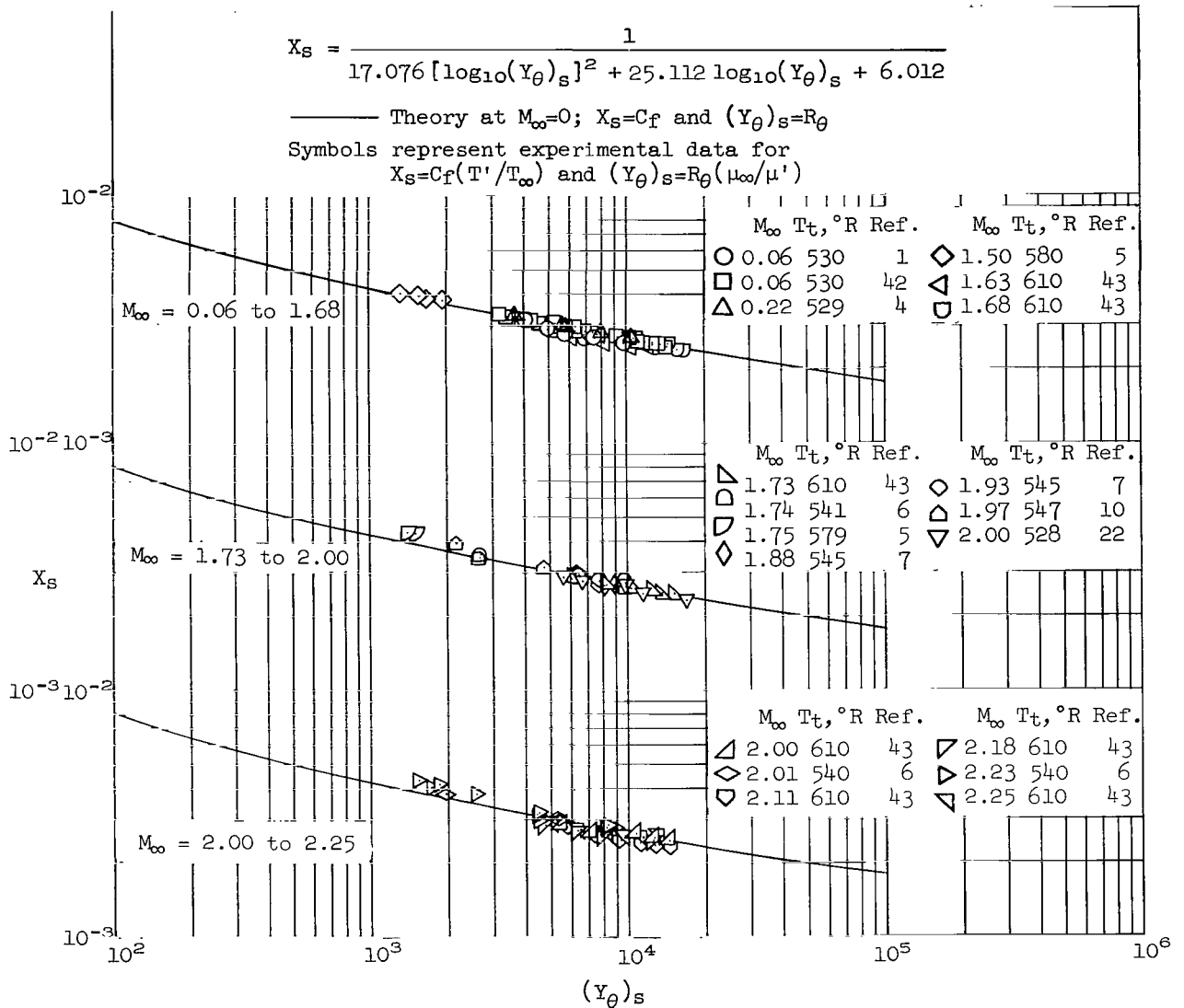
(m) $M_\infty = 4.20, 4.53$ and 4.93 .

Figure 21.- Continued.



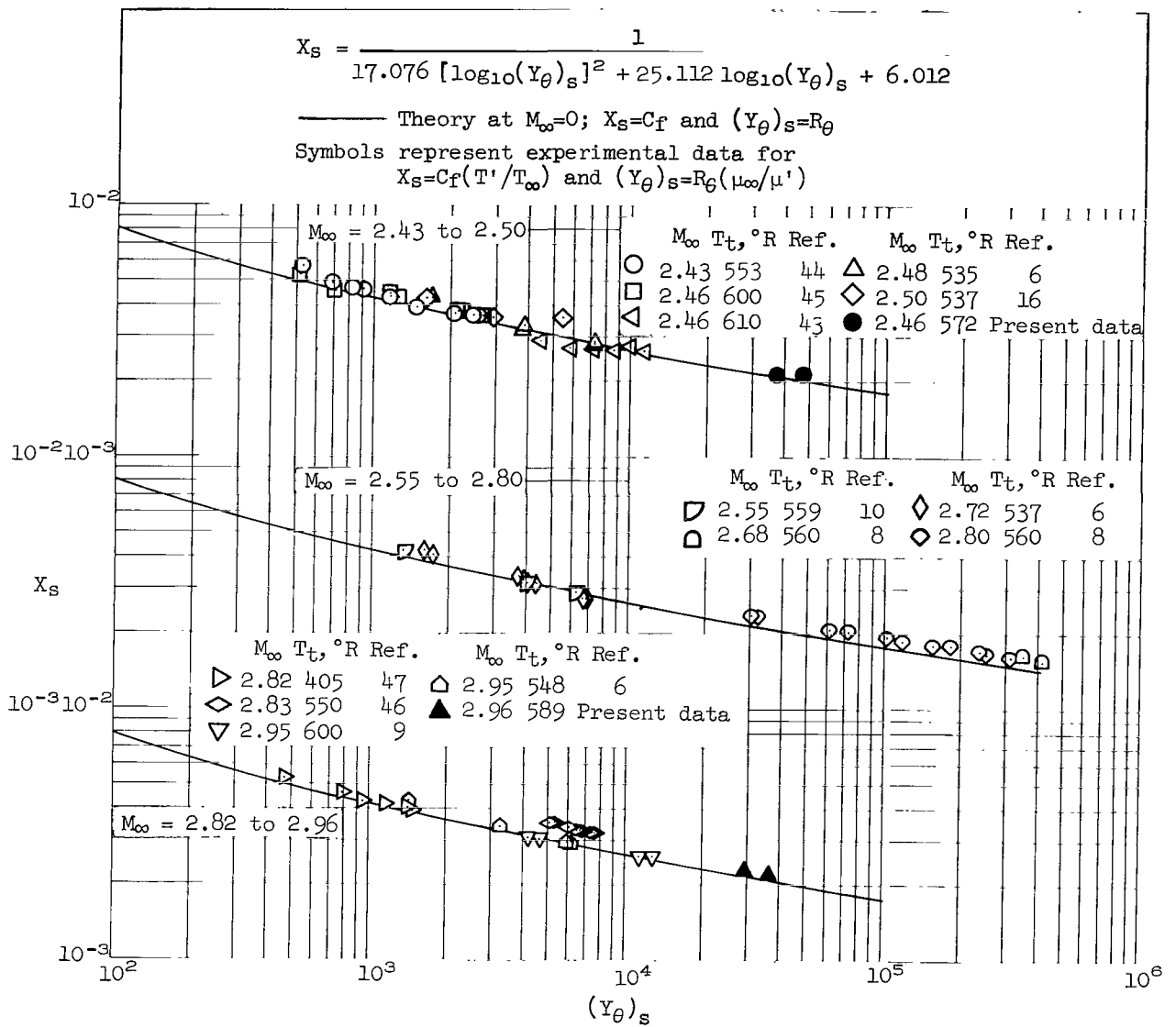
(n) $M_\infty = 5.80$ and 6.70 .

Figure 21.- Concluded.



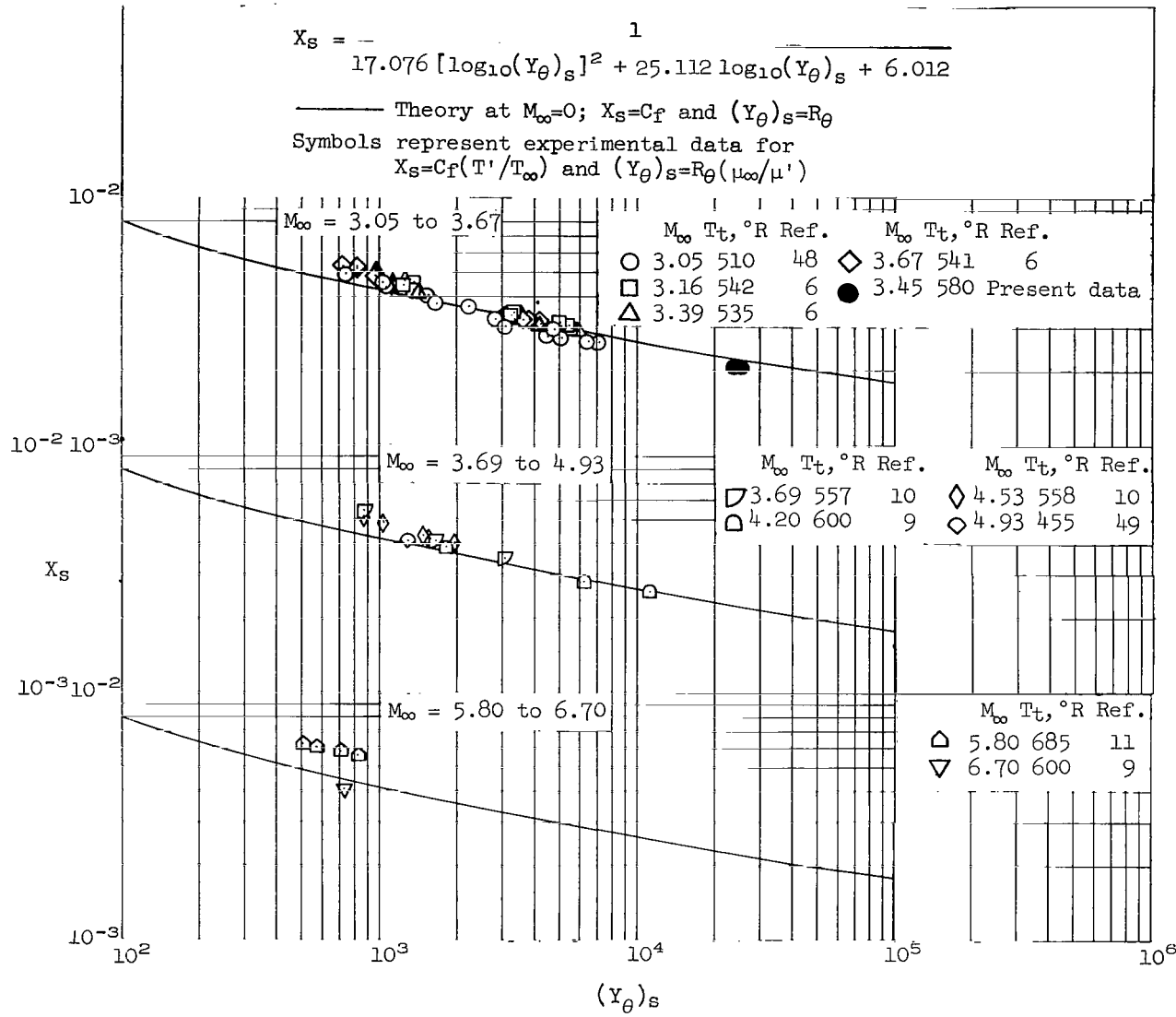
(a) $M_\infty = 0.06$ to 2.25 .

Figure 22.-- Comparison of experimental local skin-friction data on a generalized basis with C_f - R_θ theory of Sommer and Short.



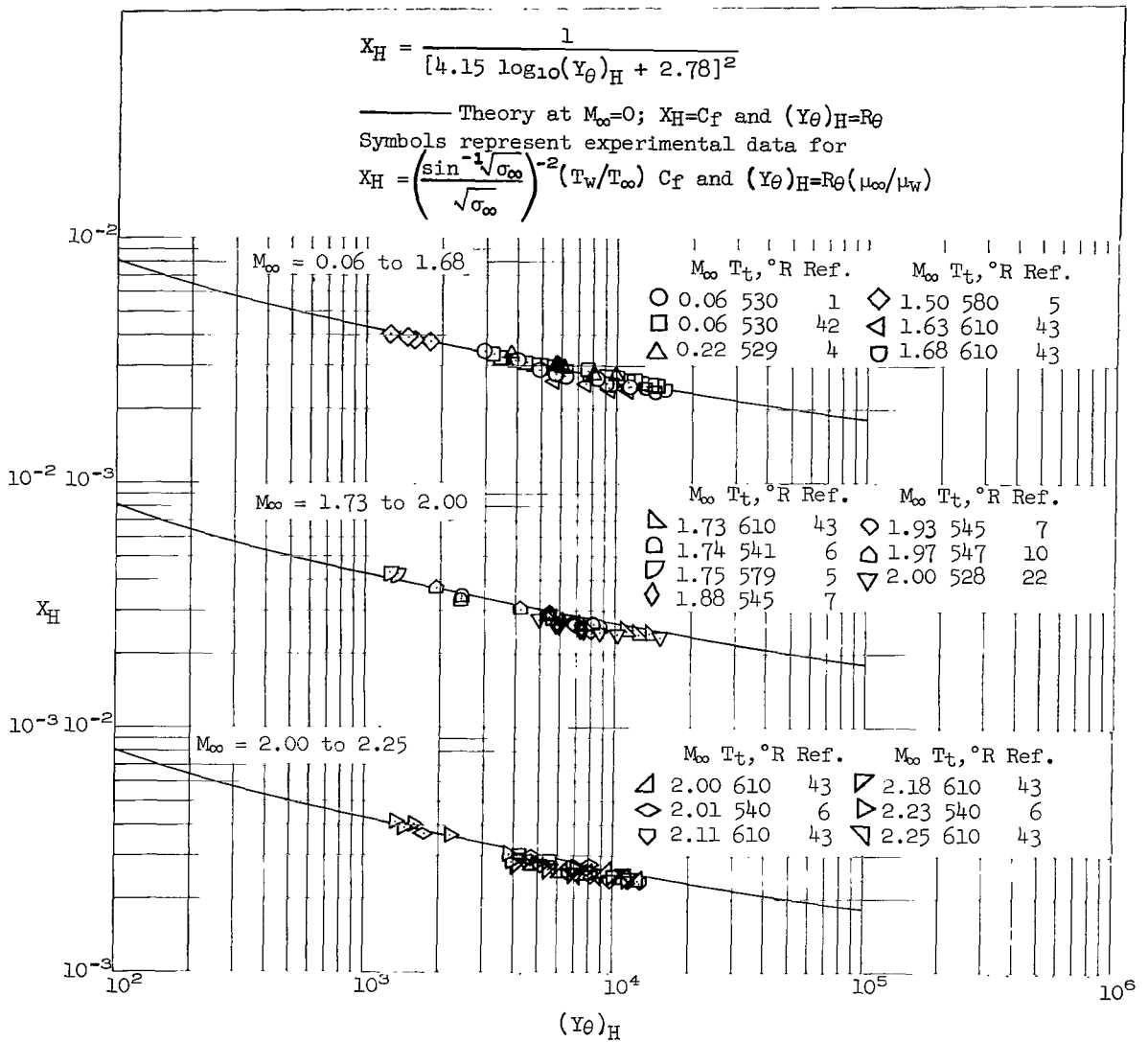
(b) $M_\infty = 2.43$ to 2.96 .

Figure 22.- Continued.



(c) $M_\infty = 3.05$ to 6.70 .

Figure 22.- Concluded.



(a) $M_\infty = 0.06 \text{ to } 2.25$.

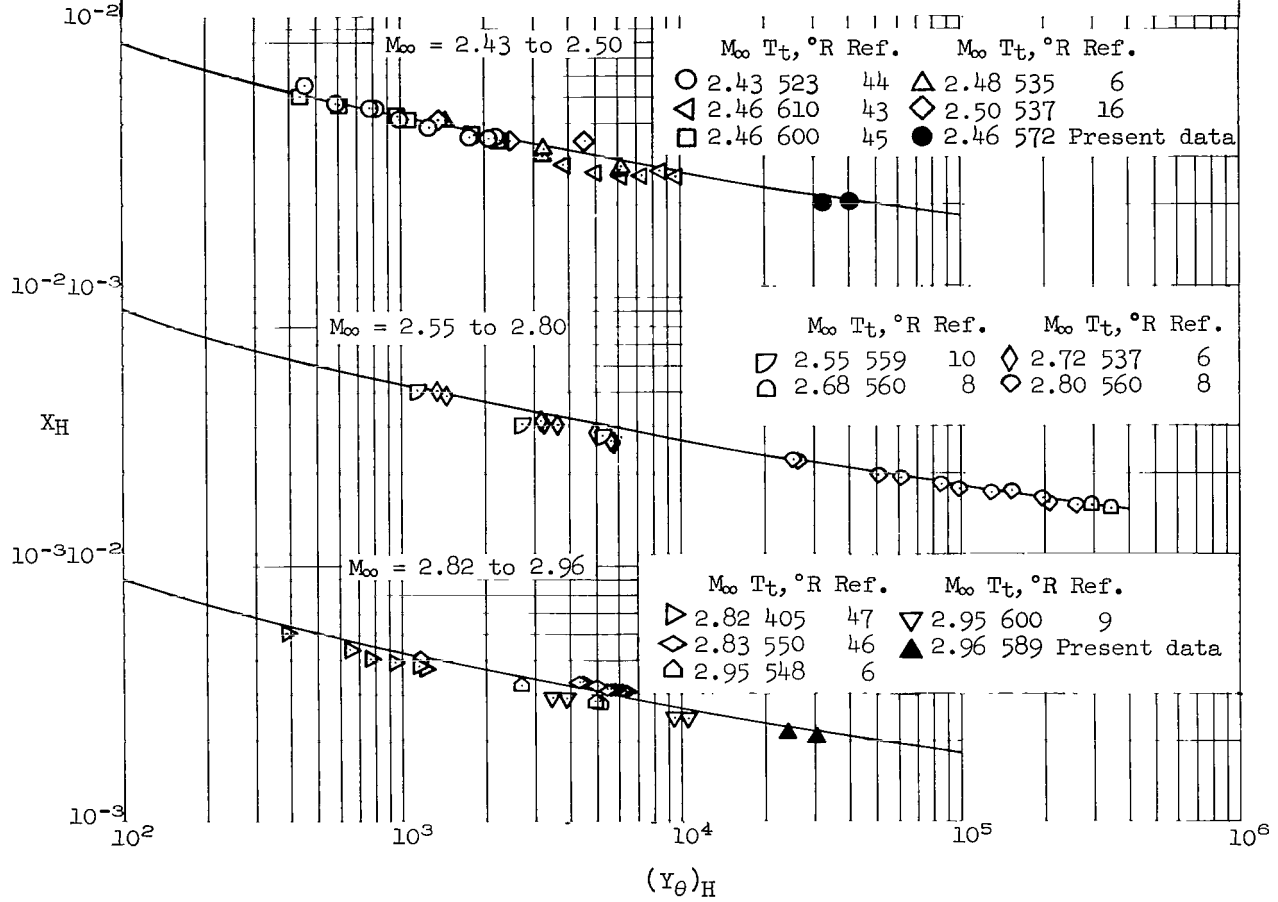
Figure 23.- Comparison of experimental local skin-friction data on a generalized basis with C_f - $R\theta$ theory of Wilson.

$$X_H = \frac{1}{[4.15 \log_{10}(Y_\theta)_H + 2.78]^2}$$

— Theory at $M_\infty=0$; $X_H=C_f$ and $(Y_\theta)_H=R\theta$

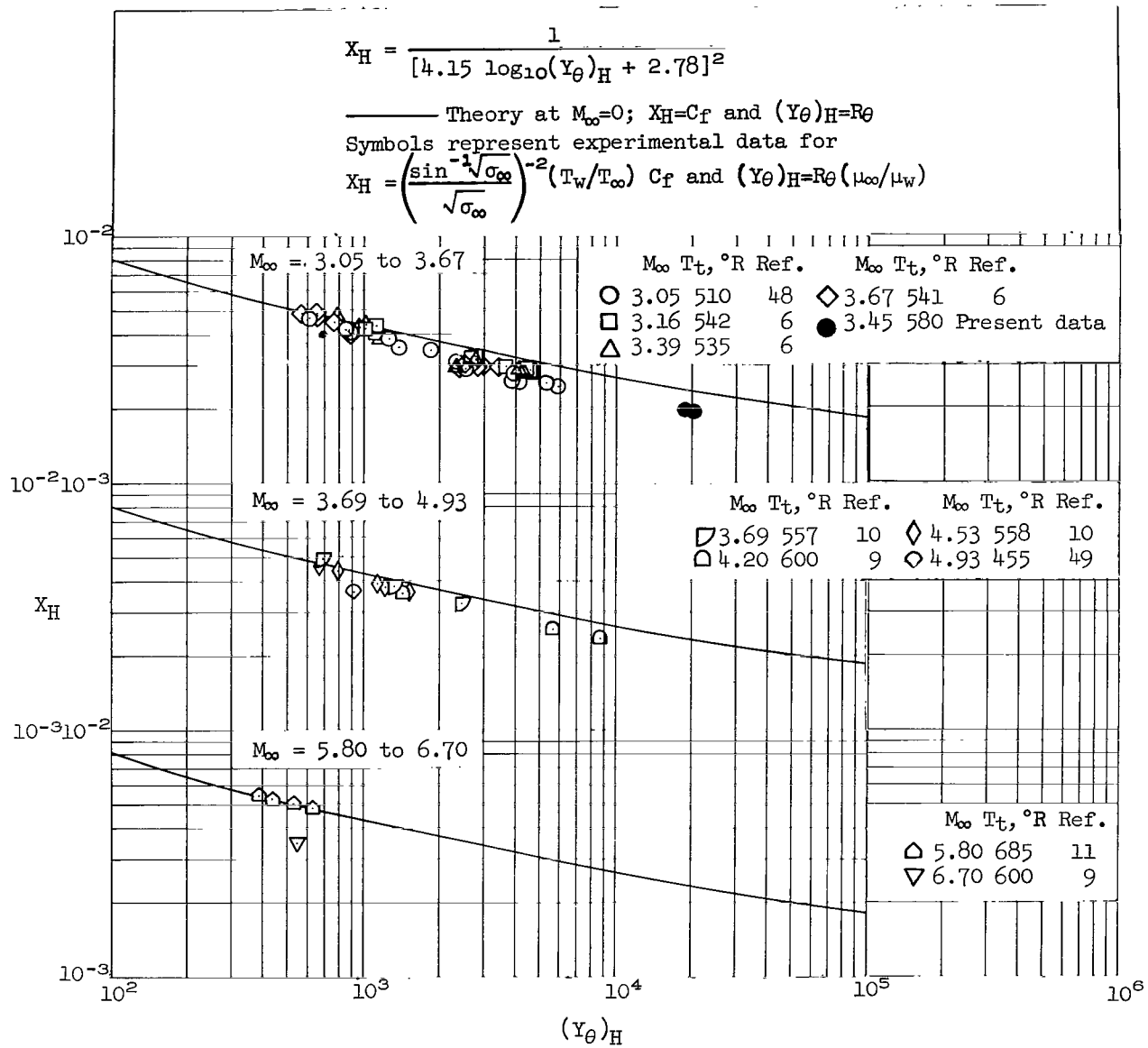
Symbols represent experimental data for

$$X_H = \left(\frac{\sin^{-1} \sqrt{\sigma_\infty}}{\sqrt{\sigma_\infty}} \right)^{-2} (T_w/T_\infty) C_f \text{ and } (Y_\theta)_H = R\theta (\mu_\infty/\mu_w)$$



(b) $M_\infty = 2.43$ to 2.96 .

Figure 23.- Continued.



(c) $M_\infty = 3.05$ to 6.70 .

Figure 23.- Concluded.

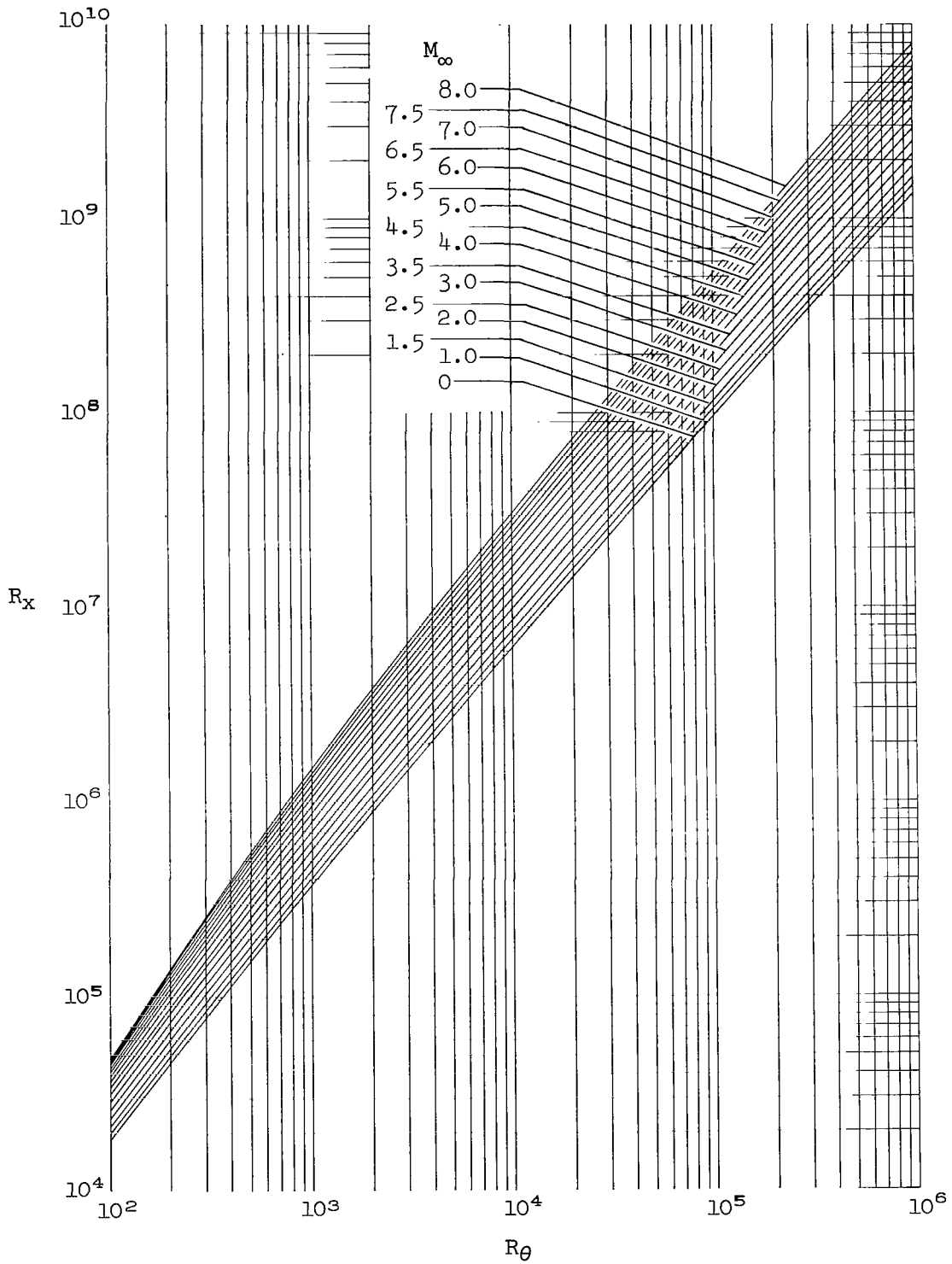


Figure 24.- Relationship between R_x and R_θ at various Mach numbers as given by the T' method of Sommer and Short. Adiabatic flat plate with $T_t = 600^\circ\text{R}$.

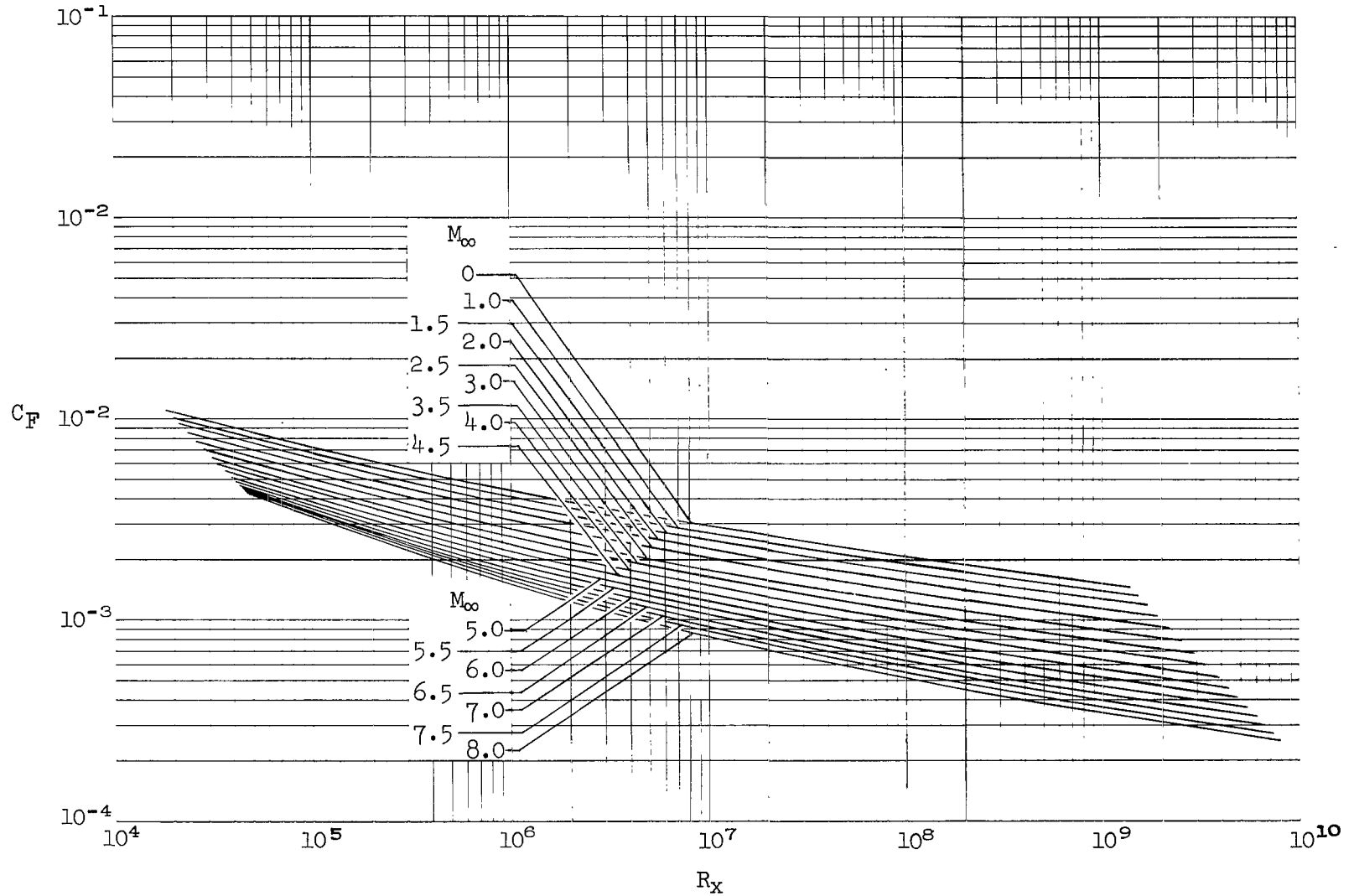
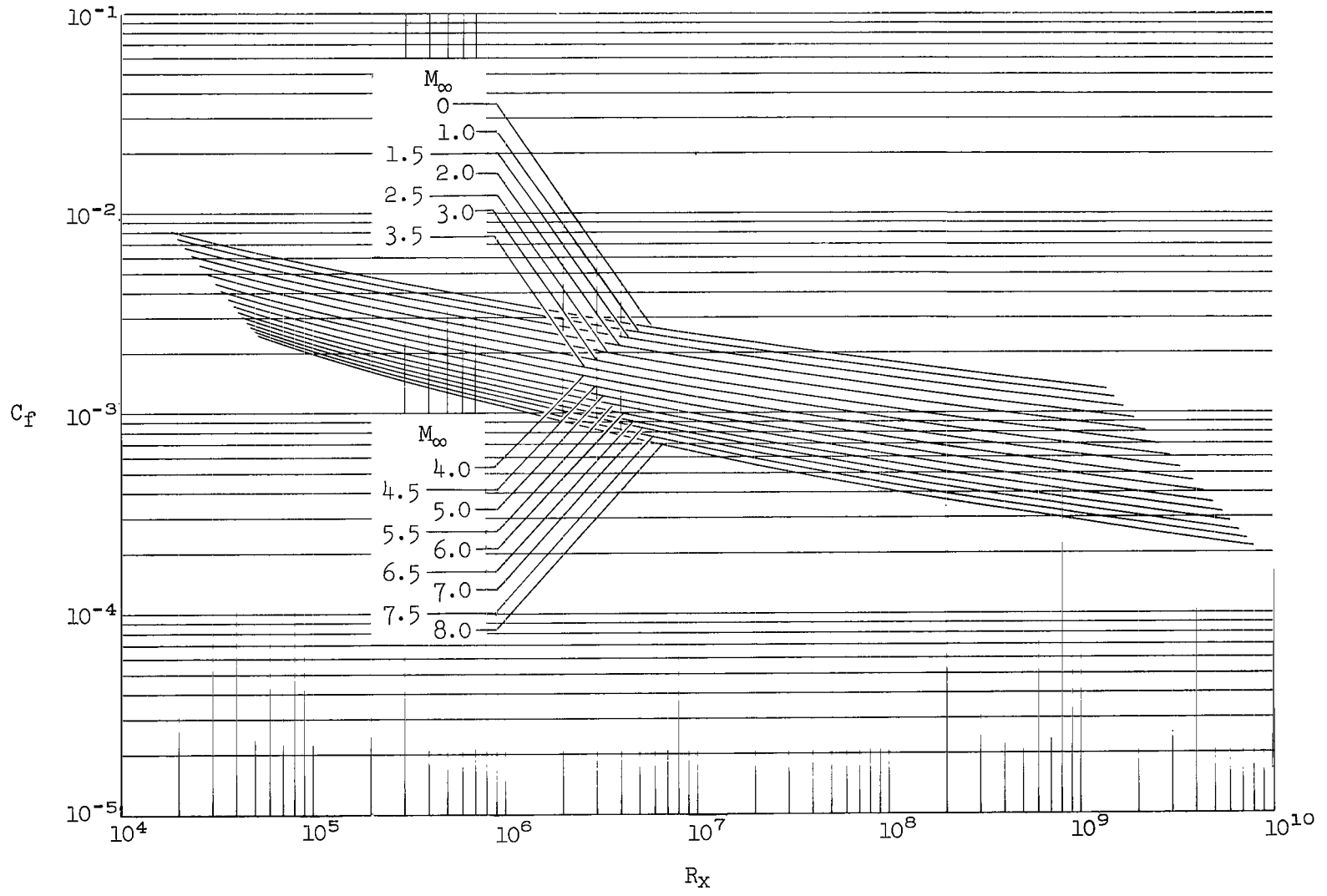
(a) C_F vs R_X .

Figure 25.- Relationship between the skin-friction coefficients and Reynolds number at various Mach numbers as given by the T' method of Sommer and Short. Adiabatic flat plate with $T_t = 600^\circ\text{R}$.



(b) C_f vs R_x .

Figure 25.- Concluded.

"The aeronautical and space activities of the United States shall be conducted so as to contribute . . . to the expansion of human knowledge of phenomena in the atmosphere and space. The Administration shall provide for the widest practicable and appropriate dissemination of information concerning its activities and the results thereof."

—NATIONAL AERONAUTICS AND SPACE ACT OF 1958

NASA SCIENTIFIC AND TECHNICAL PUBLICATIONS

TECHNICAL REPORTS: Scientific and technical information considered important, complete, and a lasting contribution to existing knowledge.

TECHNICAL NOTES: Information less broad in scope but nevertheless of importance as a contribution to existing knowledge.

TECHNICAL MEMORANDUMS: Information receiving limited distribution because of preliminary data, security classification, or other reasons.

CONTRACTOR REPORTS: Technical information generated in connection with a NASA contract or grant and released under NASA auspices.

TECHNICAL TRANSLATIONS: Information published in a foreign language considered to merit NASA distribution in English.

TECHNICAL REPRINTS: Information derived from NASA activities and initially published in the form of journal articles.

SPECIAL PUBLICATIONS: Information derived from or of value to NASA activities but not necessarily reporting the results of individual NASA-programmed scientific efforts. Publications include conference proceedings, monographs, data compilations, handbooks, sourcebooks, and special bibliographies.

Details on the availability of these publications may be obtained from:

SCIENTIFIC AND TECHNICAL INFORMATION DIVISION
NATIONAL AERONAUTICS AND SPACE ADMINISTRATION

Washington, D.C. 20546